THE ANTENNA LABORATORY

RESEARCH ACTIVITIES in ---

Automatic Controls — *Antennas* — *Echo Area Studies*
Microwave Circuits — *Astronautics* — *E M Field Theory*
Terrain Investigations — *Radomes* — *Systems Analysis*
Wave Propagation — *Submillimeter Applications*

Proceedings of the OSU-RTD Symposium
on
Electromagnetic Windows

2-4 June 1964

Vol. I

Department of ELECTRICAL ENGINEERING

THE OHIO STATE UNIVERSITY
RESEARCH FOUNDATION
Columbus, Ohio

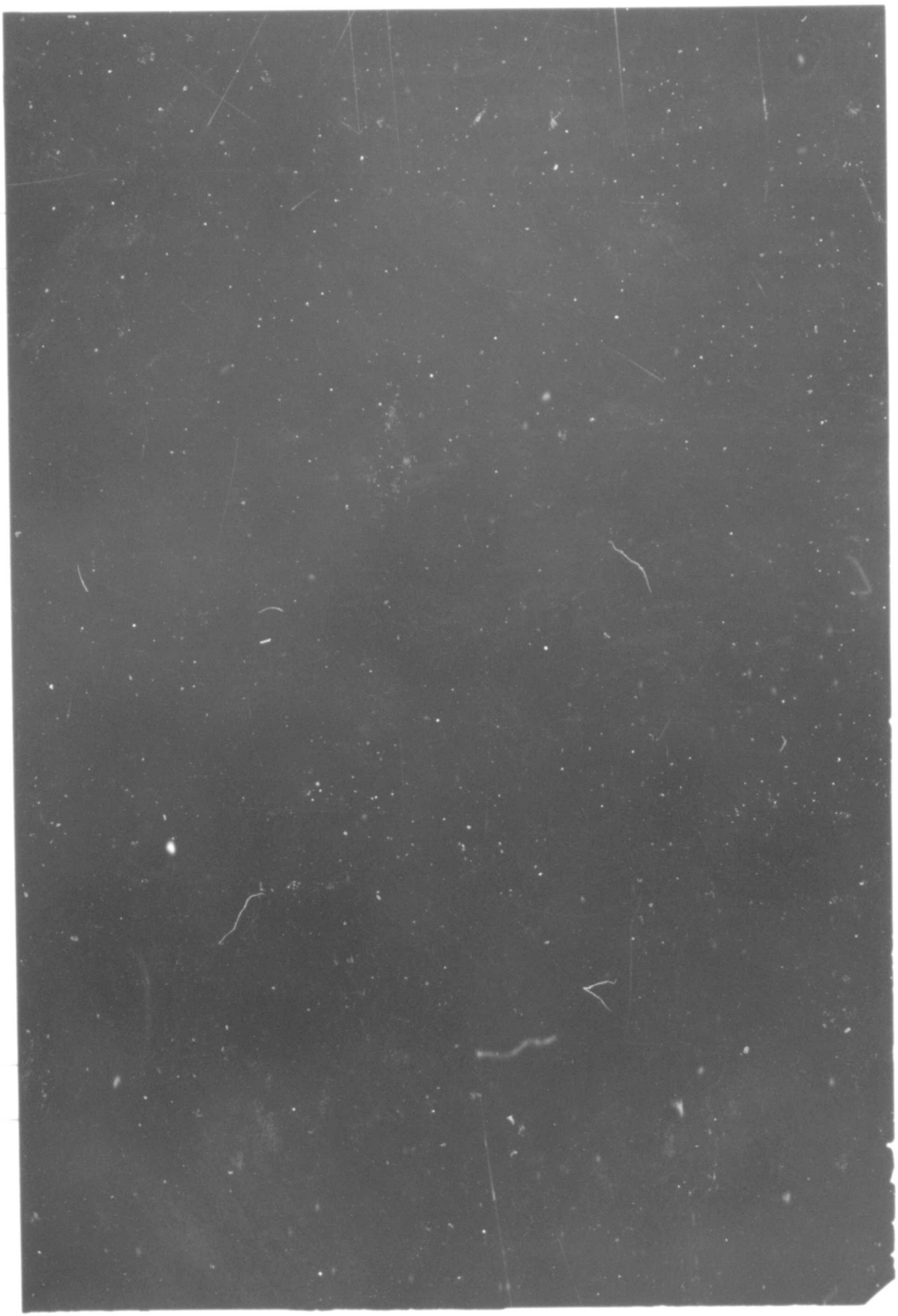

CLEARINGHOUSE FOR FEDERAL SCIENTIFIC AND TECHNICAL INFORMATION CFSTI
DOCUMENT MANAGEMENT BRANCH 410.11

LIMITATIONS IN REPRODUCTION QUALITY

ACCESSION # AD 605390

☒ 1. WE REGRET THAT LEGIBILITY OF THIS DOCUMENT IS IN PART UNSATISFACTORY. REPRODUCTION HAS BEEN MADE FROM BEST AVAILABLE COPY.

☐ 2. A PORTION OF THE ORIGINAL DOCUMENT CONTAINS FINE DETAIL WHICH MAY MAKE READING OF PHOTOCOPY DIFFICULT.

☐ 3. THE ORIGINAL DOCUMENT CONTAINS COLOR, BUT DISTRIBUTION COPIES ARE AVAILABLE IN BLACK-AND-WHITE REPRODUCTION ONLY.

☐ 4. THE INITIAL DISTRIBUTION COPIES CONTAIN COLOR WHICH WILL BE SHOWN IN BLACK-AND-WHITE WHEN IT IS NECESSARY TO REPRINT.

☐ 5. LIMITED SUPPLY ON HAND: WHEN EXHAUSTED, DOCUMENT WILL BE AVAILABLE IN MICROFICHE ONLY.

☐ 6. LIMITED SUPPLY ON HAND: WHEN EXHAUSTED DOCUMENT WILL NOT BE AVAILABLE.

☐ 7. DOCUMENT IS AVAILABLE IN MICROFICHE ONLY.

☐ 8. DOCUMENT AVAILABLE ON LOAN FROM CFSTI (TT DOCUMENTS ONLY).

☐ 9.

NBS 9/64

PROCESSOR: VM

Proceedings of the OSU-RTD Symposium on Electromagnetic Windows

2-4 June 1964

Vol. I
Session I-Objectives and New Techniques
Session II-Materials for High Temperature Applications

FOREWORD

The papers presented in this report were submitted for the Seventh Symposium on Electromagnetic Windows held at The Ohio State University, Columbus, Ohio, 2, 3, and 4 June 1964. They were compiled by Alan I. Slonim of The Ohio State University under Air Force Contract AF 33(615)-1081 administered by The Research and Technology Division, Air Force Systems Command, Wright-Patterson Air Force Base, Ohio with Richard A. Ireland serving as Task Engineer.

The proceedings are published in five volumes as follows:

Vol. I

Session I - Objectives and New Techniques
Session II - Materials for High Temperature Applications

Vol. II

Session III - Electrical Design
Session IV - Structural Design for Large Radomes

Vol. III

Session V - Fabrication and Testing of Airborne Radomes
Session VI - Hypersonic Environment

Vols. IV and V

Oral papers received too late for inclusion in Vols. I, II, and III.
Papers submitted for the proceedings only.

Vol. I
CONTENTS

SESSION I

CHEMICALLY VAPOR DEPOSITED BORON NITRIDE

P. C. Li, A. J. Capriulo, and M. P. Lepie

Raytheon Company
Research Division
Waltham, Massachusetts 02154

Abstract

Thc chemical vapor deposition (CVD) of boron nitride results in a unique material which could find application as a superior microwave and infrared window.

Process techniques are discussed for hot-pressed and CVD boron nitride. Shortcomings and advantages of both methods are outlined.

Data to be presented includes microstructure, mechanical, thermal, and electrical properties of CVD material. Like its isomorph, pyrolytic graphite, CVD boron nitride is harder, denser, stronger, and more anisotropic than the conventional material. An extremely low dielectric constant and loss tangent, which is relatively unaffected by temperature change, also make it ideal for microwave windows. No infrared absorption is observed beyond 13μ.

Introduction

The advancement of modern science is often hampered by materials problems. Conventional off-the-shelf materials are frequently inadequate for operation under the severe environmental conditions of the space age. Only by a fundamental study of material structure, processing and properties can we hope to meet this great challenge of future scientific progress.

A. Historical Background

Although boron nitride (BN) is referred to as a new material, it was prepared as early as 1842 by Balmain.[1,2] He reacted boric acid, mercuric cyanide, and sulphur and also boric acid plus potassium cyanide. In spite of the relative ease with which BN powder can be produced, it remained a laboratory curiosity until recently because of the difficulty in forming it into a useful object.

About a decade ago the Carborundum Company found that boron nitride could be processed by the hot-pressing technique. This method, however, requires the addition of a binder and fluxing agent with the resultant decrease in purity. A method that overcomes this difficulty, namely, chemical vapor deposition, has been employed by Raytheon Company for the past five years. The product is characterized by:

1. High purity
2. Theoretical density
3. Variety of shape and thickness
4. Anisotropy of crystallites.

B. Relationship with Graphite

Boron nitride is isostructural with graphite; in fact, it is commonly known as "white graphite." The x-ray diffraction patterns indicate that the two materials are almost identical. Both have a greasy feeling and possess good lubricating properties even at elevated temperatures.

There are many differences as well as similarities between graphite and boron nitride. Graphite is a semi-metal, while BN is an electrical insulator. The former can be wet by molten metals, while the latter does not react with the metals making it ideal as a crucible material. Also, BN is more oxidation resistant at elevated temperatures. Finally, the thermal conductivity of BN is somewhat superior, ranking with that of nickel.

C. Structure

Boron nitride is normally produced in the hexagonal form but two other allotropic types are known to exist. Rhombohedral BN has been reported [3] to co-exist with the hexagonal form when prepared by the fusion of sodium borate and potassium cyanide. Cubic BN is made by a high pressure technique [4] similar to that for preparing diamond.

Like graphite, BN is composed of hexagonal rings in a two-dimensional network (Fig. 1) stacked one on top of the other in varying degrees of order. Each ring is made up of alternating boron and nitrogen atoms separated by a bond length of 1.446 Å. Cubic BN has the networks stacked so that each boron atom has a nitrogen atom directly above and below it and vice-versa for each nitrogen atom. The spacing between each second layer, c-spacing, is 6.6612 Å as determined by Pease.[5] C-spacing for the cubic form[4] is 3.615 Å and for the rhombohedral form[3] it is 10.01 Å.

Process

Various raw materials have been used to produce BN. The chief source for boron is either boric acid or boron trichloride. Nitrogen is derived from ammonia although it is possible to crack molecular nitrogen at elevated temperatures.

A. Hot-Pressed Material

Gilpin [6] has desdribed the Carborundum process for the manufacture of boron nitride from the oxide and ammonia. Tricalcium orthophosphate is

blended first with boric acid in order to prevent agglomeration of the oxide at elevated temperatures. Then the mixture is heated to about 1000°C in an atmosphere of ammonia. The resultant product is next crushed and the $Ca_3(PO_4)_2$ removed by leaching with HCl. The impure BN is washed to remove HCl, dried, refired in NH_3 and the 97 percent pure product reduced to -325 mesh size by ball milling. Finally, BN billets are formed by hot-pressing in graphite molds at about 2000°C and 2000-4000 psi with a nitrogen atmosphere. The billets are easily machined to the desired shape. Although the method involves many process steps, it lends itself to mass production.

B. Chemical Vapor Deposition

The vapor deposition technique practiced by Raytheon Company for making BN is far simpler than that described above. In addition, the product is extremely pure, dense, and usually requires no machining.

Figure 2 illustrates the process with two different source materials. One method employs B-trichloroborazole, $B_3N_3H_3Cl_3$ to provide equimolar amounts of boron and nitrogen. It is a white crystalline solid which vaporizes on heating. The vapor is then swept into the reaction chamber by the N_2 carrier gas. Here it decomposes pyrolytically in the presence of a hot graphite substrate (1000°-2000°C). A simplified version of the reaction is:

$$B_3N_3H_3Cl_3 \rightarrow 3BN + 3HCl$$

The BN plates out on the graphite mandrel and the HCl is removed by the cold trap.

A second method uses BCl_3 (bp 12.5°C) and NH_3 as source gases with N_2 as a carrier. All are gases at room temperature greatly simplifying matters. The overall reaction is:

$$BCl_3 + NH_3 \rightarrow BN + 3HCl$$

Here again BN deposition is favored by elevated temperature and low pressure.

A third process has been recently developed. It differs from the others in that the product is isotropic rather than anisotropic. This can be an advantage as, for example, in the reduction of residual stresses caused by thermal expansion anisotropy.

Deposition rate for BN varies from 1-50 mils per hour and is a function of temperature, pressure, volume, of reactant gases, velocity of gases, geometry of the system, etc. Thus, a careful control of process conditions is required to assure uniformity of product.

Properties

The properties of BN are related to the source materials and the processing technique employed. Thus, an ideal way would be to report the range of values obtained for various samples. However, in order to avoid the confusion resulting from such a large collection of data, we have chosen to stress only our results with CVD BCl_3 material.

A. General Appearance

Low temperature (1000°C) CVD BN is glassy, hard, and has a yellow to brown cast. The material made above 1500°C is opaque, white, and somewhat softer. Transluscency increases with decrease in process temperature. Absolute hardness values are not available, but qualitative scratch tests indicate CVD BN is much harder than hot-pressed BN.

Figure 3 is a photomicrograph taken in polarized light of a polished cross section. The similarity to pyrolytic graphite is quite evident. Both have the same elongated cone structure which is more pronounced in the case of the graphite because the metallic gray color shows up better in reflected light.

B. X-Ray Diffraction

Boron nitride processing conditions are reflected in the x-ray diffraction patterns seen in Fig. 4. The top pattern is of hot-pressed BN. Sharp reflections of (002) and its higher order (004) indicate some degree of preferred orientation probably due to the alignment of flake-like material in the pressing operation. However, the presence of (100), (101), and (102) peaks shows that there is no true layer ordering.

The next pattern is CVD BN made at 2000°C. Here, the lack of all peaks except (002) is exactly what one observed with pyrolytic graphite. Not only do both materials have crystallite ordering, but they also show a c-spacing distance that is close (within three percent) to single crystal.

The last pattern is of low temperature (1200°C) CVD BN. The lack of any clearly defined peaks is indicative of little or no ordering. When this material is heat-treated at 1900°C for two hours, the peaks become sharp. Also, there is a shift of the (002) peak to higher angles which means a decrease in c-spacing. It appears that heat-treating causes, in addition, an increase in crystal size (narrower (002) peak) and a decrease in strain energy (sharper peaks).

C. Anisotropy

Degree of preferred orientation was measured using the technique of Guentert and Prewitt.[7,8] Rod shaped specimens were cut with their axis parallel to the deposition surface and examined by rotating at right

angles to the x-ray beam. Figure 5 shows the change in (002) intensity versus rotation angle ω. Although CVD BN is highly oriented, pyrolytic graphite exhibits an even higher degree of preferred orientation.

D. Density

The bulk density of CVD BN was determined by displacement in toluene. Figure 6 shows the effect of deposition temperature on density. There is a rapid rise in density at about 1600°C followed by an approach to theoretical density (2.27 gm/cc) at 1900°C. Even low temperature, low density material can be made extremely dense by heat-treatment under nitrogen at 1900°C.

E. Chemical Resistance

Boron nitride is remarkably inert to nearly all chemicals at room temperature. At elevated temperatures very few reagents will attack it. Thus, it makes a good crucible material for molten metals.

The oxidation resistance of CVD BN was studied by measuring its weight change in air at various temperatures. These data along with results from hot-pressed BN and graphite are presented in Fig. 7. Oxidation of CVD BN is negligible at 800°C - less than 0.2 mg/cm^2 at 70 hours. Above 800°C the oxidation rate can be expressed by an Arrhenius equation of the form,

$$K = 90\, e^{-\frac{40,000}{RT}}$$

Hot-pressed BN shows a similar activation energy of 40 k cal/mole, but the rate is orders of magnitude higher than CVD BN. The same is true for graphite versus CVD graphite. However, the mechanism of oxidation for graphite and BN is entirely different. Oxidation provides no diffusion barrier against further reaction for graphite (CO, CO_2) as in the case of BN (B_2O_3). The glassy boric oxide layer offers little protection above 1400°C because of its increased vapor pressure, higher oxidation diffusion, and low viscosity.

F. Thermal Expansion

The thermal expansion of CVD BN in both crystallographic directions was measured in the range 0°-1075°C by means of a Leitz dilatometer. Figure 8 illustrates the effects of deposition direction. For the purpose of comparison, hot-pressed BN samples were also measured perpendicular and parallel to the pressing direction.

In going from a- to c-direction the 1600°C CVD BN changes nearly two orders of magnitude in coefficient of thermal expansion (24×10^{-6} °C for a-direction versus 0.4×10^{-6} °C for c-direction). Heat-treatment

causes a decrease in expansion along the a-direction and an increase in the c-direction. An increase in deposition temperature results in a greater thermal expansion in the a-direction (0.4×10^{-6} for 1600°C material versus 3.2×10^{-6} for a 1900°C deposit). Low temperature deposits have a negative expansion below 500°C similar to pyrolytic graphite.

Hot-pressed BN also exhibits an anisotropy of thermal expansion but to a much lesser degree. This can be attributed to the mechanical orientation of crystallites by the pressing action. Both c- and a-direction expansion curves have a jog at about 400°C also reported by Taylor.[9]

G. Thermal Conductivity

The thermal conductivity of CVD BN has been measured in the a-direction. There is only a small change of conductivity with temperature going from 0.19 cal/sec/cm^2/°C/cm at 200°C to 0.17 cal/sec/cm^2/°C/cm at 845°C. Measurements have not been completed for c-direction samples but there are indications that there is an anisotropy similar to pyrolytic graphite.

H. Electrical Conductivity

Boron nitride is known[9-11] to be an excellent insulator. In the cubic form it has the highest energy[12] gap (10 ev) reported in the literature for any solid, yet when molten it becomes a good conductor.[13] Resistivity data on BN show a wide spread due to varying degrees of material purity. Also, hot-pressed BN is sensitive to the humidity because the B_2O_3 binder adsorbs moisture readily.

Room temperature DC resistance of CVD BN was measured with a megatrometer and found to be about 10^{15} ohm-cm. Using a Keithley Electrometer, measurements were extended to 1100°C. Results are shown in Fig. 9. Resistance was found to drop sharply in the high temperature range. However, even there it is a better insulator than hot-pressed BN and most other materials.

I. Mechanical Properties

The room temperature flexural strength of CVD BN was determined with 7/8 in. beams of the material in three-point loading with an Instron testing machine. Values ranged from 18 to 30 x 10^3 psi depending on the source material and temperature of deposition. For hot-pressed BN the value is 15.8 x 10^3 psi. Figure 10 shows the effect of temperature on strength. In the range RT to 2000°C CVD BN, like pyrolytic graphite, does not decrease in strength but actually becomes stronger at elevated temperatures.

Compressive strength perpendicular to the ab-plane is 72.3×10^3 psi. Static moduli of elasticity also in the ab-plane are 2.7×10^6 psi and 4.3×10^6 psi for samples loaded in compression and in tension, respectively. Poisson's ratio is negative and less than 0.1.

J. Dielectric Properties

Figure 11 is derived from measurements made at MIT[14] on CVD BN at 4.8 Gc with the electrical field parallel to the field of deposition. The relative dielectric constant (5.12) does not change with temperature from RT to 500°C. Even over the range RT to 1200°C temperature coefficient of the dielectric constant is lower than other microwave window materials. This is highly desirable in cases where radar reception is subject to disruption due to radome heating.

Equally remarkable is the extremely low loss tangent (0.00014 at RT) and its negligible temperature coefficient (0.00005 at 1200°C). No other dielectric has such a consistently low tan δ. The low loss permits the use of increased microwave power and thereby greater radar sensitivity.

Low tangent and dielectric constant at 5 Gc is shown in Fig. 11 for hot-pressed BN [14] also. Loss tangent is greater than CVD BN and not as low as for fused silica.

K. Infrared Transmission

Figure 12 is an absorption curve of the near IR range for a one mil thick specimen perpendicular to the a-plane run on a Perkin-Elmer Infracord with a NaCl prism. There is about 40 percent transmission in the near IR except for absorption bands at 6-8 microns and at 13 microns. Figure 13 also shows absorption coefficient in the intermediate IR range to 35 microns measured on a Perkin-Elmer model #112 with a CsBr prism. There appears to be excellent transmission here with no absorption bands observed. No data is presently available for this material in the far IR.

Conclusions

Boron nitride is a unique material in that it is a high temperature, non-oxide dielectric that is refractory even under drastic environmental conditions.

Chemical vapor deposition of boron nitride produces a substance with property values depending on source materials, process temperature, heat-treatment, etc. Since growth from the vapor is essentially an atom-wise process, the product is dense, pure, and usually highly anisotropic, similar to single crystals, although an isotropic form has also been produced. A variety of shapes can be made without resorting to binders, fluxes or other additives.

An examination of the properties of CVD BN reveals that it deserves serious consideration as an infrared and microwave window material. High strength (3×10^4 psi), low elastic modulus (2×10^6 psi), and low expansion coefficient (2×10^{-6} °C) combine to make it thermal shock resistant. The dielectric constant is relatively low (5.1 at x-band) and changes little with increasing temperature. No other dielectric shows such a low loss tangent (10^{-4}) and temperature coefficient of loss at the same 10^{10} cps frequency. Infrared transmission studies also look promising for CVD BN. The material has absorption peaks at 6-8 and 12-13 microns, but with no further peaks out to 35 microns.

REFERENCES

1. Balmain, W. H., J. Prakt-Chem., 27, 422 (1842).
2. Balmain, W. H., Phil. Mag., 21, 170 (1842).
3. Herold, A., Marzluf, B., and Perio, P., Compt Rendu., 246, 1866, (1958)
4. Wentorf, R. H., Jr., J. Chem. Phys., 26, 956, (1957).
5. Pease, R. S., Acta Cryst., 5, 356 (1952).
6. Gilpin, J. W., Chem. Eng., 70, 110 (1963).
7. Guentert, O. J., Prewitt, C. T., Raytheon Company, Technical Memorandum T-196, (1959).
8. Guentert. O. J., et al, Nature, 193, 570 (1962).
9. Taylor, K. M., Ind. Eng. Chem., 47, 2506 (1955).
10. Podszeus, E., and Angrew, Z., U allgem. chem., 30, 156 (1917).
11. Ingles, T. A. and Popper, P., "Special Ceramics," Proceedings of a Symposium by the Br. Ceram. Res. Assoc., Academic Press, Inc. New York, 1960, pp. 144-169.
12. Geller, S., J. Phys. Chem. Solids, 10, 340 (1959).
13. Wentorf, R. H., Jr., J. Phys. Chem., 63, 1934 (1959).
14. Westphal, W. B., Techn. Rept. 182, Lab. Insul. Res., MIT, Oct. 1963.

BLANK PAGE

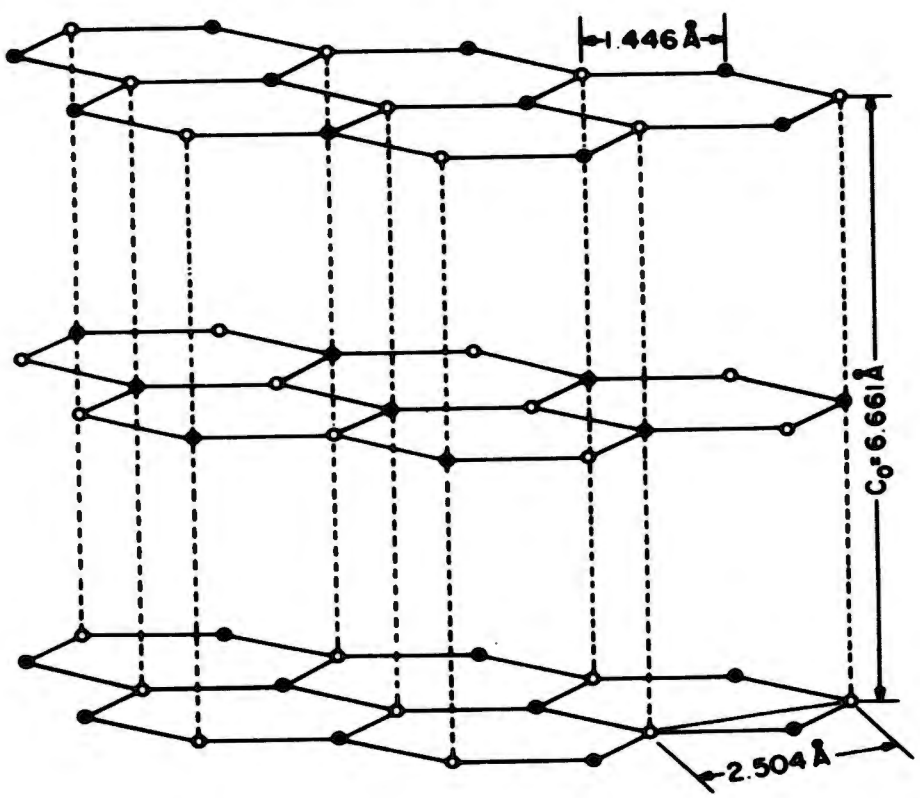

(a)

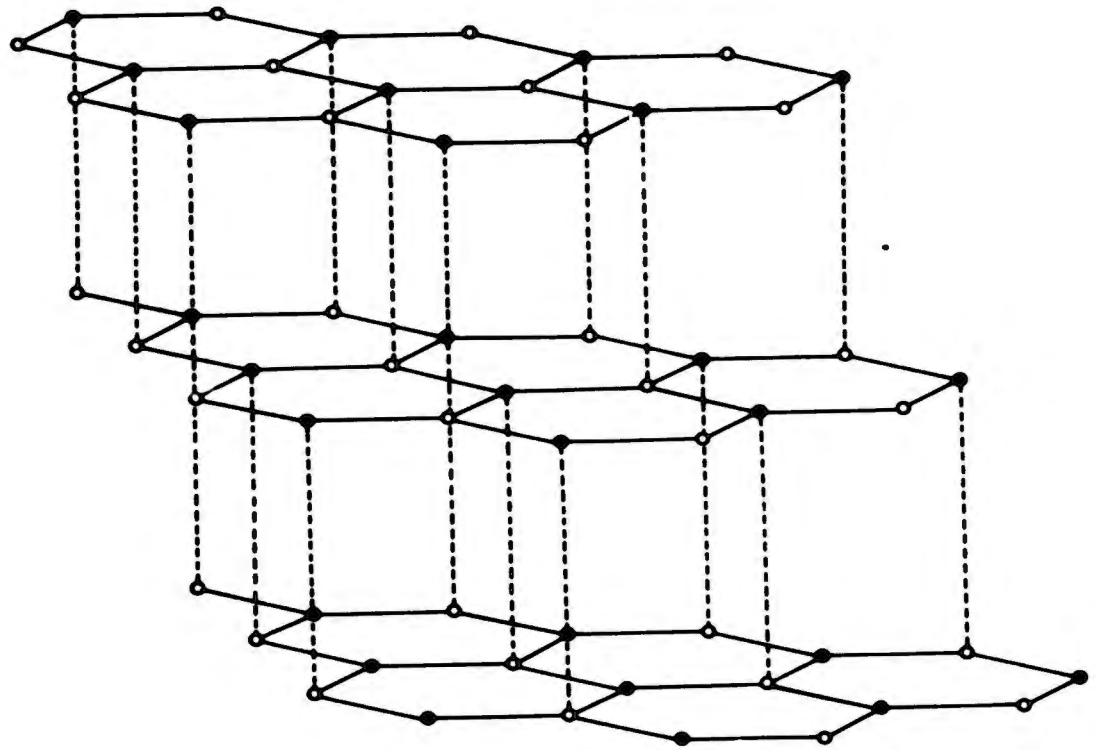

(b)

A

● Boron

○ Nitrogen

BORON NITRIDE (a) Hexagonal structure; (b) Rhombohedral layer structure

FIGURE 1

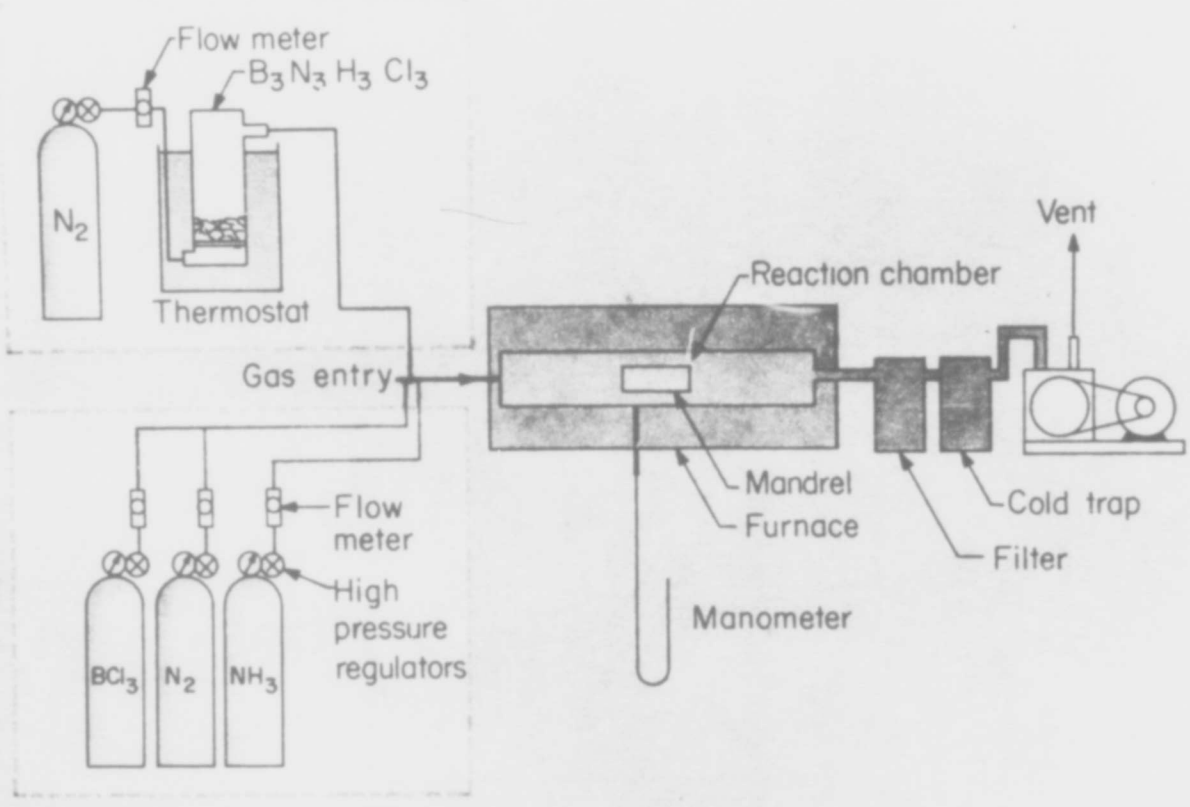

APPARATUS FOR VAPOR DEPOSITION OF BORON NITRIDE FROM BCl_3 AND NH_3 OR $B_3N_3H_3Cl_3$

FIGURE 2

Photomicrograph of Pyrolytic BN (50X)

(a)

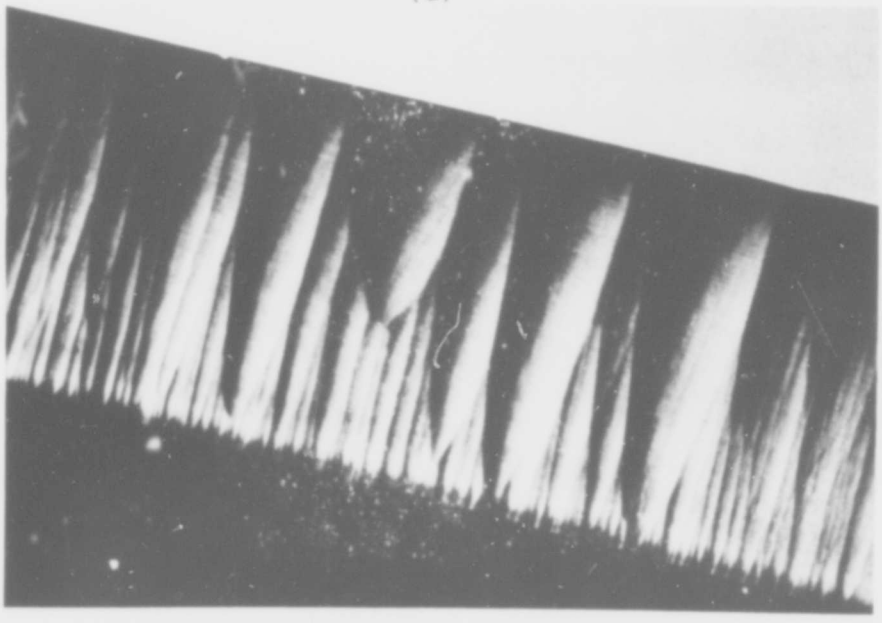

Photomicrograph of PYROGRAPHITE (100X)

(b)

FIGURE 3

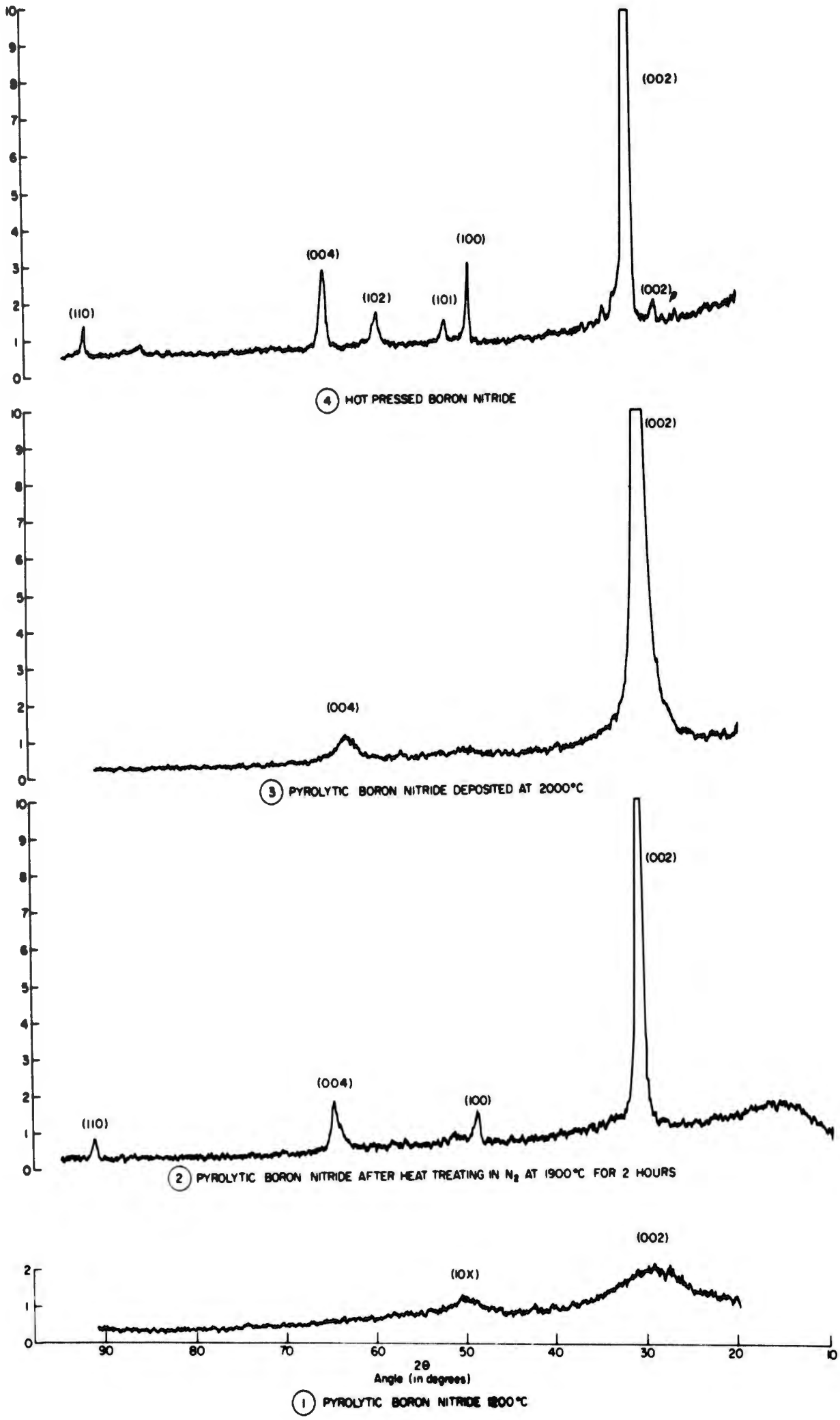
(110)
(004)
(102)
(101)
(100)
(002)
(002)
4 HOT PRESSED BORON NITRIDE
(004)
(002)
3 PYROLYTIC BORON NITRIDE DEPOSITED AT 2000°C
(110)
(004)
(100)
(002)
2 PYROLYTIC BORON NITRIDE AFTER HEAT TREATING IN N_2 AT 1900°C FOR 2 HOURS
(10X)
(002)
90
80
70
60
50
40
30
20
10
2θ
Angle (in degrees)
1 PYROLYTIC BORON NITRIDE @ 00°C

FIGURE 4

A

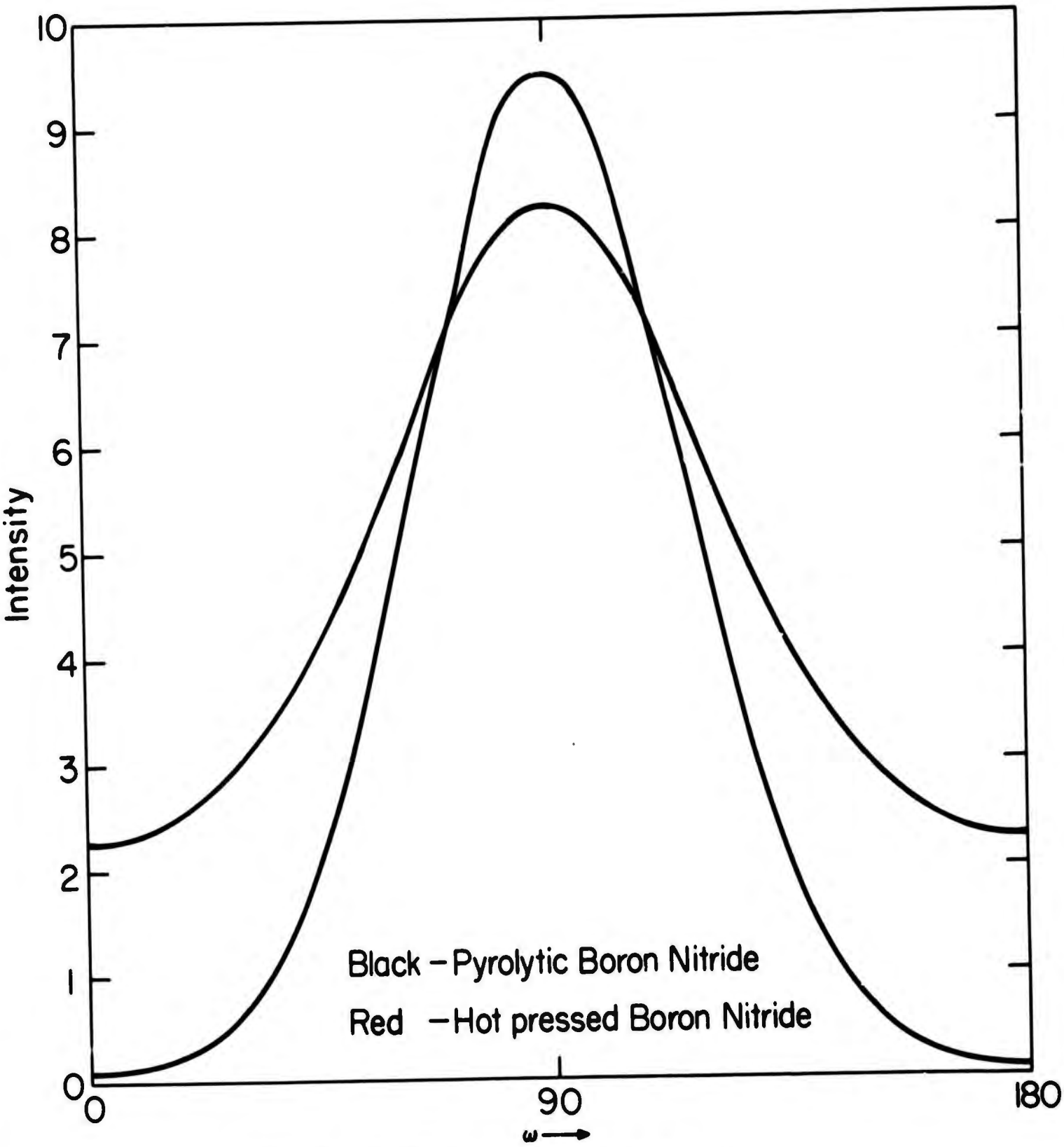

DEGREE OF PREFERRED ORIENTATION

FIGURE 5

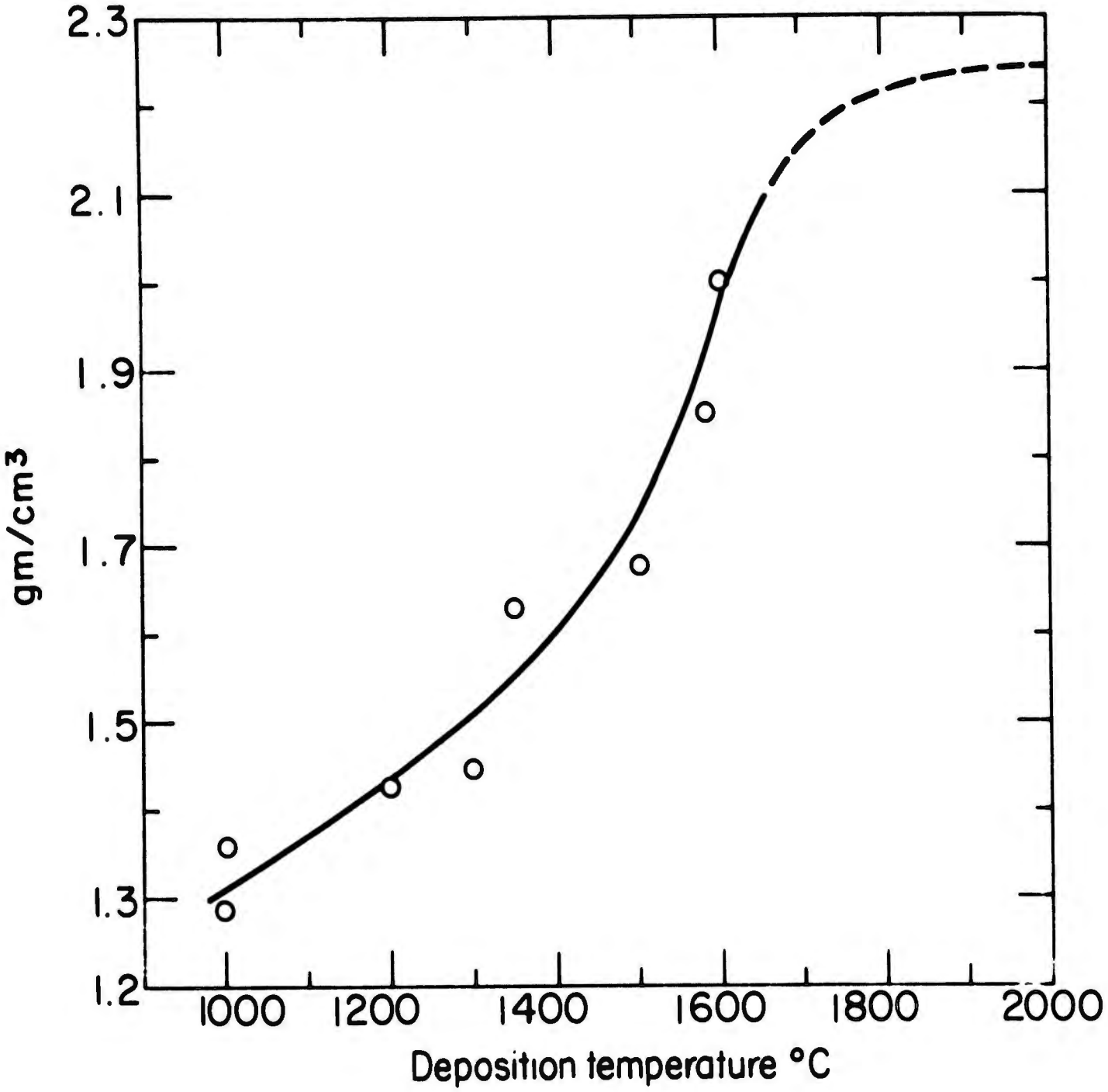

DENSITY OF PYROLYTIC BN
FIGURE 6

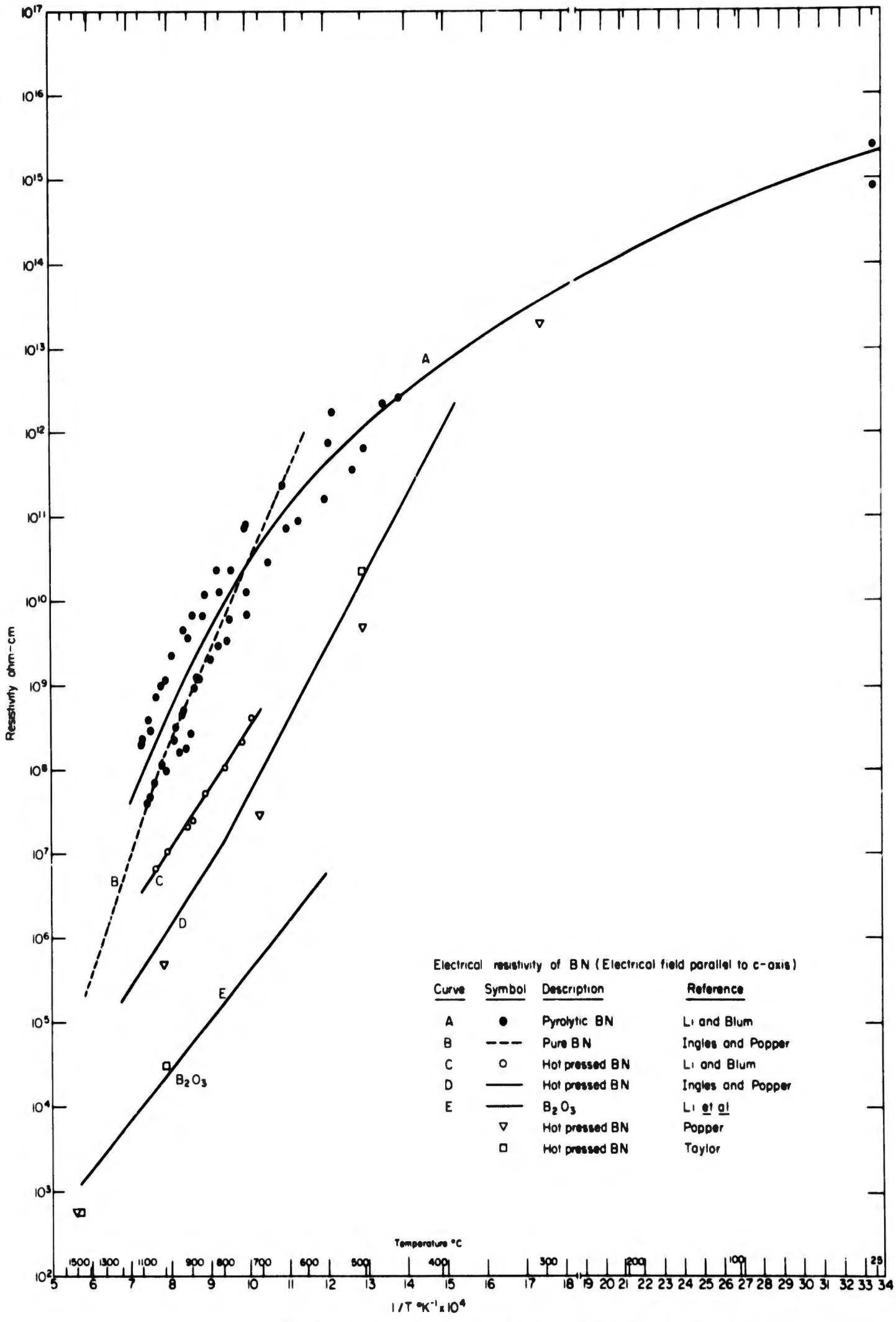

ELECTRICAL RESISTIVITY VS TEMPERATURE

FIGURE 7

A

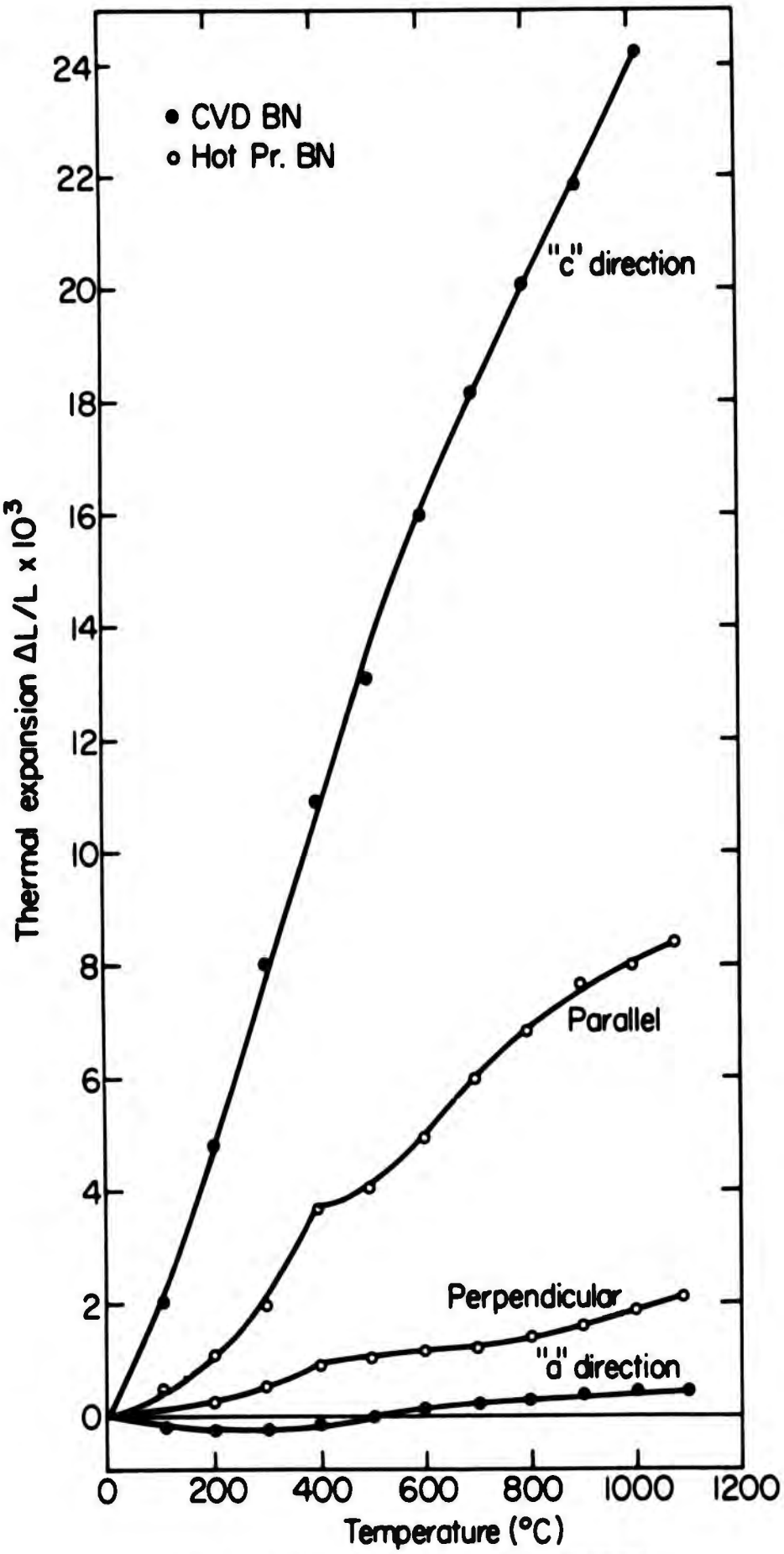

THERMAL EXPANSION OF BORON NITRIDE

FIGURE 8

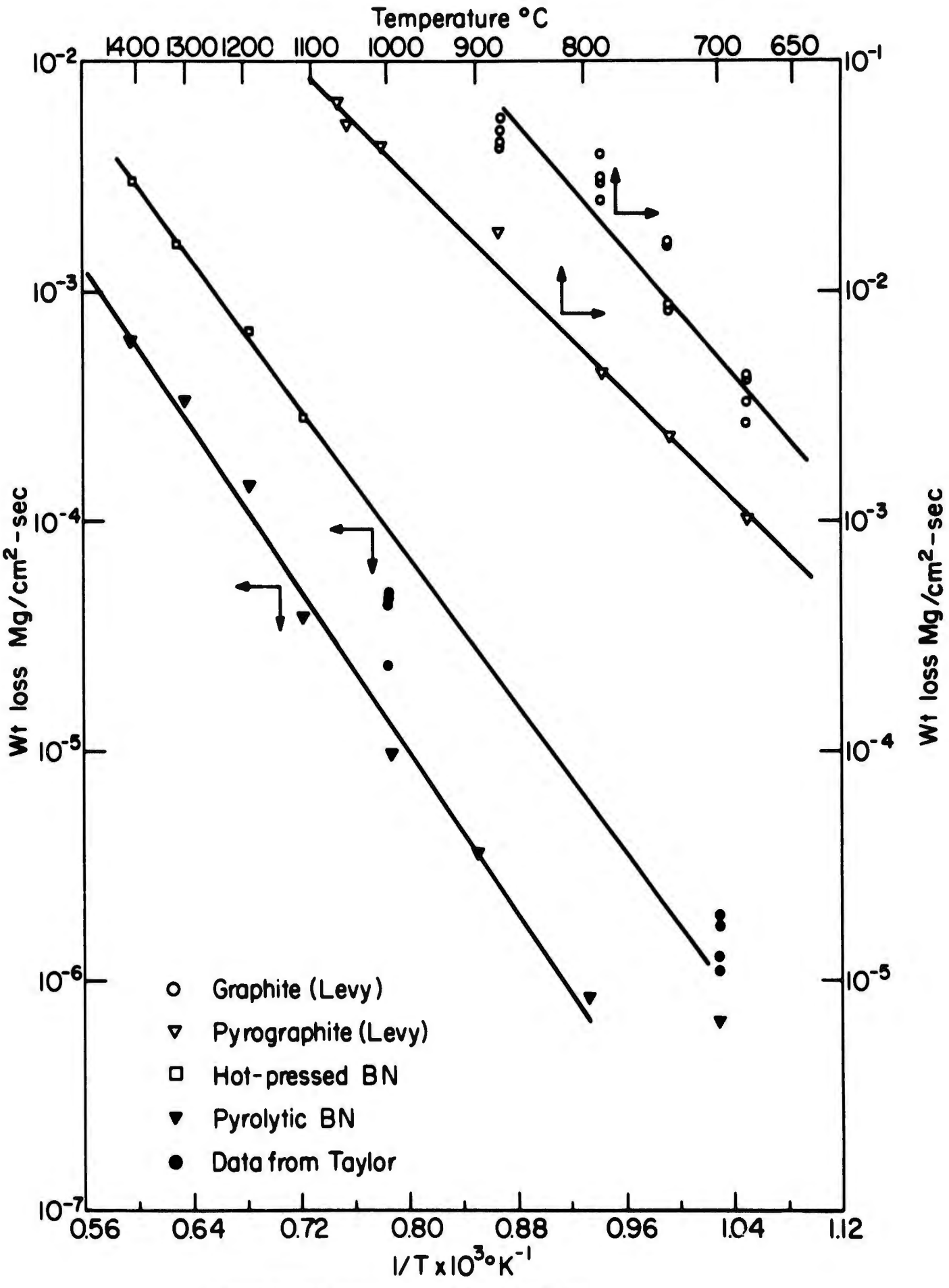

OXIDATION OF GRAPHITE AND BN
FIGURE 9

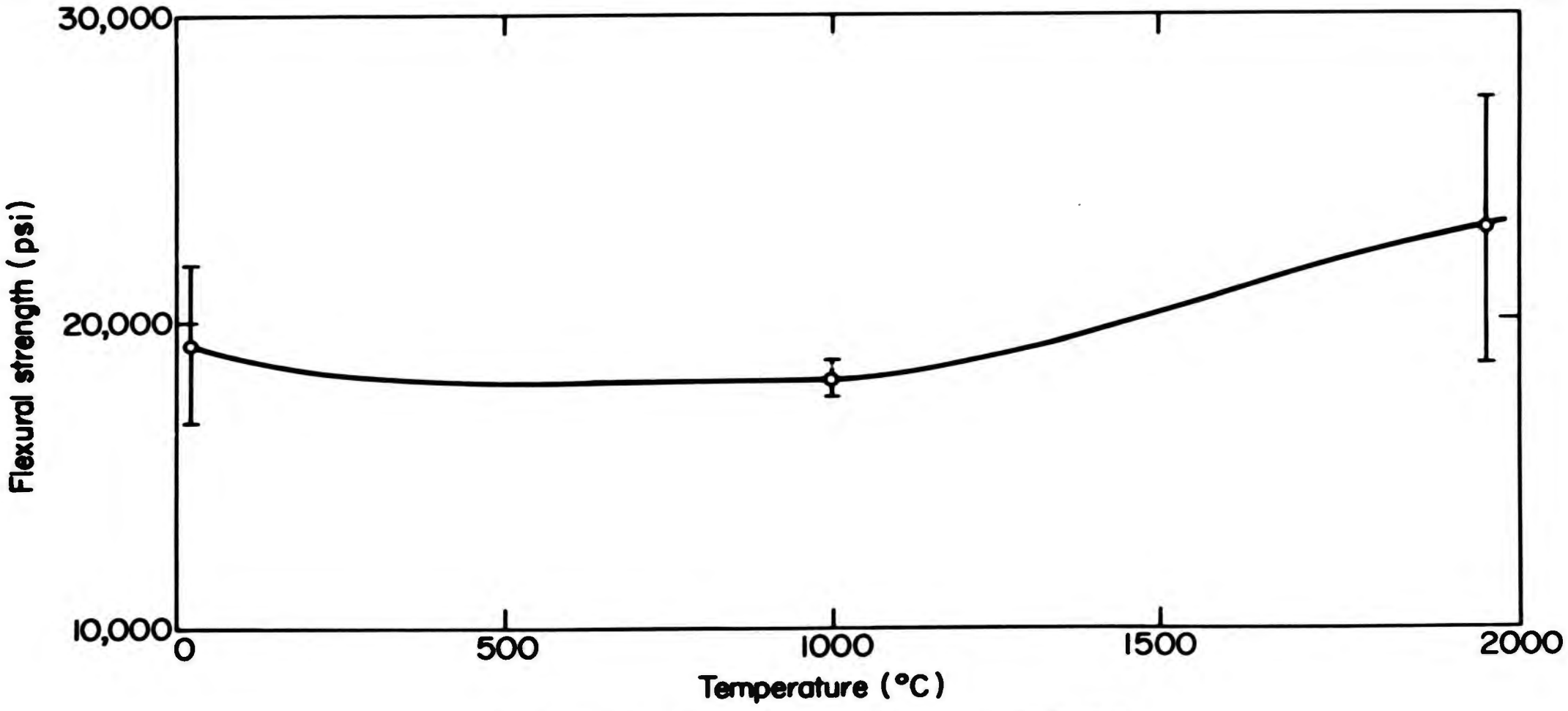

STRENGTH VS. TEMPERATURE OF CVD BN

FIGURE 10

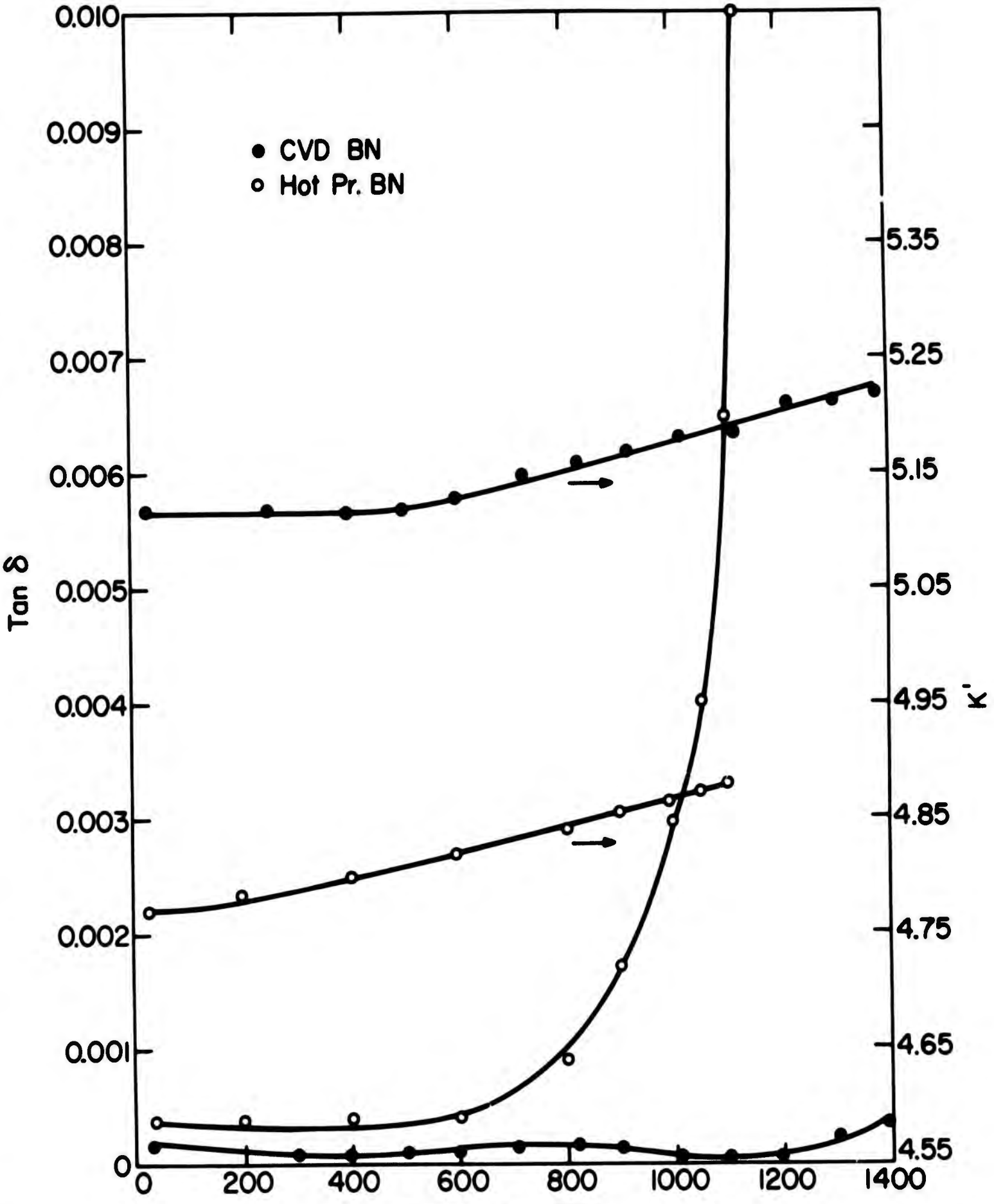

DIELECTRIC PROPERTIES OF BN

FIGURE 11

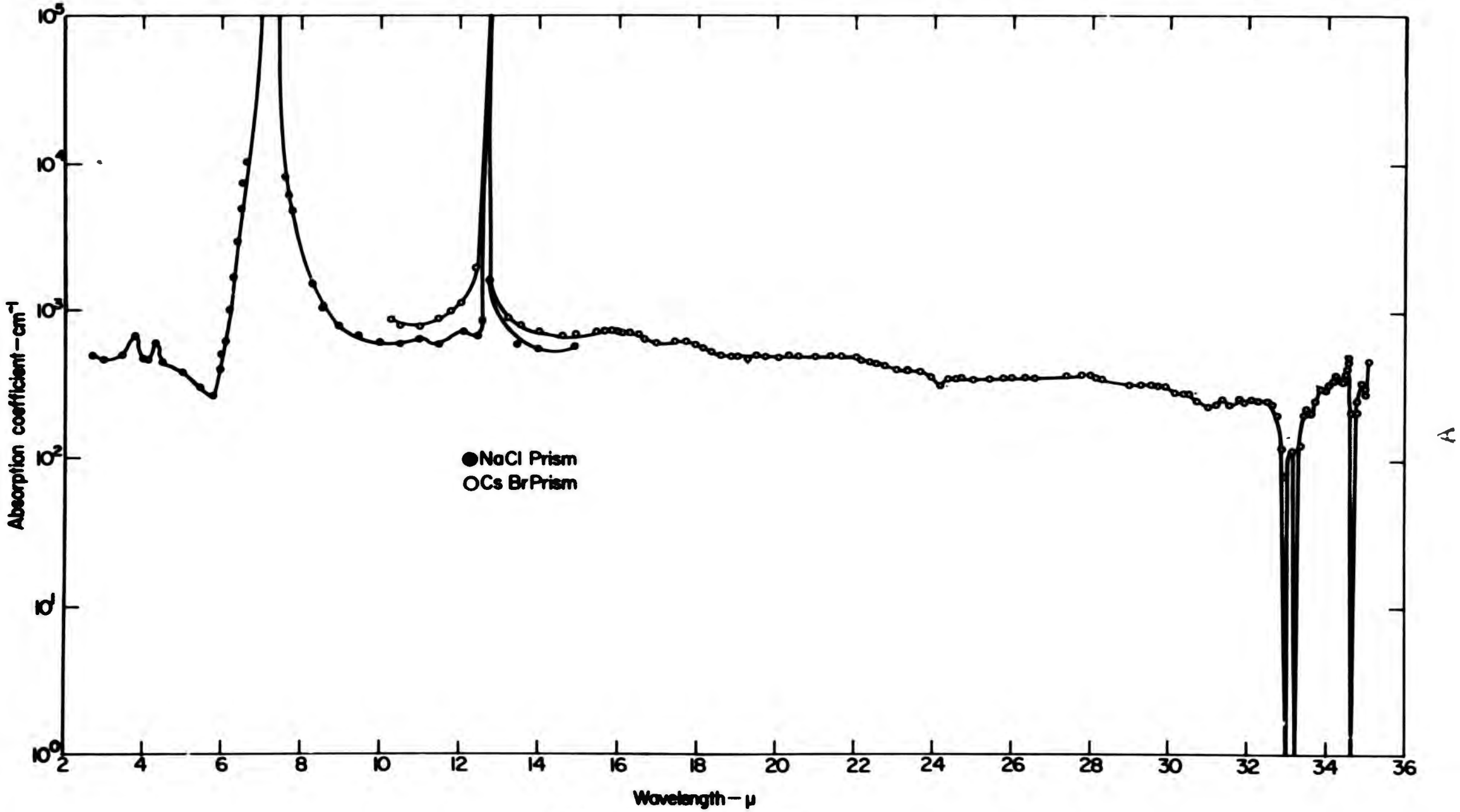

IR ABSORPTION OF CVD BN

FIGURE 12

SLOT CLOSURES FOR A 2500°F ANTENNA

by

W.H. Wheeler
P.M. Winslow
L.E. Gates

INTRODUCTION

Glide re-entry vehicles, upon reentering the earth's atmosphere, are subjected to surface temperatures up to several thousand degrees Fahrenheit. Although ablative plastics and refractory heat shields are satisfactory for protecting large portions of a vehicle, the antenna window system presents a more serious problem. Materials used for this purpose must pass an electromagnetic signal, and must not degrade at high temperatures. Under Air Force sponsorship, Hughes Aircraft Company undertook a small program to develop a materials system for a planar array antenna designed for operation under a typical glide re-entry pattern. Ultimately the antenna must be suitable for multiple re-entry missions. This requirement excluded considerations of ablative radome materials due to the inherent electrical degradation.

Because of a limited time schedule and uncertainties in the expected performances of materials, several approaches were studied simultaneously:

1. A refractory metal slot array with the slots individually closed and hermetically sealed with ceramic dielectric windows.

2. A refractory metal slot array with the slots closed mechanically but not hermetically with shrink fitted dielectrics.

3. A refractory metal slot array coated with a high temperature vitreous enamel that also fills and seals the slots.

4. A slot array fabricated of metallized ceramic waveguide elements.

5. Special high temperature composite metal-ceramic waveguide structures.

The selected test specimen configuration consisted of waveguide end plates each containing one slot in the center and oriented parallel to the "E" plane dimension of the waveguide.

MATERIALS SELECTION

Ceramics

Ceramic dielectrics capable of long term operation at 2500°F include alumina, beryllia, magnesia, spinel, mullite, zircon, fused silica, and several composite compositions. Materials deemed most applicable to this program were zircon and mullite, because of close thermal expansion matching with molybdenum, and alumina because of exceptional dielectric properties at elevated temperatures, and close thermal expansion matching with columbium.

Metals

The primary considerations in selection of the metallic material for the waveguides were: (1) high temperature capability, (2) coefficient of expansion matching that of the dielectric material, (3) density, (4) the ability to apply an oxidation resistant coating, (5) fabricability, (6) availability, and (7) cost. Electrical conductivity is important also, but the other requirements restricted the choice of materials to those that do not have exceptional electrical conductivity. The only materials that meet these requirements are refractory metals and alloys and certain precious metals. The former depend upon oxidation resistant coatings for high temperature service while the latter are oxidation resistant. Precious metals were not considered because of cost and availability.

Molybdenum or columbium were the preferred choices of the refractory metals. Molybdenum has a coefficient of expansion closely matching that of mullite and zircon, and molybdenum oxidation resistance coating technology is further advanced. Columbium has the advantage of better fabricability because of its ductility which is retained after heating to 2500°F. Because molybdenum stock was readily available, and because fabrication technology is similar for either system, molybdenum was chosen as the waveguide metal.

HERMETICALLY SEALED WINDOWS

Hot Pressing Studies

A laboratory induction heated hot pressing apparatus, Figure 1, was utilized for diffusion bonding ceramic powders into molybdenum waveguide endplates. Pressing studies were first conducted with the ceramic powders to establish optimum pressure, time, and temperature for preparation of strong, nonporous specimens with the lowest possible carbon contamination. Schedules for hot pressing were established as follows:

Material	Temperature, °C	Pressure, psi	Time, Minutes
Mullite	1600	4500	10
Zircon	1600	4000	10
	1600	3300	10

Studies were then undertaken between zircon and molybdenum and between mullite and molybdenum. Alumina was bonded to molybdenum using a thin platinum interlayer. After attainment of successful bonding to the metal, alumina was found to be poorly matched in thermal expansion with molybdenum. Specimens generally cracked upon removal from the press, or upon cool-down to room temperature. However, alumina fragments were well bonded to the metal. The use of 0.002 inch platinum foil was found very effective in obtaining reliable bonds between molybdenum and mullite. A high quality diffusion bond between mullite and molybdenum may be seen in Figure 2.

THERMAL CYCLING TESTS

A zircon window bonded directly to molybdenum with platinum at the interface, and two similarly bonded mullite windows were found to be helium leak tight before thermal cycling. After cycling the zircon window to 2690°F, helium leakage was excessive. The two mullite windows were cycled to 2720°F and to 2910°F before retesting for leakage. The former showed a slight leakage; the latter was helium leak tight.

Difficulty was experienced in pressure bonding of zircon to molybdenum due to the reactivity of zircon with carbon vapors from the graphite hot pressing die. This resulted in bonding between zircon and the graphite plungers with subsequent deterioration of the die. Work was therefore continued only with mullite windows where this problem was not encountered. The dielectric properties of mullite were also expected to be better than those of zircon at 2500°F. Hot pressed mullite windows are shown in Figure 3.

Oxidation Protective Coatings

The molybdenum parts were coated with molybdenum disilicide by a commercial process* to provide the required oxidation protection. The coatings were applied to a nominal thickness of 0.003 inch and were oxidized at 2000°F for 15 minutes. With the samples prepared, the edges of the molybdenum were extremely brittle and appeared to exfoliate. This was apparently due to diffusion of the disiliciding vapors into the lamellar structure of the molybdenum. By deburring and rounding off edges this problem was alleviated.

A bonded mullite window was subjected to dielectric transmission measurements before and after application of the molybdenum disilicide. This was done to determine if there was an interaction between the ceramic window and the coating process that might alter the transmission characteristics. A four db loss in transmission was noted, and is attributed to non-uniformities in the disilicide coating around the window, reactions between the ingredients used in the disilicide process and the mullite, and the change in electrical resistance of surfaces of the molybdenum after coating.

---

*Chromizing Corporation

SHRINK-FITTED WINDOWS

Ceramic discs of alumina, mullite, and zircon were procured for preparation of mechanically closed windows. The discs were 0.375 inch diameter by 0.050 inch thick. Molybdenum waveguide end plates were prepared from 0.050 inch sheet stock, and 0.375 inch holes were machined in their centers.

The end plates were heated to 800°F, providing a diametrical difference of about 0.001 inch. The cold ceramic discs were pressed into the hot end plates, and the metal shrank to the dimension of the ceramic. These end plates are shown in Figure 4. The use of this type of window would require pressurizing of the antenna, with constant replenishing of the pressurizing gas lost due to leakage. For some aircraft, this might not be objectionable.

ENAMELED WAVEGUIDE

A number of high temperature glass compositions previously developed by Hughes Aircraft Company for other purposes appeared promising for use as refractory dielectrics. Expansion coefficients of these materials were calculated, and three were selected for studies of their adherence to molybdenum. Compositions, fusion points, and calculated thermal expansion coefficients are given in Table 1.

TABLE 1

Compositions and Properties of High Temperature Enamels

Enamel No.	Constituents	Amount (%)	Fusion Temperature (°C)	Calculated Thermal Expansion (in/in -°C)
R45	SiO_2	36.0	1475	6.40×10^{-6}
	Al_2O_3	48.0		
	MgO	16.0		
R74	SiO_2	50.0	1450	5.18×10^{-6}
	Al_2O_3	22.5		
	MgO	7.5		
	ZrO_2	20.0		
R99	SiO_2	50.0	1580	4.99×10^{-6}
	Al_2O_3	27.0		
	MgO	3.0		
	ZrO_2	20.0		

Rods were prepared from the glass compositions and fritted using an induction heated apparatus. The frits were ground into fine powder for sprinkling or prepared as slip for dipping and applied to molybdenum test strips. Heating was accomplished using a laboratory resistance heated vacuum furnace. Because of the vacuum and the high temperatures involved it was generally difficult to achieve enamel maturity without boil-off or bubble formation. In general, the expansion match was satisfactory, and subsequent heating in a helium atmosphere yielded uniform coatings without pinholes.

Enameled specimens were re-heated in air to 2500°F for one minute. The molybdenum appeared to be well protected from oxidation by the three enamels, but it was found that enamel number R-74 was soft at 2500°F, resulting in its elimination. Compositions R-45 and R-99 were hard at this temperature. Sections of enameled molybdenum before and after exposing to 2500°F in air are shown in Figure 5. A scratch made at 2500°F with a quartz rod appears in the R-74 enamel.

CERAMIC WAVEGUIDES

Methods for forming ceramic waveguides with precision internal dimensions were studied. The intent was to metalize the interior of the waveguide except at the slot location, thus providing a refractory antenna element capable of operation at 2500°F.

Initial attempts were made to fabricate ceramic waveguide using wax mandrels. Dip coating the mandrels with alumina slip was found to be unsuitable due to excessive shrinkage cracking.

A special alumina spraying slip was prepared with an organic binder and an alcohol vehicle. This material was sprayed onto a heavily waxed, precision machined mandrel. As the particles traveled from the spray gun to the mandrel, the alcohol evaporated so that the particles stuck tightly and built up a thick layer with no drying shrinkage. The formed waveguide section was easily removed from the mandrel by gently warming and melting the wax. The piece was fired and is shown in Figure 6. The internal geometry was maintained precisely. The process is very promising for fabricating ceramic waveguides with the required internal tolerances. Additional experiments show that with appropriate tooling,flanges may be fabricated as an integral part of a waveguide section.

SPECIAL COMPOSITES

Means of bonding dielectric windows to refractory metal waveguide elements were briefly considered. The conventional silicate and phosphate cements were found with a few experiments to provide insufficient adherence to molybdenum at 2500°F to warrant further studies. The aforementioned high temperature enamels were evaluated as adhesives and were found to provide excellent adherence, but appeared to offer no advantage over direct diffusion bonds. Mullite and zircon specimens that were successfully bonded to molybdenum with a refractory enamel are shown in Figure 7.

WAVEGUIDE TEST SPECIMENS

Waveguide Fabrication

To facilitate more accurate electrical transmission tests, two molybdenum waveguide assemblies were fabricated from .040" sheet. Steps .015" deep were machined in the edges of the sheets so that they were self-jigging to form the rectangular box configuration of the waveguide. Electron beam welds were made on the four edges. End plates containing hot pressed ceramic windows were machined with a step around the perimeter so that they were self-locating in the ends of the waveguides. An end plate was then electron beam welded to each waveguide. A characteristic of electron beam welds is a high depth-to-width ratio of the weld with consequent low heat input and relatively low distortion. The minor distortion that occurred in these parts was removed by creep forming the waveguides between steel plate jigs in a hydrogen atmosphere furnace at 2000°F for 1 hour. After this treatment, the dimensions conformed to those specified in Figure 8. Figure 9 shows one of the waveguide assemblies after welding.

Oxidation Protection

A molybdenum disilicide diffusion coating was applied to the external surfaces of one of the waveguides. Some discoloration of the mullite window occurred during the disiliciding process. This turned out to be a shallow surface reaction, and it was removed by selective abrasive cleaning. In the hot pressing operation, the platinum apparently was extruded around the edge of the window. There appeared to be a reaction between this platinum and the silicon fluoride used in the coating process. The interior of the waveguide was filled with inert material to prevent the coating of the inside surfaces. The purpose of leaving the interior bare was to achieve the best electrical conductivity along the inner surface. Molybdenum is reported to have a resistance of 35 micro-ohm-cm at 2500°F and molybdenum disilicide has reported resistivity values ranging from 80 to 300 micro-ohm-cm at 2500°F. This antenna fabrication concept requires that the waveguides be pressurized with dry inert gas to prevent oxidation of the internal surfaces.

Microwave Transmission Tests on Waveguide Assemblies

Prior to disiliciding, two of the waveguide assemblies were subjected to microwave transmission tests. The results are shown in Table 2 for signals radiated into a matched load, Case 1, and into free space, Case 2. Some of the insertion loss may be attributed to the lower electrical conductivity of the molybdenum waveguide surface, but this was not determined quantitatively.

SUMMARY AND CONCLUSIONS

Technology has been established for several methods of closing and sealing slots in high temperature planar array antennas. The most promising system incorporated mullite windows hot pressed into molybdenum waveguide end plates. The diffusion bond developed in this system was enhanced with the use of a thin platinum foil interlayer. A window of this type was found to be

helium leak tight after thermal cycling to 2910°F. The system alumina-columbium should yield similar results.

Fabrication of molybdenum waveguides to specified dimensional requirements by electron beam welding was demonstrated. Electron beam welding was also found to be suitable for welding an end plate containing a ceramic window to waveguide tubing. The molybdenum waveguide containing a mullite window was readily coated with molybdenum disilicide without serious electrical degradation of the window.

Molybdenum can be successfully coated with a high temperature porcelain enamel for oxidation protection and sealing. The enamel can also be used to provide adherence between molybdenum and mullite or zircon windows.

Ceramic waveguide fabrication to close internal dimensional tolerances appears feasible.

TABLE 2

Microwave Transmission Tests on Waveguide Assemblies

	Specimen Number	
	1	2
Case 1, signal radiated into a matched load		
Resonant frequency-minimum VSWR	9.120 gc	9.028 gc
VSWR	1.235	1.165
Insertion loss	0.35 db	0.45 db
Case 2, signal radiated into free space		
Resonant frequency-minimum VSWR	8.950	8.876
VSWR	1.085	1.130

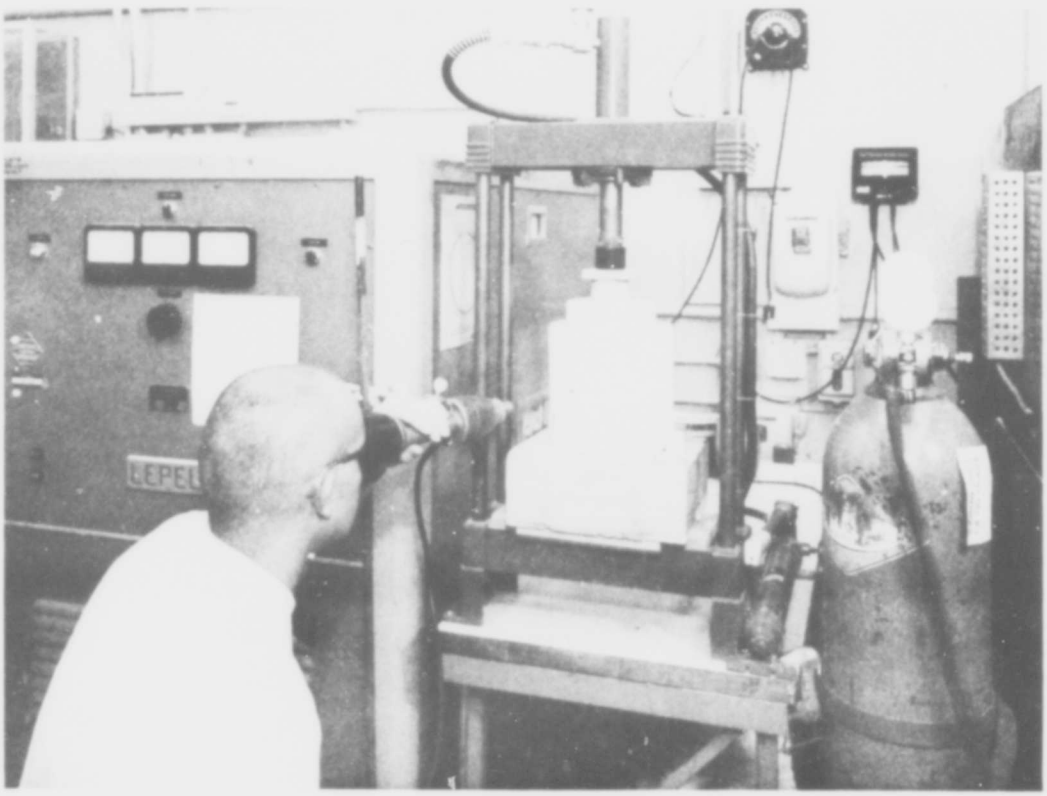

Figure 1. Laboratory hot press facility.

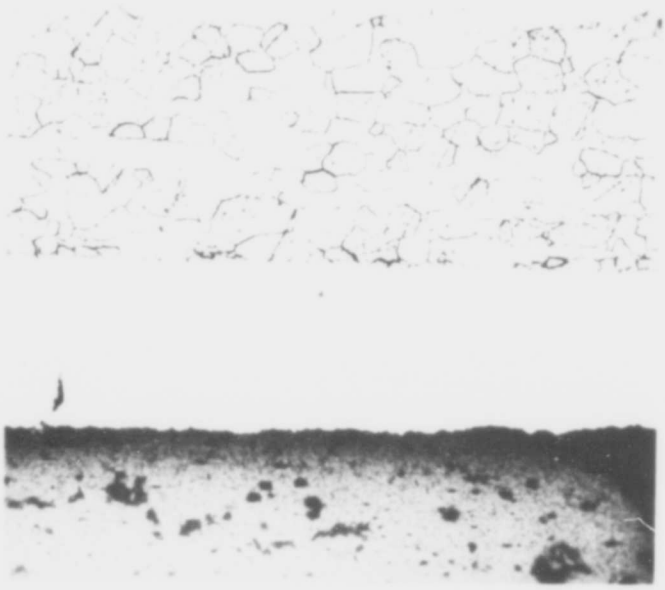

Figure 2. Mullite to molybdenum bond with platinum interface, 200x magnification. Neg. No. 00888.

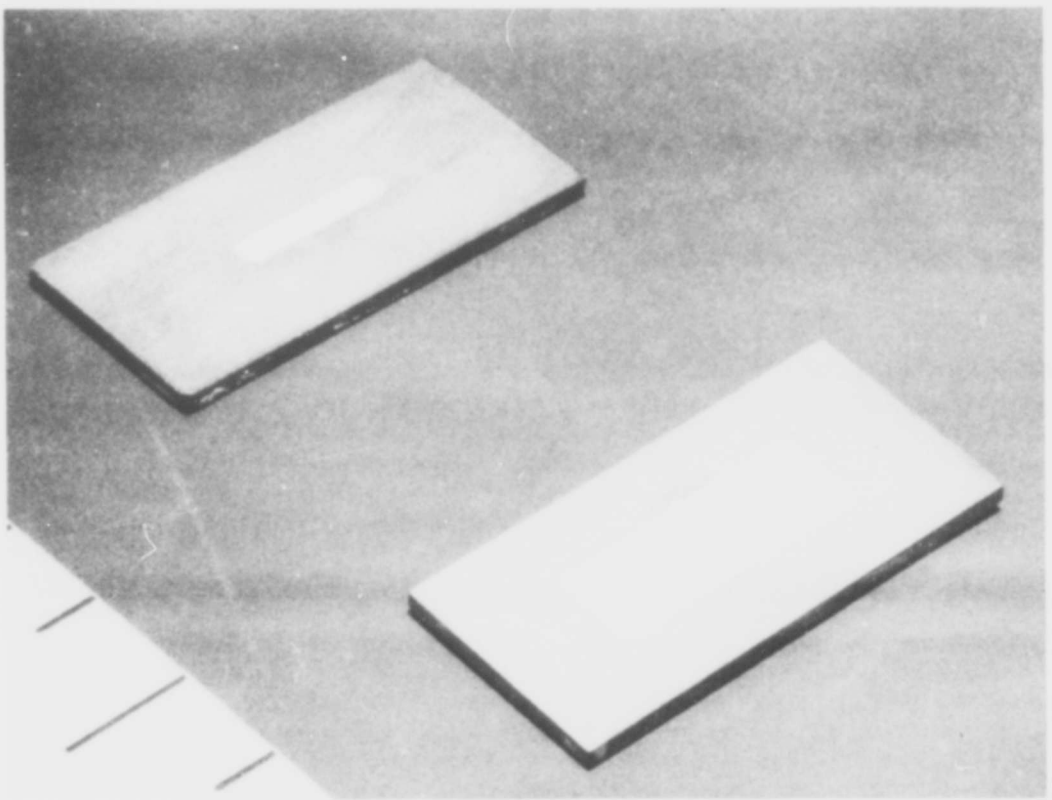

Figure 3. Hot pressed mullite windows in molybdenum end plates.

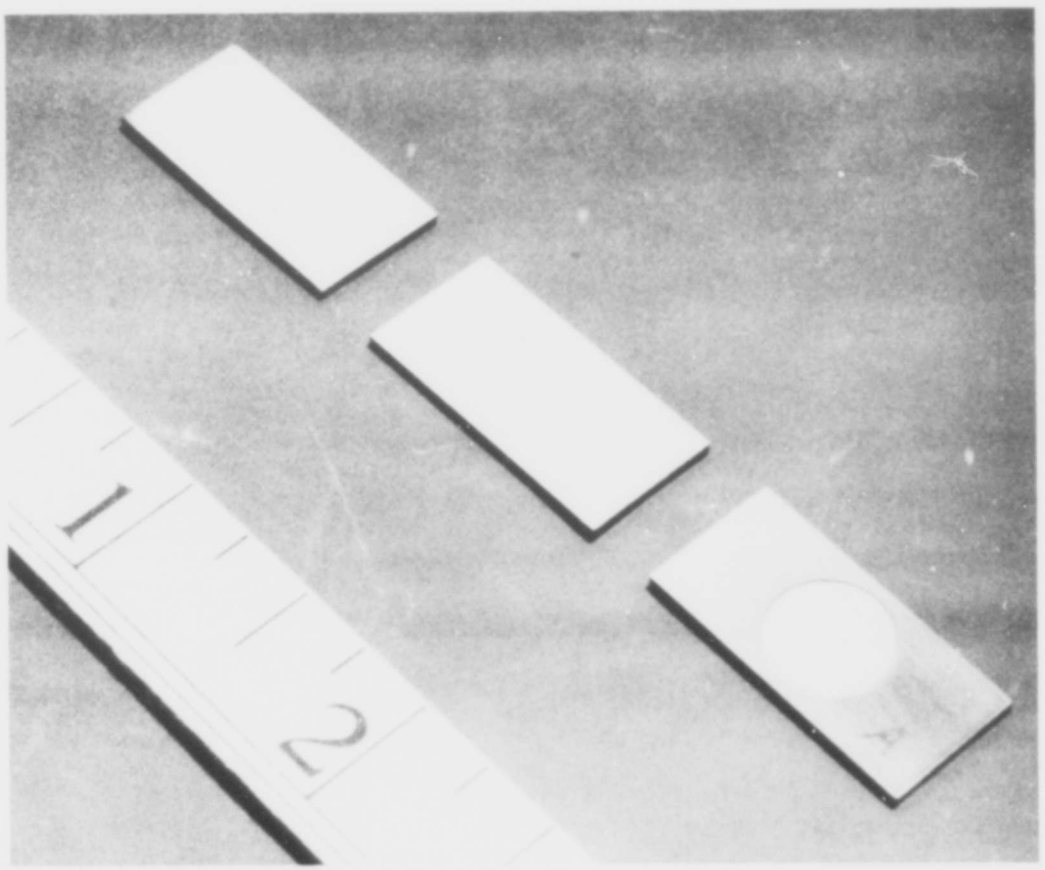

Figure 4. Mullite, zircon, and alumina windows shrink fitted in molybdenum end plates.

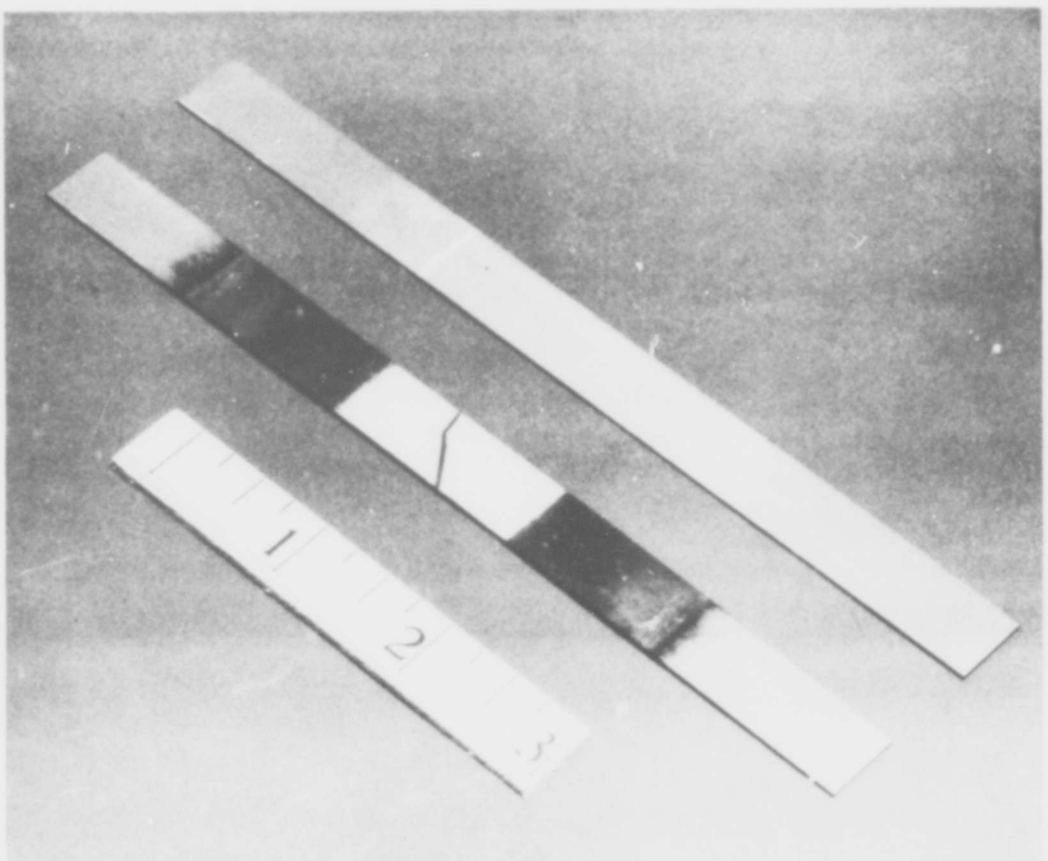

Figure 5. Glazed molybdenum sections before and after exposure to 2500°F in air.

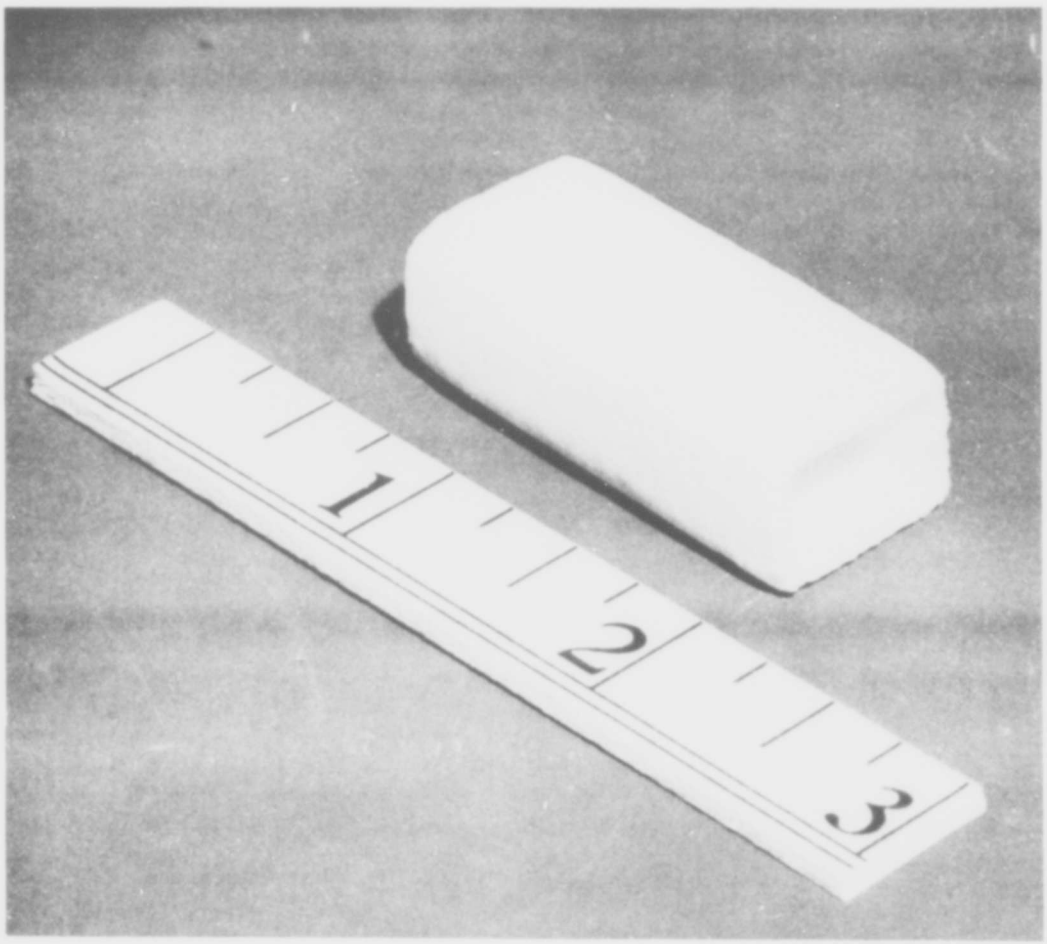

Figure 6. Alumina waveguide section.

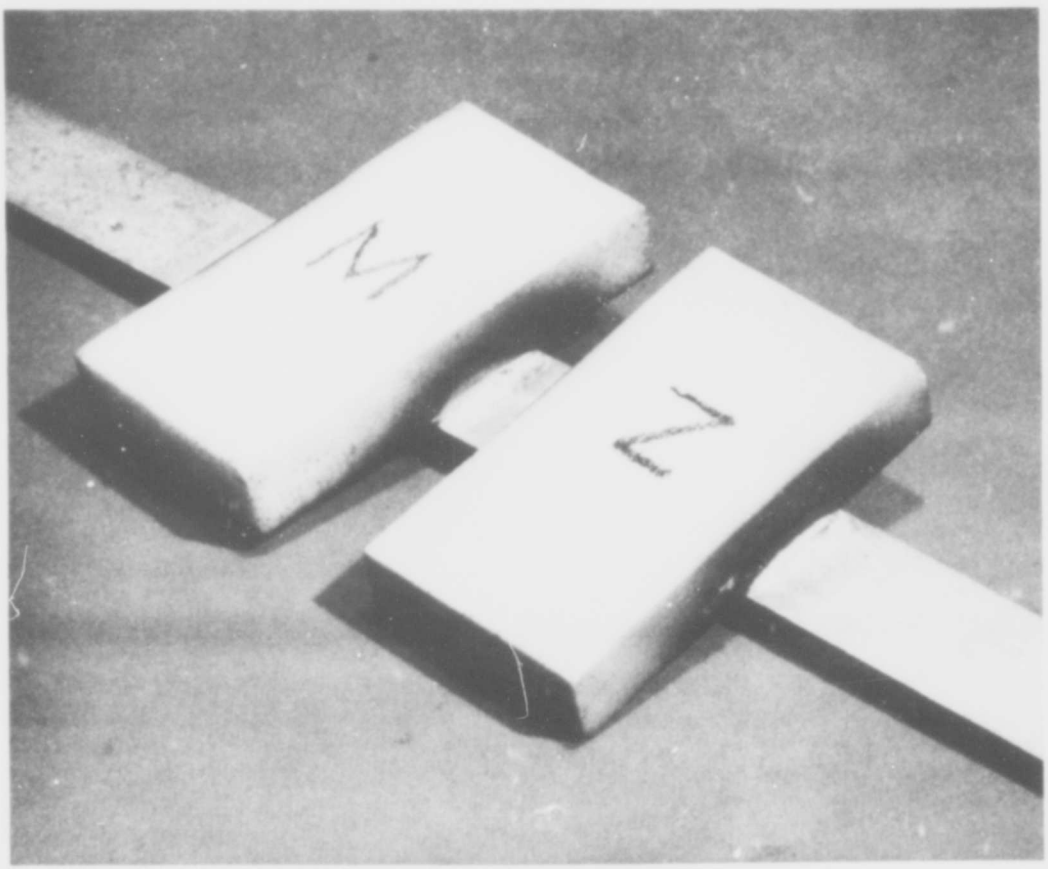

Figure 7. Mullite and zircon windows attached to molybdenum strip with glass adhesive.

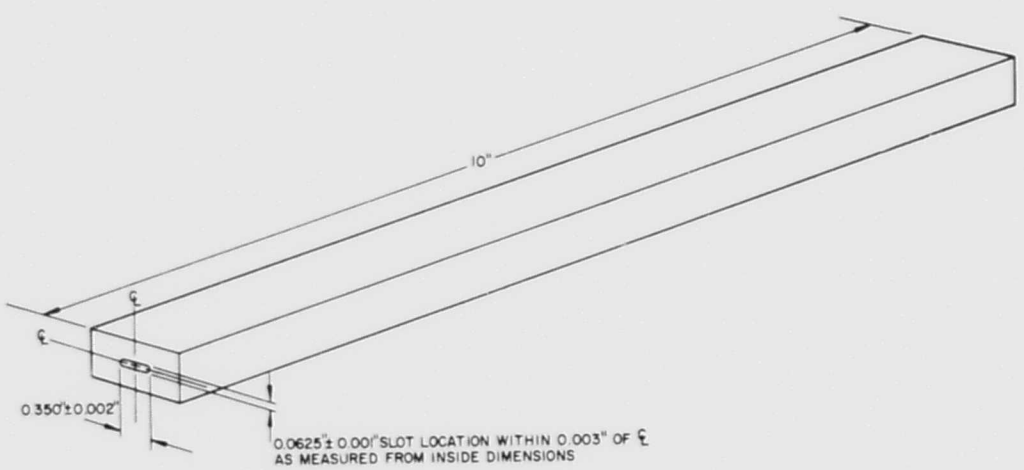

GENERAL NOTES:

1. WAVEGUIDE I.D., 0.400"x 0.900"±0.003"
2. WAVEGUIDE WALL THICKNESS, 0.040"±0.003"
3. MAXIMUM AXIAL CAMBER, ±0.003" OVER ENTIRE LENGTH
4. 1/32" MAXIMUM RADIUS ON ALL INSIDE CORNERS
5. INSIDE SURFACE FINISH 32 rms

Figure 8. High temperature waveguide test section material: electron beam welded molybdenum.

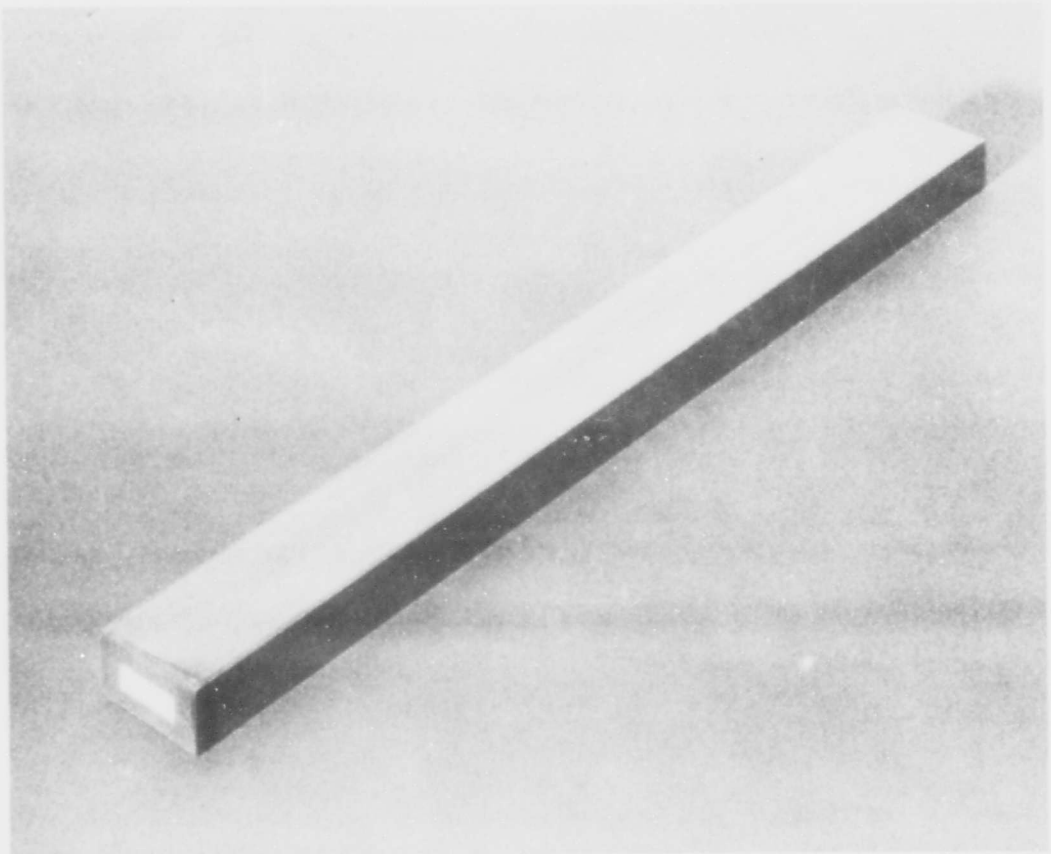

Figure 9. Electron beam welded molybdenum waveguide with mullite window.

SESSION II

THE MEASURED ELECTRICAL CHARACTERISTICS OF SEVERAL ABLATIVE AND SOME NON-ABLATIVE HIGH TEMPERATURE RADOME MATERIALS

By

T. Larry Norin
The Boeing Company
Aero-Space Division
Seattle, Washington

INTRODUCTION

The problem of aerodynamic heating of ballistic nose cones and other re-entry vehicles is one of extreme importance and must be given considerable attention in the design of radomes or antenna windows for hypersonic vehicles. Depending on the specific mission of a given hypersonic vehicle, it may encounter peak heating rates as high as 6,000 BTU/FT^2/SEC. A typical ballistic missile nose cone may encounter peak stagnation point heat flux as high as 2500 BTU/FT^2/SEC with a total exposure time of 1 to 1.5 minutes. For vehicles on a more gradual re-entry path, the peak heating rate may be only 100 BTU/FT^2/SEC; but a typical exposure time may be as much as 5 to 10 minutes. Needless to say, the large heat fluxes produced by aerodynamic heating of the re-entry vehicle are quite detrimental if allowed to transfer their thermal energy to an antenna or associated systems. The ablative radome then, is a possible solution to the problem of thermal protection in addition to electrical transparency, structural and aerodynamic requirements.

This paper presents the results of X-band electrical tests as performed on six ablative materials. The purpose of this work was the evaluation of electrical performance at temperatures from ambient through ablation temperatures including measurements made during the ablation process. This data, combined with structural and thermal considerations, can aid the antenna window designer in choosing a material that will most nearly satisfy all the requirements of an antenna window for a given hypersonic vehicle.

THE ABLATION PROCESS

Ablation is a self-cooling, mass transfer process which is initiated when a sufficient quantity of heat is absorbed by a material surface to cause varying amounts of melting, vaporization, sublimation and depolymerization in which gaseous and solid products are formed. The solid products normally take the form of a heated residue which is injected into the hypersonic boundary layer in the case of a re-entry vehicle.

A very desirable characteristic of ablation as a cooling method is the self-contained features of the process. Other cooling methods require extra weight and volume. Such methods as heat sinks, heat shields, insulation, and circulation of coolants are considerably more complex. Another outstanding feature of the ablation cooling method is a compensating increase in the ablation rate to give additional thermal protection as the material

heat input increases. Ablation cooling is very effective for extremely high heating rates of relatively short duration. Therefore, an ablative material radome provides a relatively simple but very reliable means of protecting an antenna from extremely high heating rates.

For the general case, a radome material undergoing ablation will include a layer of material in the molten state nearest the heat source which may eventually take the form of a char or other residue. This layer is followed by a region which is undergoing heating and will decompose and become molten if the heating process continues. An unheated or virgin portion of the radome material is the final region of the "thermal model" before reaching the antenna or other structure being protected. Eventually all the protective material would ablate and be injected into the boundary layer if sufficient heat were applied.

As a radome material ablates, the electrical thickness changes. The material becomes considerably more lossy and the electrical performance is degraded. When considering the use of an ablative radome material, one must consider such factors as the maximum allowable degradation in electrical performance and the amount of thermal protection needed. These fundamental requirements must be considered before, during, and after the ablation process occurs since the radome configuration is continually changing. If the change in an ablative radome's electrical properties is prohibitively detrimental to the performance of a system, the only alternative is to use a thermally stable non-ablative material and provide some other means of meeting the thermal protection requirement.

ABLATIVE MATERIALS CONSIDERED

Due to the mechanism of ablation, ablative materials generally fall into one of the following categories:

REINFORCED PLASTICS - various plastic resins reinforced with either organic or inorganic fibers to form a composite material. A carbonaceous char layer forms during ablation.

PURE THERMOPLASTICS - ablation differs from most reinforced plastics by lack of carbonaceous char formation after the material sublimes.

GRAPHITES - characterized by combustion only at the material surface and a relatively low ablation rate. The combustion of a graphite causes a net reduction of the heat transfer through the material. Graphites are not generally of interest for electromagnetic window applications due to their poor electrical properties.

OXIDES - oxide ceramics such as alumina, beryllia, and magnesia which have excellent electrical properties, are poor ablators since they are chemically and physically stable at extremely high temperatures. These temperatures are too high to permit the use of these materials for thermal protection of many systems. High temperature systems using oxide materials may require some other method of thermal protection.

Most ablation materials with radome applications fall into the reinforced plastics group.

Table I is a description of six ablative materials (cork, phenolic nylon, Teflon, Duroid, Thermolag, and Avcoat) which were evaluated. All these materials except Teflon are in the reinforced plastics category. Teflon is a thermoplastic.

X-BAND HIGH TEMPERATURE TRANSMISSION GAUGE

A high temperature transmission gauge (Figures 1 and 2) was used to measure the power transmission characteristics of the test materials. Temperature and attenuation measurements were made as heat was applied and surface temperature increased, and were continued as the material underwent ablation.

Basically the transmission gauge consists of a large water cooled steel chamber with the inside lined by a silicon carbide refractory microwave absorber. A 12 x 12 inch test panel of the material under investigation is heated by a radiant heat source consisting of 37 1500 watt quartz glass lamps in a configuration 16 inches wide and 18 1/2 inches high. The maximum heat radiated from this source is on the order of 20 to 25 $BTU/FT^2/SEC$. The test panel is located 9 inches from the lamp reflector. The test panel surface temperature is monitored by thermocouples located at various points on the heated side of the panel from which a mean surface temperature is obtained. The power transmission through the test panel is monitored by a pair of platinum-coated ceramic, conical horn antennas. The horn antennas are parallel polarized and the angle of incidence at the material surface is 60 degrees; approximately Brewster's angle for the materials tested. Using this configuration, reflections are minimized and the losses encountered are due primarily to the absorption properties of the test material.

MEASURED ATTENUATION

By comparative measurements with and without the test panel in place, the power attenuation as a function of sample surface temperature and exposure time was measured using a minimum of three samples of each ablation material. Data presented in Figures 3 through 5 are typical of the test results. Photographs of the materials before and after ablation are shown in Figures 6 through 11. In these photographs it is noted that the residue remains on the material surface. During a typical hypersonic re-entry, most of the residue would be injected into the boundary layer.

When observing these test results, one notes the range of maximum surface temperatures which were achieved for the various materials. The materials which achieved relatively low maximum surface temperatures are superior from a thermal protection standpoint. However, time in a given environment is very important when considering both the thermal protection and the maximum power attenuation which might be encountered during a given flight profile. The data presented here may be considered worst case data for most re-entry environments since the lossy residue remained on the material surface. The total heat quantity applied was comparable to that which would be encountered by an electromagnetic window in a relatively severe hypersonic re-entry environment.

ABLATIVE MATERIALS TESTED

MATERIAL	THICKNESS	DENSITY	DESCRIPTION	MANUFACTURER
CORK (ARMSTRONG 2755)	.50 IN.	32.78 LBS/FT^3 0.525 GM/CM^3	NATURAL CORK GRANULES WITH RESORCINOL BINDER	ARMSTRONG CORK COMPANY LANCASTER, PA.
PHENOLIC NYLON (TAYLORON P/N)	.50 IN.	73.54 LBS/FT^3 1.178 GM/CM^3	PHENOL FORMALDEHYDE RESIN REINFORCED WITH NYLON (6-6 POLYIMIDE) FABRIC	THE TAYLOR FIBRE COMPANY SAN CARLOS, CALIFORNIA
TEFLON (TFE)	.50 IN.	128.61 LBS/FT^3 2.06 GM/CM^3	POLYTETRAFLUOROETHYLENE	E. I. DUPONT DE NEMOURS & COMPANY, WILMINGTON, DELEWARE
DUROID (ROGERS 5650)	.30 IN.	138.97 LBS/FT^3 2.226 GM/CM^3	TEFLON REINFORCED WITH CERAMIC FIBERS	ROGERS CORPORATION ROGERS, CONNECTICUT
THERMOLAG (T-500 EX 167)	.25 IN.	79.72 LBS/FT^3 1.277 GM/CM^3	PROPRIETARY ITEM WITH THE MANUFACTURER	THE EMERSON ELECTRIC MANUFACTURING COMPANY, ST. LOUIS, MISSOURI
AVCOAT (TYPE II)	.50 IN.	65.61 LBS/FT^3 1.051 GM/CM^3	EPOXY-POLYAMIDE RESIN MODIFIED WITH PHENOL, GLYCINE, PRECIPITATED SILICA AND COLOR TONER	AVCO CORPORATION CINCINNATI, OHIO

TABLE I

MEASURED X-BAND DIELECTRIC PROPERTIES

In addition to the attenuation measurements described above, which are of a composite nature, it is desirable to determine in detail the dielectric properties of the materials at elevated temperatures. Knowledge of the dielectric properties of an ablative material, at temperatures below the ablation point, allows one to calculate electrical performance before ablation occurs and aids in determining the electrical effects of heating throughout the material.

A resonant cavity dielectrometer was utilized to measure the dielectric constant and loss tangent of the ablative materials and several non-ablative organic materials of current interest.

ABLATIVE MATERIALS

Dielectric properties of the ablative materials were measured at stabilized temperatures from ambient to the point where the material under test began to smoke and decompose. Tests were not conducted at higher temperatures due to the inhomogeneity of the materials as the surface ablates and to prevent clogging the precision resonant cavity dielectrometer with residue. The dielectric constant and loss tangent data are plotted in Figures 12 and 13 respectively.

SOME NON-ABLATIVE HIGH TEMPERATURE ORGANIC MATERIALS

Some recent measurements have been made of the dielectric properties of several high temperature organic materials with applications related mainly to supersonic aircraft environments and to some missile radome applications. These materials, to be more precise, might be called "poor ablators" rather than "non-ablators" since they may ablate to some extent.

Materials measured were DuPont SP polyimide resin, laminates of PI-2101 polyimide and "E" glass, DC-7141 silicone and "E" glass, and silicone with asbestos reinforcement. The dielectric constant and loss tangent data are plotted in Figures 14 and 15 respectively. Data was taken at 100 degree temperature increments with at least a 10 minute exposure time at each temperature.

The polyimide resin was supplied by DuPont and the silicone-asbestos laminate by Raybestos-Manhattan. The silicone and polyimide laminates with "E" glass reinforcement were fabricated at Boeing.

SUMMARY

Table II is a summary of the pertinent ablative material electrical properties as measured. The representative maximum attenuation values as tabulated were obtained by averaging the absorption losses for each of three material samples after a 7 minute exposure time in the high temperature transmission gauge.

From an electrical performance standpoint, the non-charring Teflon is considerably superior to the char-forming materials. However Teflon without reinforcement is dimensionally unstable when heated. The reinforced plastics are more desirable from both the structural and thermal protection standpoints. Therefore a compromise must be made in choosing an ablative material to meet the thermal, structural, and electrical requirements of the radome in the selection of a satisfactory material.

MATERIAL	ROOM TEMPERATURE DIELECTRIC PROPERTIES DIELECTRIC CONSTANT	LOSS TANGENT	REPRESENTATIVE MAXIMUM ABSORPTION LOSS
Teflon	2.05	.00013	0.6 db
Duroid	2.78	.0039	1.2 db
Avcoat	2.78	.0195	4.0 db
Thermolag	4.26	.0180	6.8 db
Phenolic Nylon	3.35	.035	7.3 db
Cork	1.91	.042	15.0 db

TABLE II

The polyimide and silicone laminates will not withstand the extreme heating rates that the other ablative materials will take, and therefore do not generally find application as electromagnetic windows for re-entry vehicles. However, these materials do show promise for large radomes of the supersonic (mach 3) aircraft variety where long-term radome temperatures may be as high as 600 to 700°F. The silicone-asbestos laminate is quite lossy at elevated temperatures and does not appear as desirable from an electrical standpoint as the "E" glass laminates. The maximum long-term temperature capability of the "E" glass reinforced polyimide and silicone laminates is primarily a function of the structural stability of the material since the dielectric properties do not change significantly at temperatures up to 700°F.

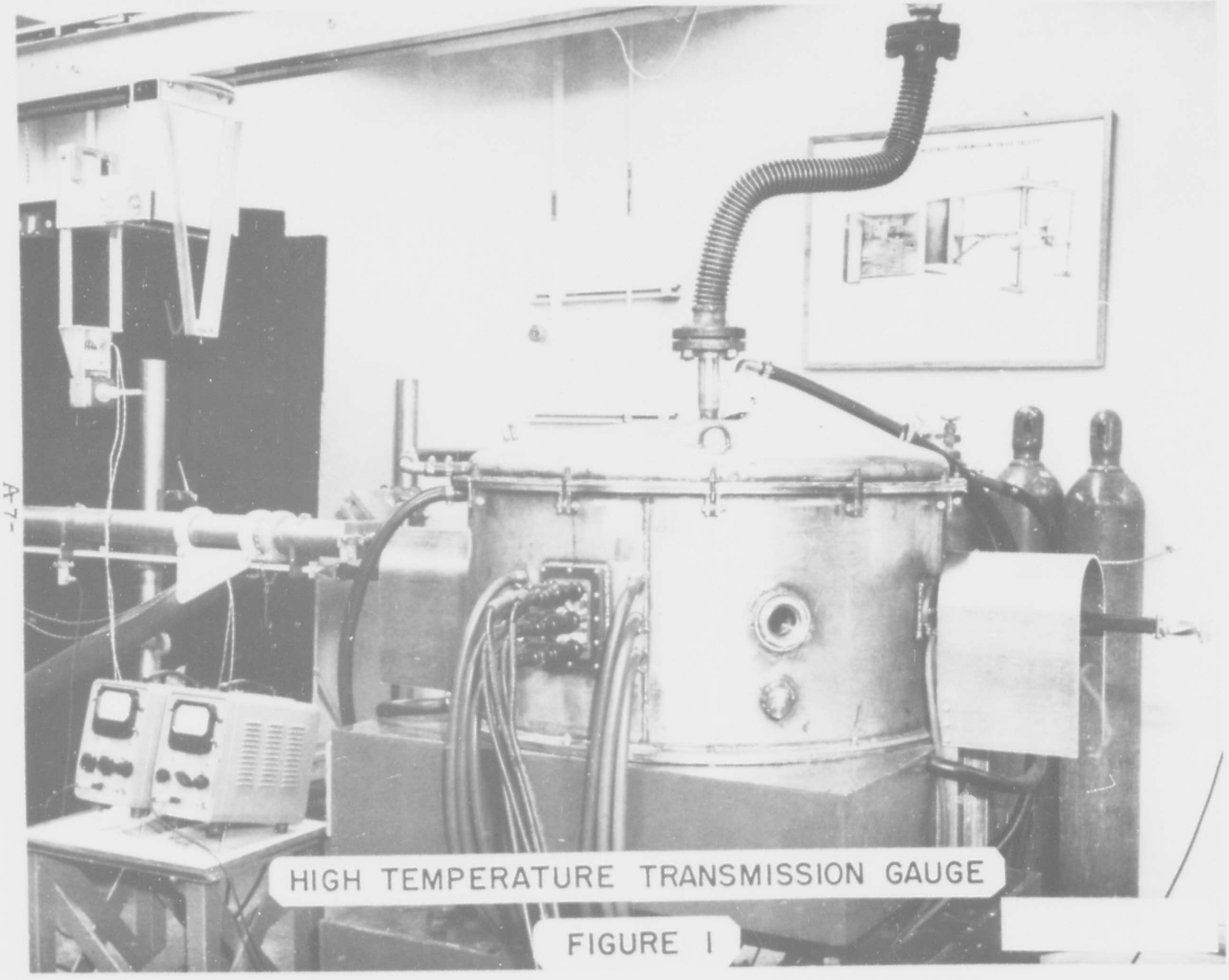

HIGH TEMPERATURE TRANSMISSION GAUGE

FIGURE 1

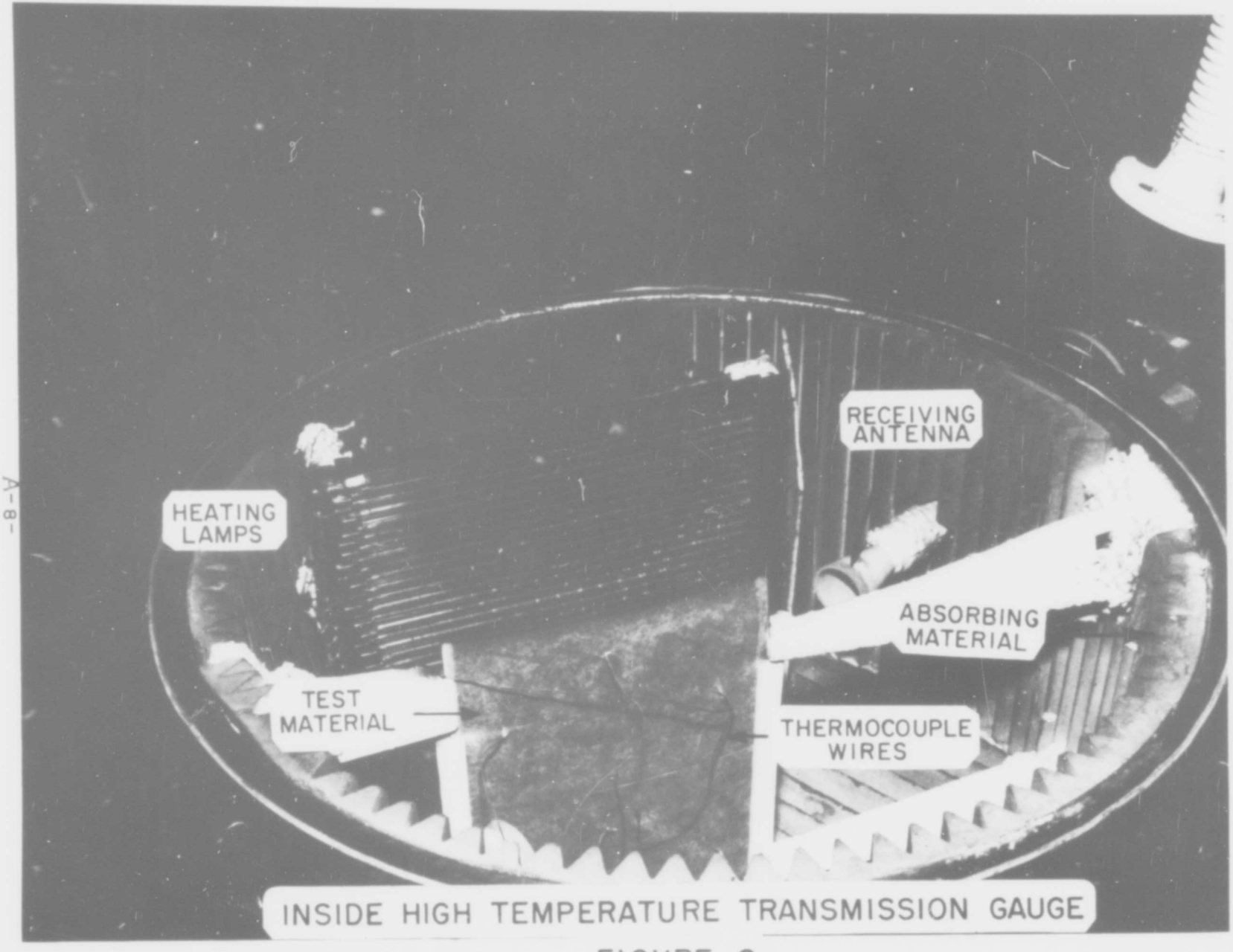
HEATING LAMPS
RECEIVING ANTENNA
ABSORBING MATERIAL
TEST MATERIAL
THERMOCOUPLE WIRES
INSIDE HIGH TEMPERATURE TRANSMISSION GAUGE

FIGURE 2

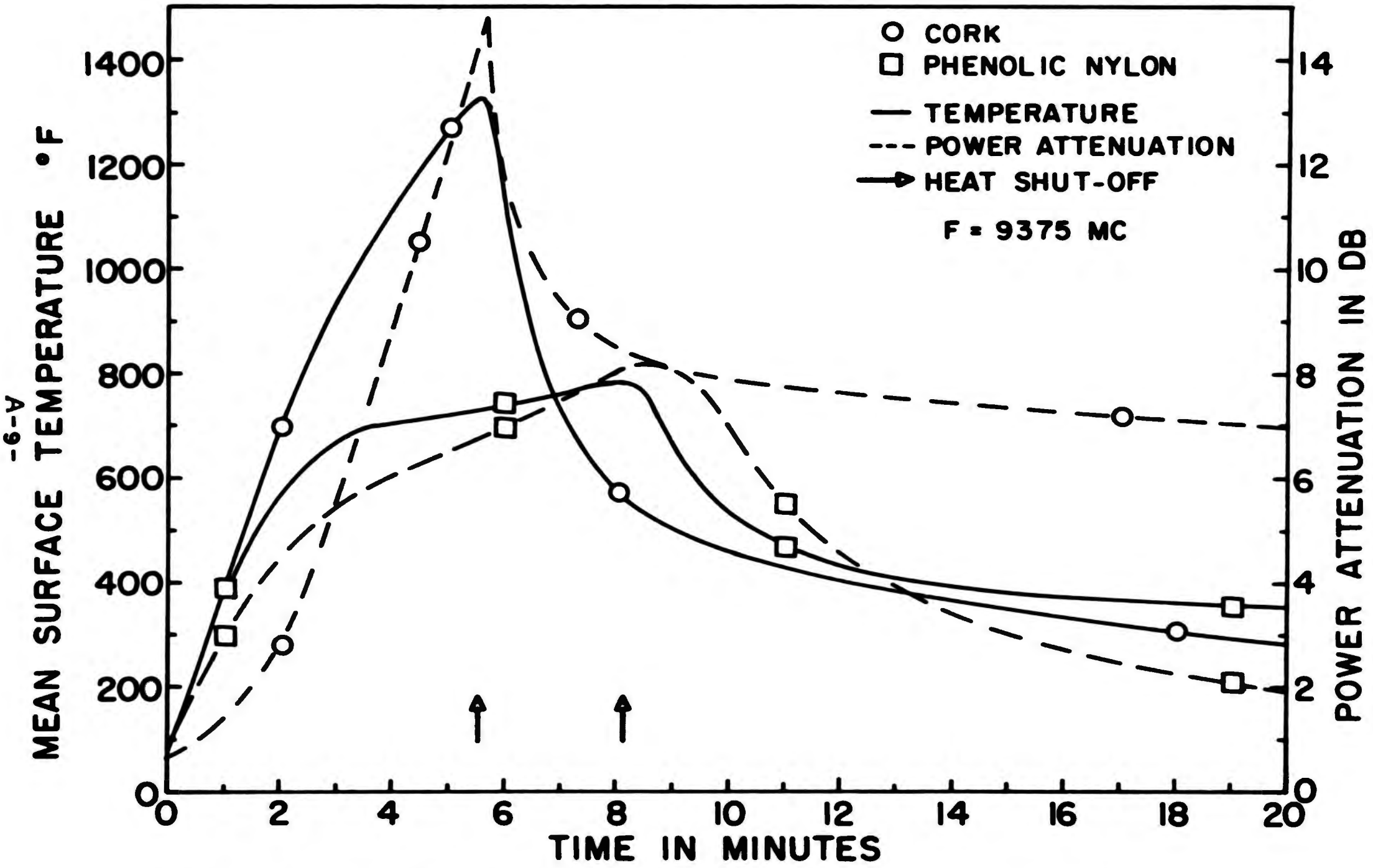

ATTENUATION AND TEMPERATURE VS TIME FIGURE 3

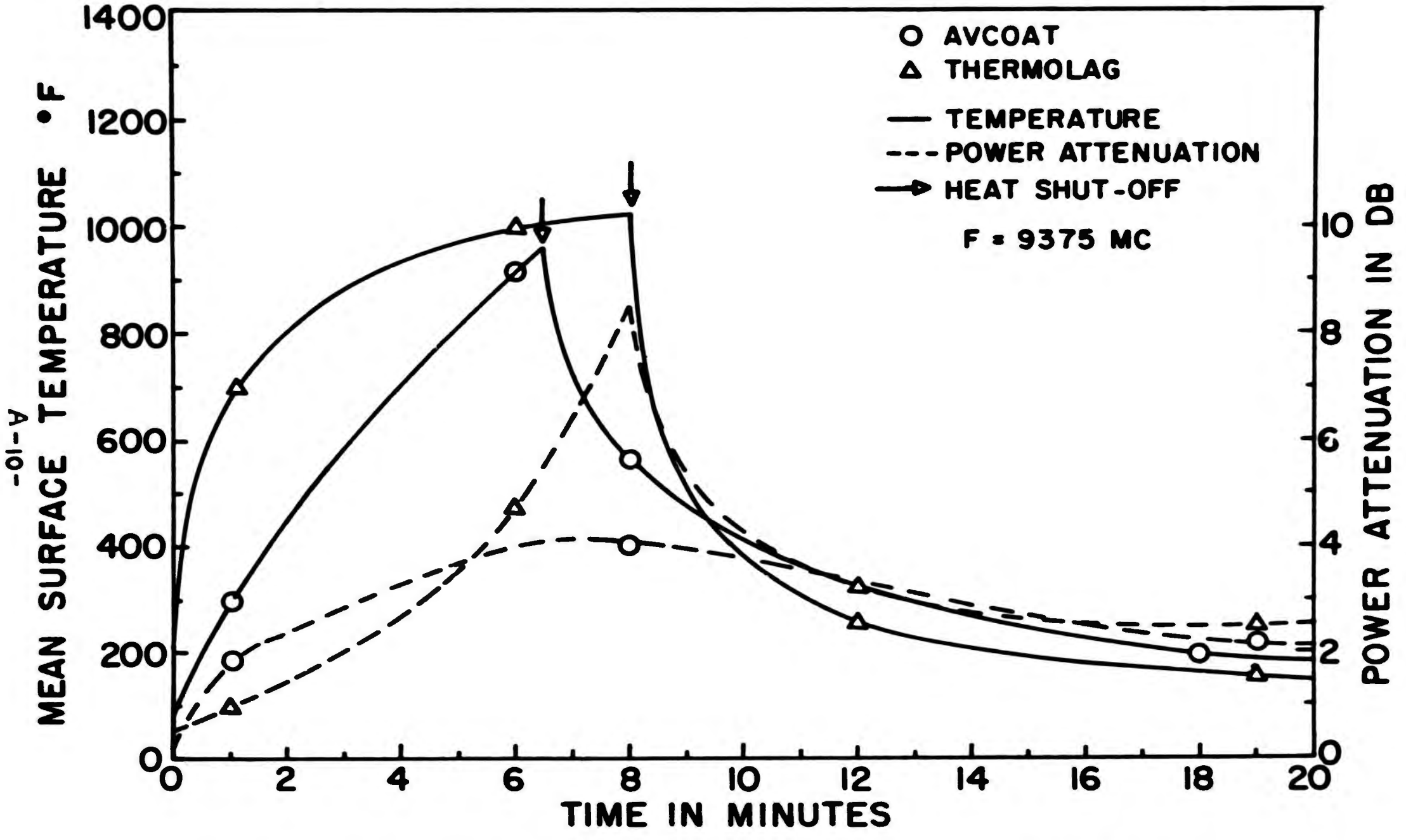

ATTENUATION AND TEMPERATURE VS TIME FIGURE 4

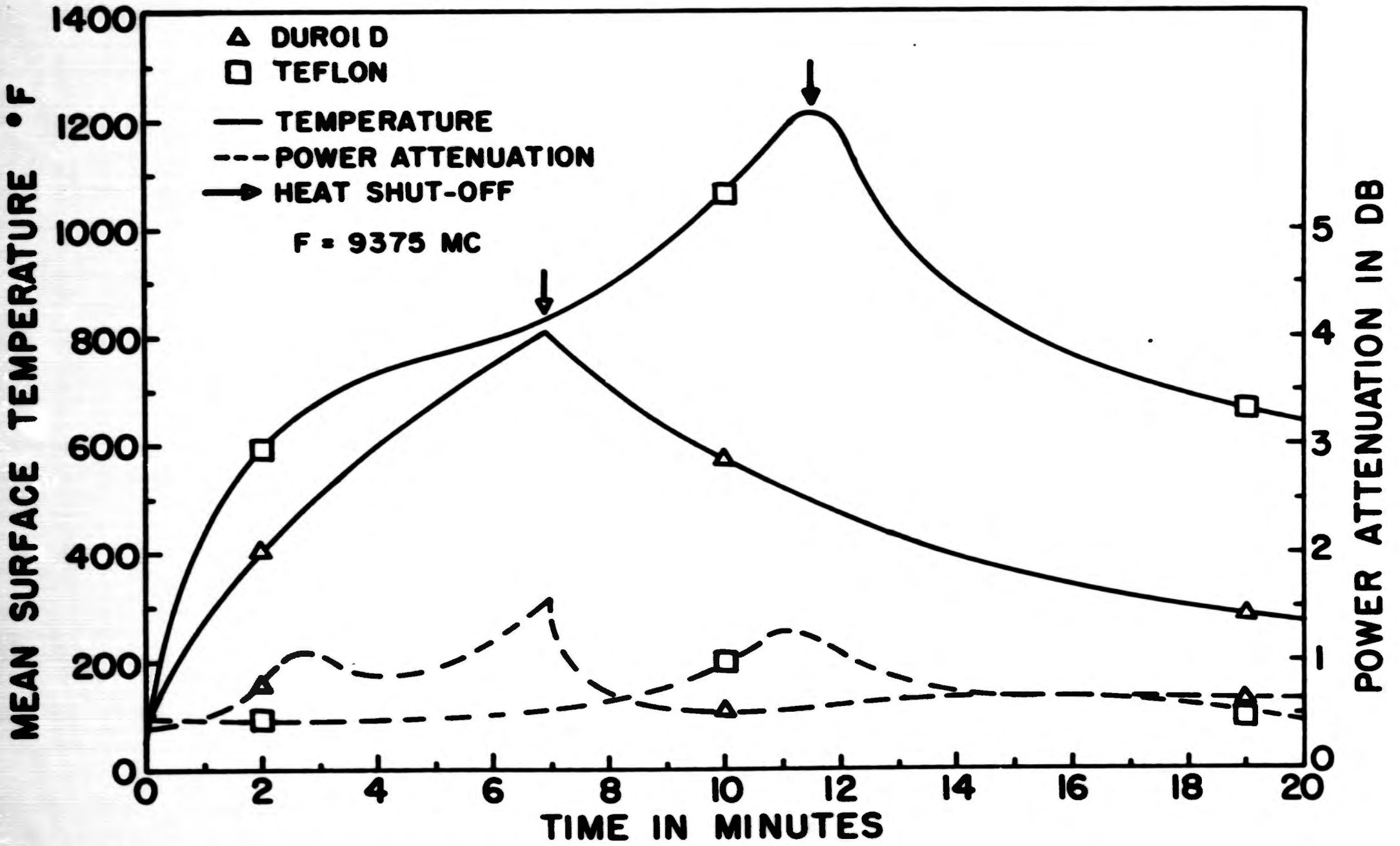

ATTENUATION AND TEMPERATURE VS TIME FIGURE 5

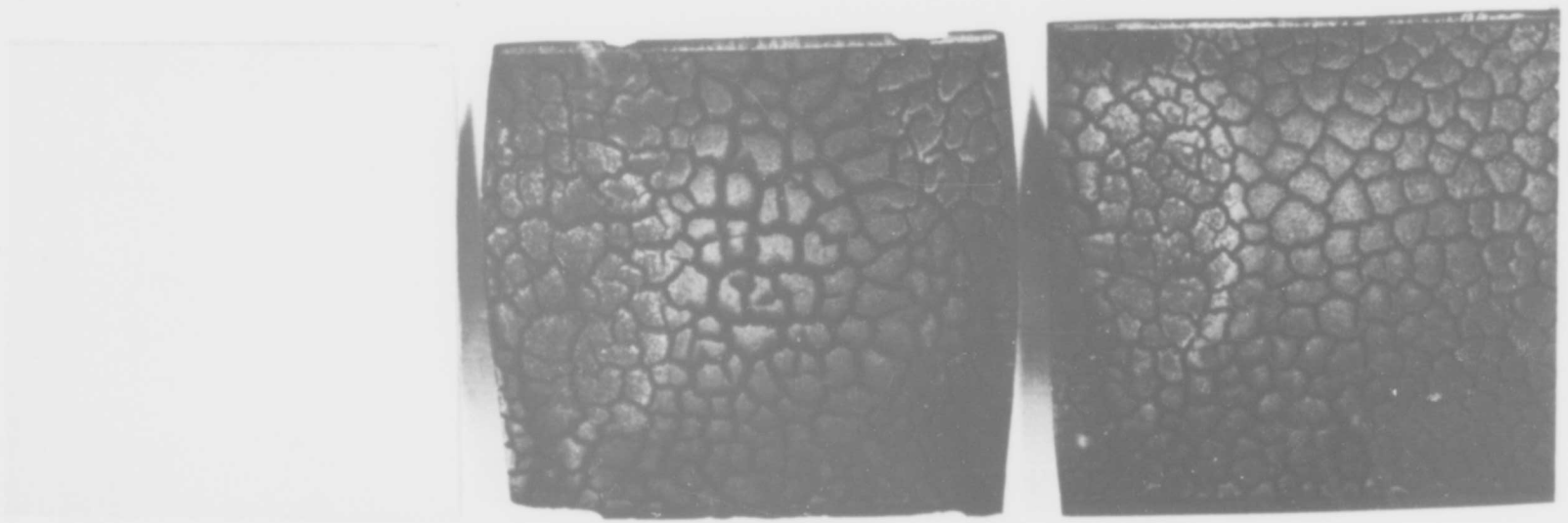

BEFORE ABLATION TEST

AFTER ABLATION TEST

MATERIAL: ARMSTRONG 2755 CORK

FIGURE 6

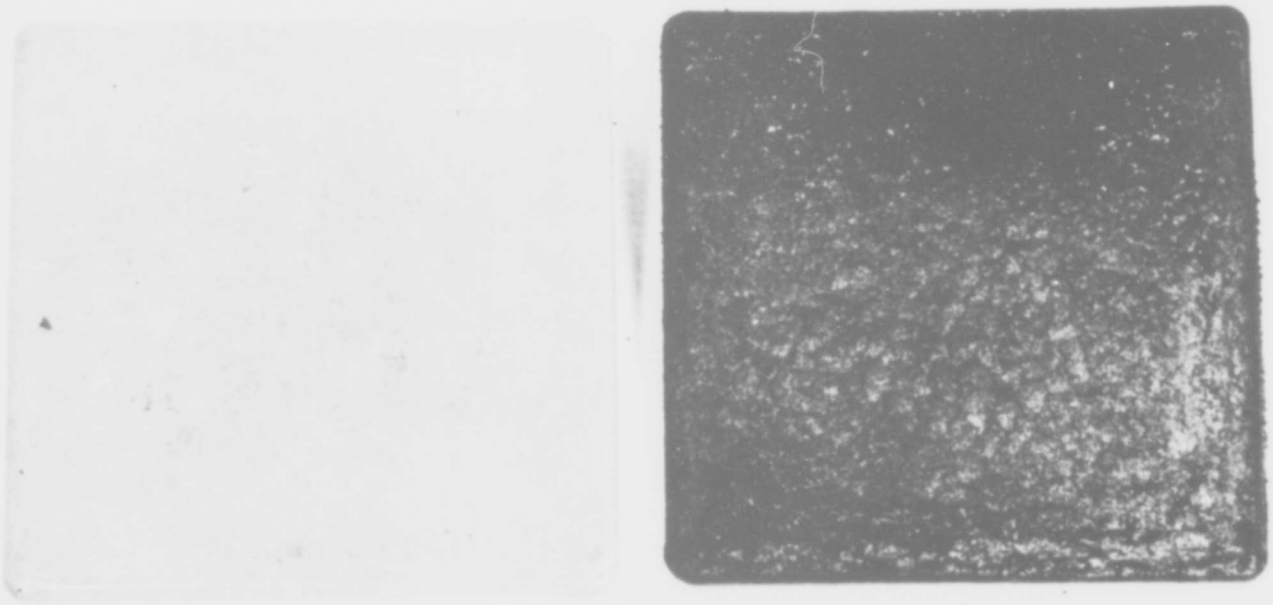

BEFORE ABLATION TEST AFTER ABLATION TEST

MATERIAL: TAYLORON PHENOLIC NYLON

FIGURE 7

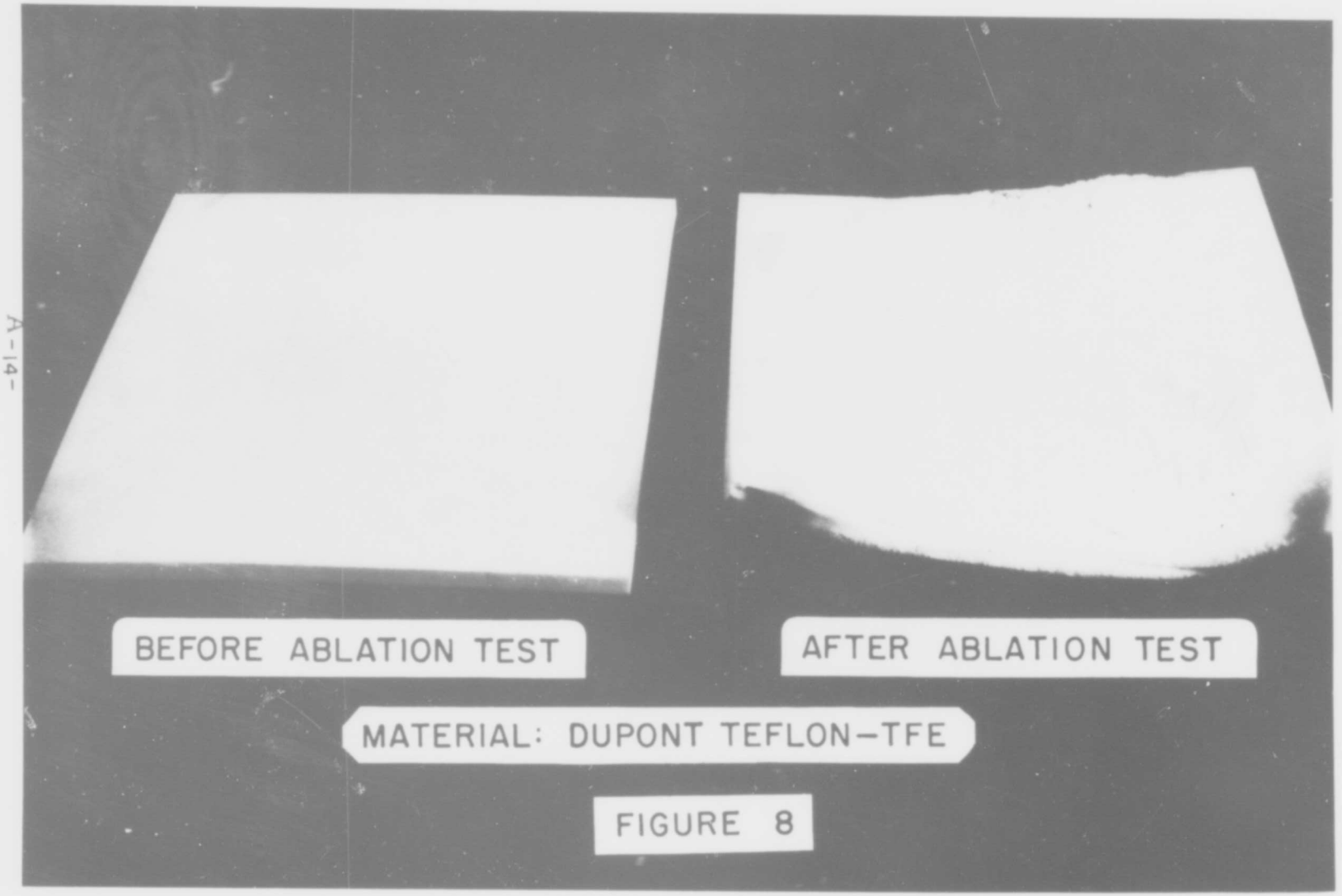
BEFORE ABLATION TEST
AFTER ABLATION TEST
MATERIAL: DUPONT TEFLON–TFE

FIGURE 8

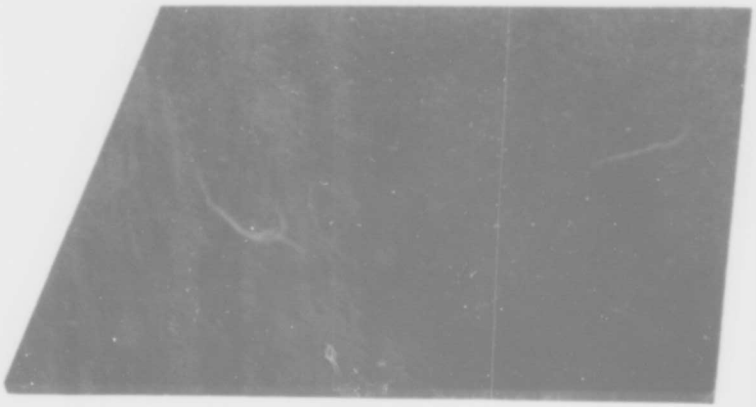

BEFORE ABLATION TEST

AFTER ABLATION TEST

MATERIAL: ROGERS DUROID 5650

FIGURE 9

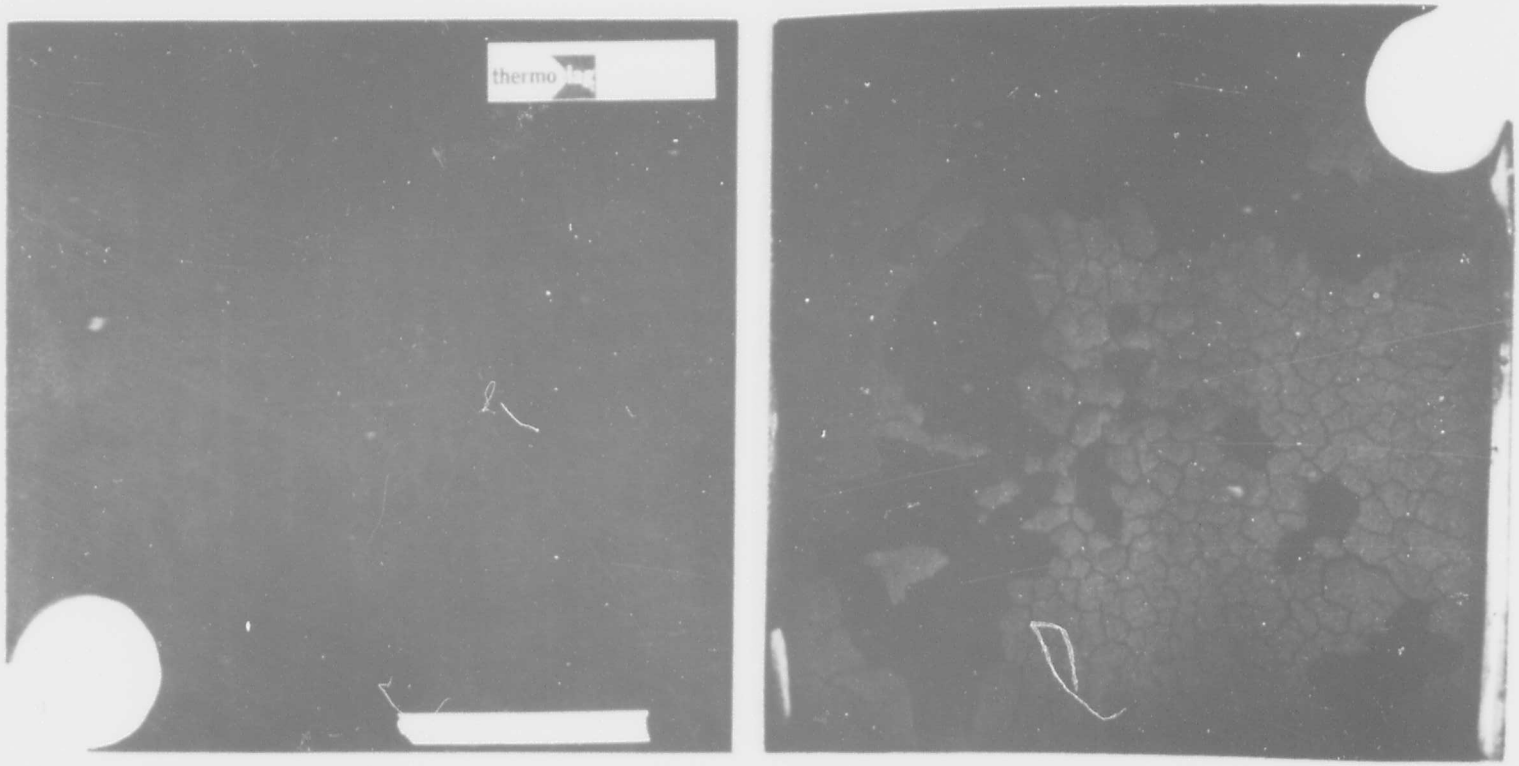

BEFORE ABLATION TEST

AFTER ABLATION TEST

MATERIAL: EMERSON ELECTRIC THERMOLAG-500

FIGURE 10

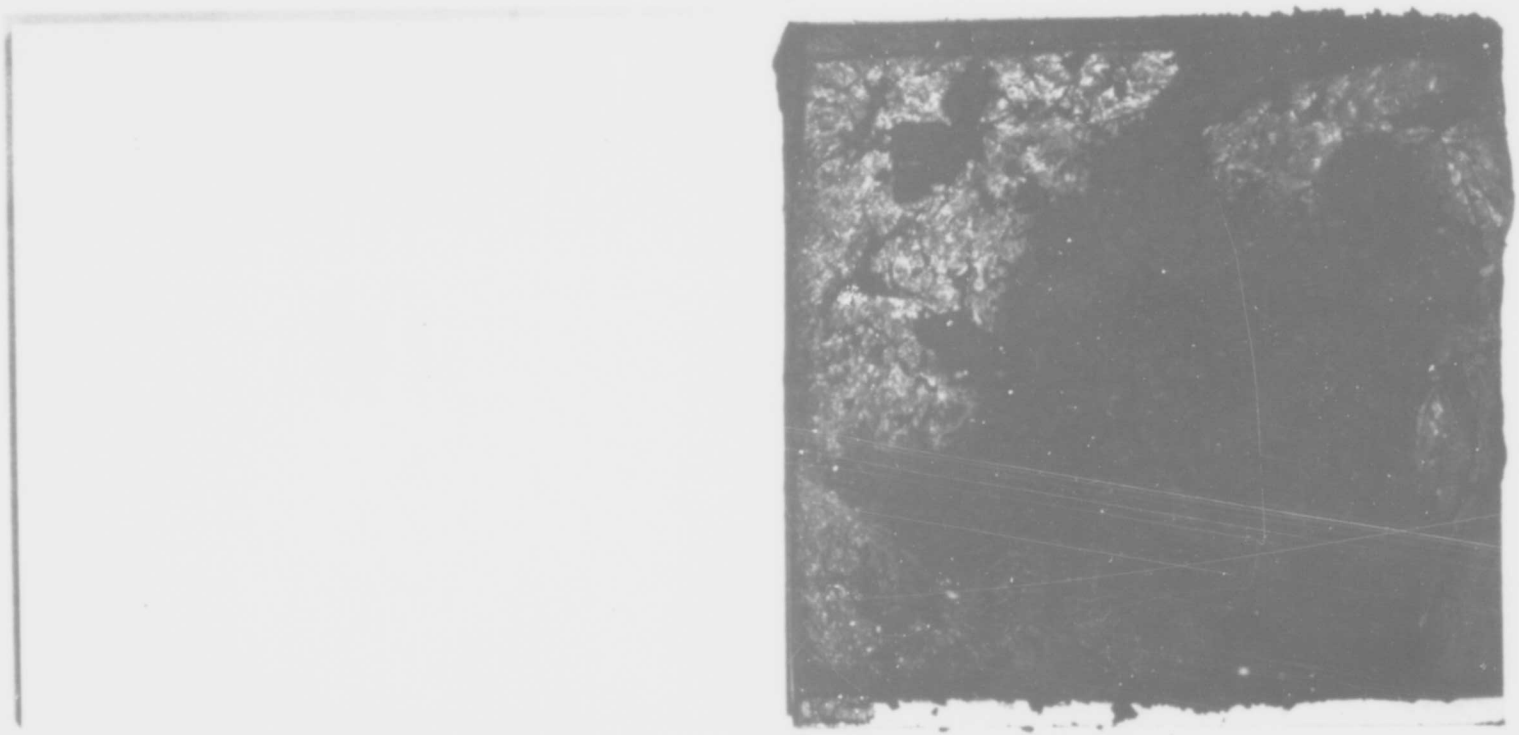

BEFORE ABLATION TEST AFTER ABLATION TEST

MATERIAL: AVCOAT-II

FIGURE 11

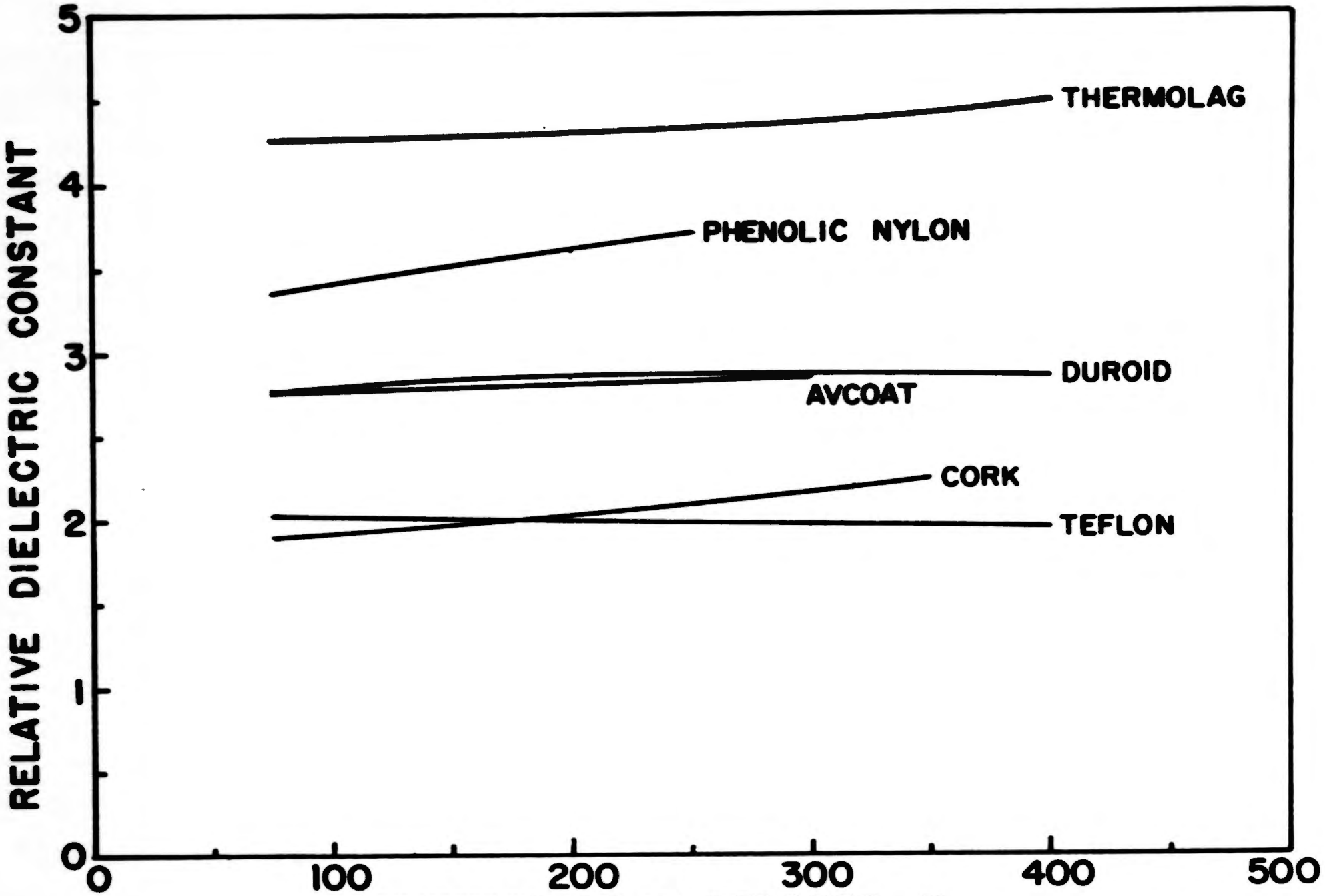

ABLATION MATERIALS DIELECTRIC CONSTANT VS TEMPERATURE

FIGURE 12

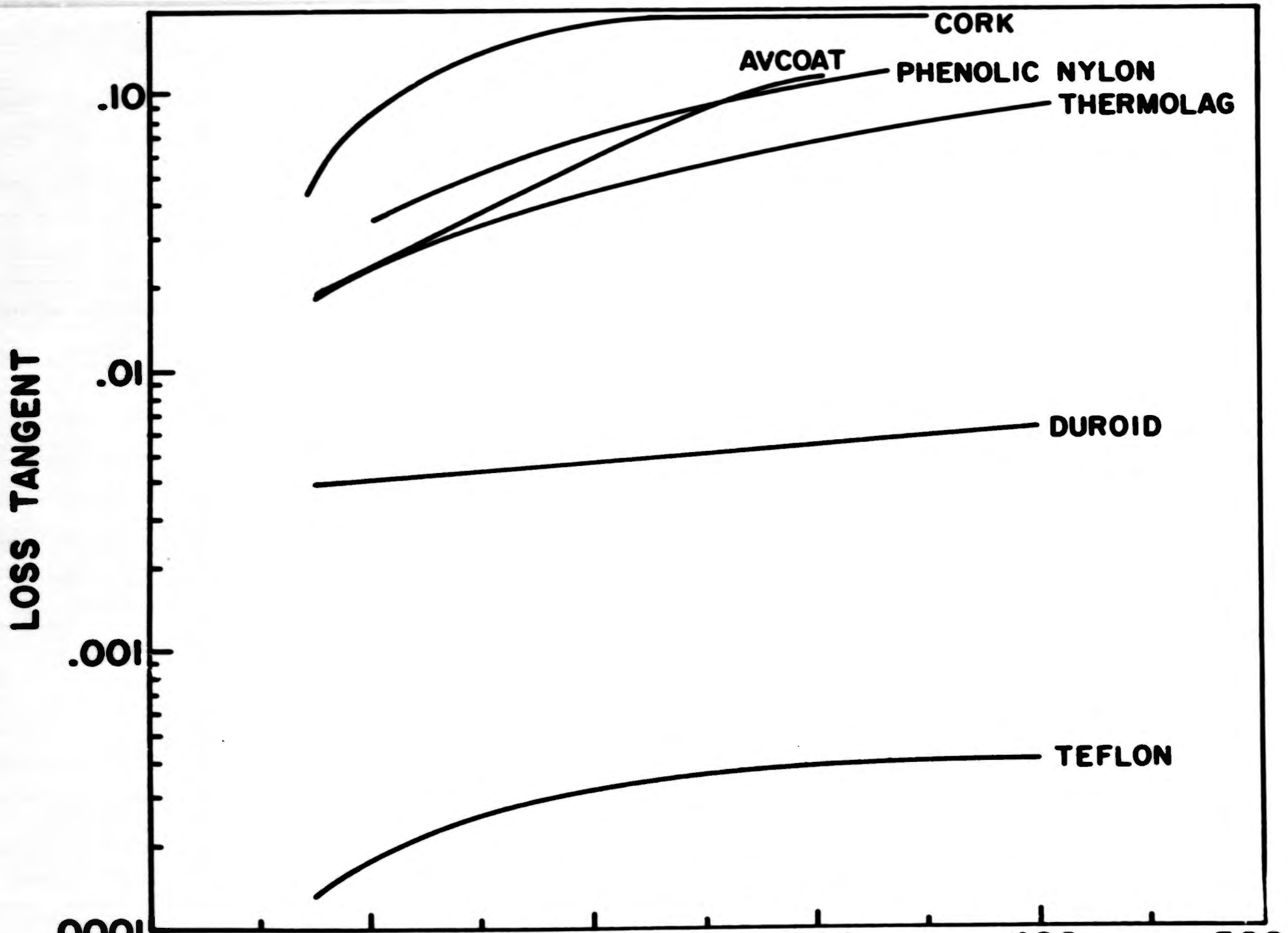

ABLATION MATERIALS LOSS TANGENT VS TEMPERATURE
FIGURE 13

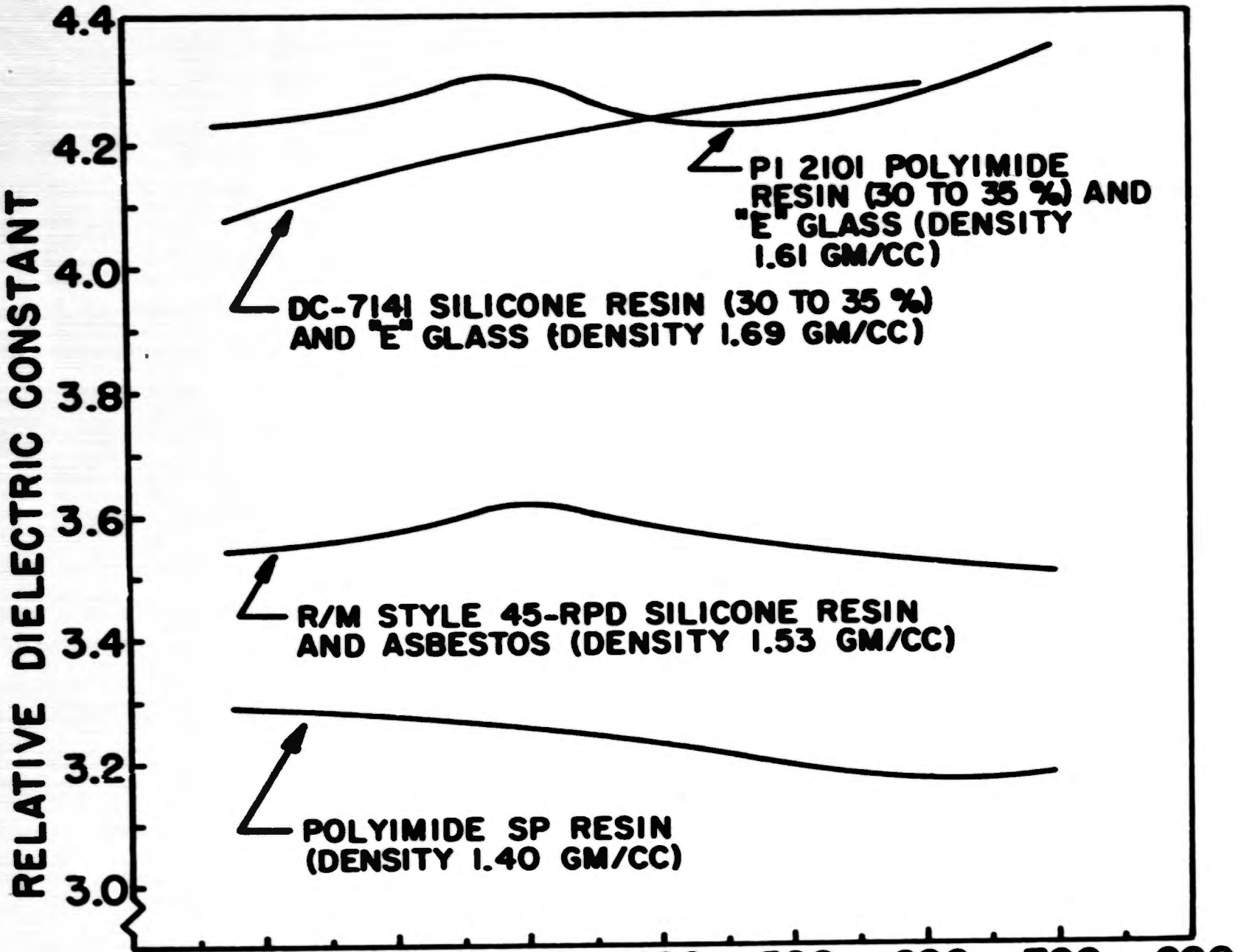

DIELECTRIC CONSTANT VS TEMPERATURE FIGURE 14

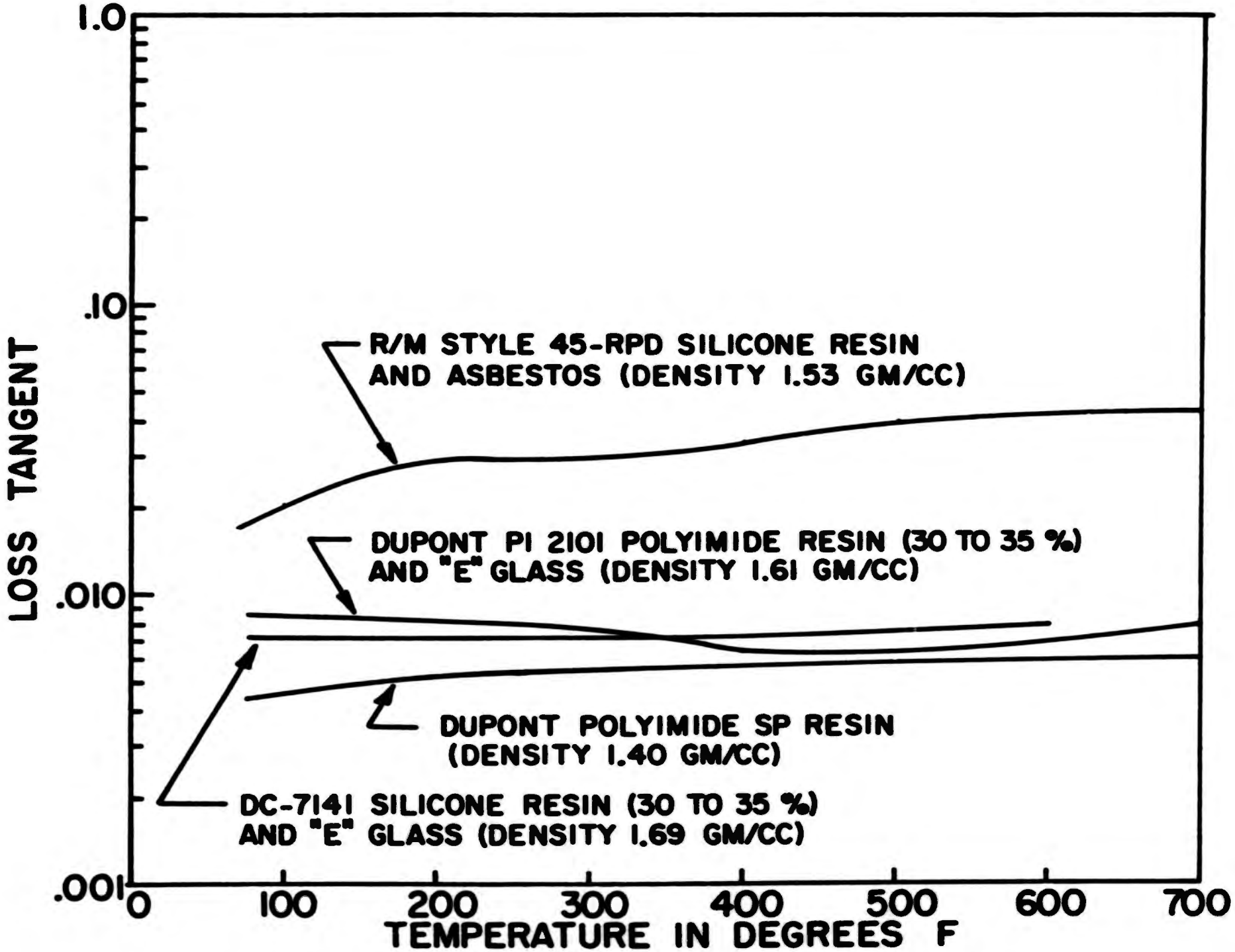

LOSS TANGENT VS TEMPERATURE FIGURE 15

DEVELOPMENT OF A 1200°F RADOME

Vance A. Chase
Senior R&D Engineer

R. L. Copeland
R. & D. Engineer

Brunswick Corporation
Defense Products Division
Marion, Virginia

The research in this document was sponsored by the Air Force Avionics Laboratory, Wright Patterson Air Force Base, Ohio under contract No. AF 33(657) 11469.

I. INTRODUCTION

This project is devoted to the development of large fibrous reinforced lightweight radomes based on an inorganic aluminum phosphate matrix, which will operate effectively in the temperature range of 800 to 1200°F for prolonged periods of time. The target objectives, as specified in the development contract, are as follows:

A. The dielectric constant shall be held to a minimum consistent with performance, but shall in no event exceed the value of 5.5.

B. The composite developed shall have a temperature coefficient of dielectric constant of not more than 5.0×10^{-4} where,

$$E = \frac{E_T - E_o}{E_o T}$$

E_o = Dielectric Constant at 70°F
E_T = Dielectric Constant at 1200°F
T = Temperature

C. The loss tangent shall be less than .005 at 70°F and not more than .02 at 1200°F.

D. The average one-way power transmission shall be not less than 85 percent of the impinging energy for all angles of incidence up to and including 60°.

E. Power reflection back into the antenna by the radome sample shall be less than two percent of the impinging energy.

F. The structural composite shall absorb less than 0.02 percent moisture.

G. The flexural strength shall be at least 25,000 psi at 70°F and 10,000 psi at 1200°F.

H. The composite shall have an Izod impact strength of at least ten foot pounds.

The work reported herein encompasses the first twelve months effort on the program.

The composite developed is based on an aluminum phosphate matrix and Owens Corning's S-994 fiberglass. A protective coating of Dow Corning's 805 silicone resin is applied to the glass fabric to prevent its degradation.

The fiber glass is treated with the unreacted aluminum phosphate and passed through a heated zone. The pre-preg obtained is similar to those based on conventional thermosetting resins and may be stored for four weeks at temperatures on the order of 45°F. Laminated structures are obtained at pressures of 100 psi and 300-350°F for one hour followed by a postcure to 600°F.

II MECHANICAL PROPERTIES

Tensile strengths, compression strengths, flexural strengths and modulus have been measured on glass reinforced aluminum phosphate laminates at temperature up to 1200°F.

The test results of flexural specimens over the subject temperature range have been very encouraging. An average flexural strength in excess of 21,000 psi at room temperature after a postcure to 600°F and in excess of 25,000 psi at 1100°F has been obtained. These data are shown in Figure 1. It was determined that the fabric weave pattern is significant in obtaining high strength at elevated temperatures. This is illustrated in Figure 1 by the improved strength of 143 fabric laminates over 181 fabric laminates at temperatures above 800°F. Tensile specimens have shown high tensile strength at room temperature but fall off rapidly at temperatures above 800°F. Efforts to improve this condition have been quire satisfactory. Using the theories expounded in Sectior VI the tensile strength at 1000°F has been increased more than one hundred rcent (Figure 3).

Compression strength data has been obtained over a room temperature to 1200°F range. Compression strength is very stable versus temperature with the maximum value being obtained at 1100°F (Figure 4).

Measurements of Izod impact strength were made on specimens after exposure to various elevated temperatures. The impact resistance of the composite appears to be effected by exposure to elevated temperatures. However, the strength after a two hour exposure to 800°F is more than 50% above target goal, (Figure 9).

III. THERMAL AND PHYSICAL PROPERTIES

Coefficient of linear thermal expansion was measured for the reinforced material over a room temperature to 1200°F range. Data has been obtained both in the direction of the reinforcement and across the reinforcing plies.

Thermal conductivity was measured up to 1200°F and a thermal shock merit index was calculated based on data obtained at 1200°F. Values such as specific gravity and specific heat have been obtained. (Figure 0).

IV. ELECTRICAL PROPERTIES

The reinforced ceramic material has been evaluated for dielectric constant, loss tangent, transmission, reflection and insertion phase delay. Temperature coefficient of dielectric constant was calculated based on room temperature and 1200°F data. (Figures 5, 6 and 9).

The electrical properties of the S-994 glass reinforced ceramic have proved to be excellent for radome applications. The low dielectric constant and loss tangent, which are stable over the room temperature to 1200°F range, result in a larger acceptable tolerance on the radome wall thickness, high transmission effeciency and broadband characteristics.

V. RADOME DEVELOPMENT

A. Fabrication

To demonstrate the feasibility of the material and manufacturing techniques developed, a 65" ogive shape radome was designed and fabricated The electrical esign (half wave wall at 10 gc) required a wall thickness of 0.360". This thickness was obtained from 39 plies of glass fabric preimpregnated with aluminum phosphate. The reinforcement was Style 143, S-994 glass fabric with a protective coating of DC-805. The matrix system was the standard ratio 1A, aluminum phosphate. The first step in "pre-preg" preparation was treating the heat cleaned fabric with a solvent solution of DC-805 and drying for 5 minutes at 250°F. The coated fabric was impregnated 50% by weight with phosphate matrix 1A and "B" staged at 250°F. The prepreg was laid up on a male mandrel. The first twelve plies were laid up in six stages of two plies per stage. After each stage the part was pressure wrapped and pre-cured two hours at 250°F. The last 27 plies were applied in nine stages of three plies per stage with each stage pre-cured two hours at 250°F. At the end of each twelve ply stage, the part received an additional cure of two hours at 300°F. After the final lay-up the radome was postcured 12 hours at 450°F.

Other steps in the fabrication process involved grinding to thickness, applying and curing the seal coat and trimming and attachment of ring and nose plug.

Figure 11 shows the radome being ground to thickness. Figure 12 shows the finished radome with nose plug and mounting ring attached.

B. Stress Analysis

To determine performance at high temperature for a large reinforced ceramic radome, a stress analysis was performed based on 181 Style fabric laminates. The radome analyzed was approximately three times the size of the one fabricated under this contract. The radome was analyzed for the major considerations used in radome design, i.e., tensile stress, compressive stress and stability. The margins of safety for these considerations are as follows:

Consideration	Margin of Safety
Tensile Stress	3.06
Compressive Stress	3.49
Stability	6.02

The temperature profile for the analyzed radome (Figure 2, item 1 Appendix) shows a nose temperature of 1200°F and an attach area temperature of 900°F. The above values of margin of safety were based on this profile. Had the radome attach area been 1200°F (requiring a nose temperature of approximately 1500°F) the margins of safety for tensile stress, compressive stress and stability would have been 0.41, 4.8 and 7.2 respectively. These values and the design analysis are significant in that they show that the strengths of the reinforced ceramic material are sufficient for the successful development of a high performance radome.

C. Radome Range Testing

The antenna utilized for electrical testing the radome, was a parabolic amplitude sensing 4-lobe mono-pulse type operating in the pencil beam mode.

Transmission measurements were conducted over a frequency band from 9.375 KMCS to 10.200 KMCS in increments of 200 MCS. The tests were performed as follows using both horizontal and vertical polarizations as referenced to the radome.

1. Horizontal Polarization: Azimuth scans of ± 40° at antenna elevation angles of 0°, ± 5°, ± 10°, and -20° at a roll angle of 0°.

2. Vertical Polarization: Azimuth scans of ± 40° at an antenna elevation angle of 0° at a roll of angle of 0°.

Figure 13 is a graph of average transmission versus frequency for an azimuth scan of ± 40° at the 0° elevation, 0° roll antenna look position.

The optimum test frequency for horizontal polarization was approximately 9.850 KMCS ± .20 KMCS and the minimum transmission value at this frequency was 87.8%. The optimum test frequency for vertical polarization was 9.675 KMCS ± .25 KMCS and the minimum transmission value was 84.5%. As the accompanying graph indicates the radome transmission characteristics are excellent over a rather broad frequency band (925 MCS). It appears that this broadbanded effect would have extended further had the test been extended further down the frequency scale.

The electrical transmission characteristics of the subject radome were superior to those usually associated with a radome of this configuration particularly across a frequency band of this width. The use of this type of material appears to represent a definite advancement in the state-of-the-art as applied to transmission capabilities of streamlined radomes.

VI. PROBLEM AREAS AND FUTURE WORK

The major problem areas with the reinforced aluminum phosphate are strength decrease after thermal aging and tensile strength reduction at elevated temperatures after short term exposure. The unusual flexural strength versus temperature curve has also caused concern. The causes for these problems have been well defined and steps are being taken to eliminate them.

Preliminary investigation has shown our approaches to be correct as evidence of the improved thermal aging and short term tensile strength reported later in this section of the report.

The probability for elimination of these problems appears to be very good.

The following is a discussion of the major problem areas and the methods designed to alleviate them.

A. Thermal Aging

The theory has been postulated, that decreases in flexural strength after aging at elevated temperatures (Figure 10) can be alleviated by reducing the large difference between the thermal expansion of the matrix and the glass reinforcement.

Prior to an extensive investigation into the effects of matrix expansion, it was considered necessary that the expansion theory be substantiated. Laminated specimens were prepared with low expansion silica fillers added to the standard matrix formulation. The reinforcement was style 143, S-994 glass fabric coated with DC-805. One set of specimens was prepared using 5% silica (Cab-O-Sil) ®, another using 10% silica (5 micron particles).

These specimens were aged 25 hours at 800°F and tested for flexural strength at room temperature. The highest flexural strength previously obtained from a specimen subjected to these aging conditions was 8,837 psi. The flexural strengths of the specimens containing silica fillers are shown below:

Silica Filler	R.T. Flexural Strength After 25 hrs. at 800°F	Increase Over Standard Laminate
5%	9,400 psi	5.5%
10%	10,940 psi	20.5%

The reduced flexural strengths after thermal aging can be attributed in part to the phenomenon of static fatigue. This term is used in glass technology to describe the time function of strength under static load. Essentially it states that a glass fiber loaded at 50% or higher of its ultimate strength will fail as a function of time. The higher the load the shorter time to failure. The stress on the glass at elevated temperature no doubt is of a magnitude sufficient to cause static fatigue.

The percent elongation to rupture for S-994 at 1000°F is 3%. A load equivalent to one-half of the ultimate strength of S-994 at 1000°F would result in 1.2% elongation of the filament. However, the fabric reinforced laminate does not produce an ideal situation in regard to uniform loading of the glass. The twists and weave of the fabric reinforced aluminum phosphate laminate results in areas of high stress concentration.

Figure 8 shows a theoretical 0.8% elongation of the glass due to expansion differences at 1000°F. This is evidently great enough to produce high areas of stress concentration and introduce static fatigue.

B. Loss of Tensile Strength at Elevated Temperature

Decrease in tensile strength at elevated temperature has proved to be a problem with the composite. A set of specimens prepared using the standard matrix with 5% silica filler was tested at 1000°F after short term exposure. The average for five specimens was nearly 100% greater than any value obtained previously using the standard laminates. (Figure 3).

Figure 8 shows the percent linear thermal expansion for the standard 1A matrix, percent expansion for S-994 glass and percent expansion for the 1A matrix containing 10% silica. This graph also shows the theoretical differences in S-994 and matrix ratio 1A. The 10% addition of low expansion filler reduces this percent difference in thermal expansion for the matrix and reinforcement from .57% to .47% at 800°F. It may also be seen from this graph that 10% silica will offer little advantage over the standard ratio during 1000°F aging because the curves begin to coincide.

It was felt that the preliminary work was sufficient to confirm the theory that differences in thermal expansion of the matrix and reinforcement are a factor in the loss of strength after thermal aging.

Continued effort is being directed toward altering the expansion characteristics of the matrix to bring it more closely to that of the reinforcement. Indications are that substantial improvements over the strength properties reported here may be expected as an outcome of this work.

C. Unusual Flexural Strength Versus Temperature

The flexural strength curve versus temperature for the glass reinforced aluminum phosphate laminates is, to say the least, unusual. The increase in strength from 800 - 1100°F has caused much concern. However, we now feel that this phenomena may be explained by two factors. (1.) Aluminum phosphate undergoes a reversible β to α phase change at approximately 1100°F. This phase change is accomplished by a volume increase and appears to start as low as 800°F as evidence of the expansion coefficient curve for the matrix (Figure 7). During this phase change the molecular structure of the matrix is in a mobile state which allows better stress distribution between the reinforcing fibers, It is interesting to note that the matrix expansion curve closely follows the flexural strength curve. (2.) The large expansion of the matrix stresses the reinforcing fibers at elevated temperatures. This results in a structure similar to pre-stressed concrete. For short term conditions this effect is beneficial, but under long term heating the reinforcement can be damaged by static fatigue. Current work with additives which alter the thermal expansion of the matrix show promise of straightening the flexural strength curve to some degree.

VII. CONCLUSIONS

1. A major portion of the target goals for the project have been met or exceeded.
2. Large size radome fabrication can be effectively accomplished from the glass reinforced aluminum phosphate material in much the same manner as with conventional glass reinforced plastics.
3. The successful fabrication of a large, lightweight radome capable of performing satisfactory in a thermal environment of at least 1000°F is a substantial advancement of the "state of the art" for the radome field.
4. A slight decrease in the thermal expansion of the matrix will offer increases in flexural strength after aging at elevated temperature and higher tensile strength at elevated temperature.
5. The current room temperature tensile values (30,000 psi) are adequate for meeting the 1200°F goal (10,000 psi) if the degrading side effect of thermal expansion differences between the reinforcement and matrix can be eliminated.

FIGURE 1
Flexural Strength For Glass Reinforced $AlPO_4$

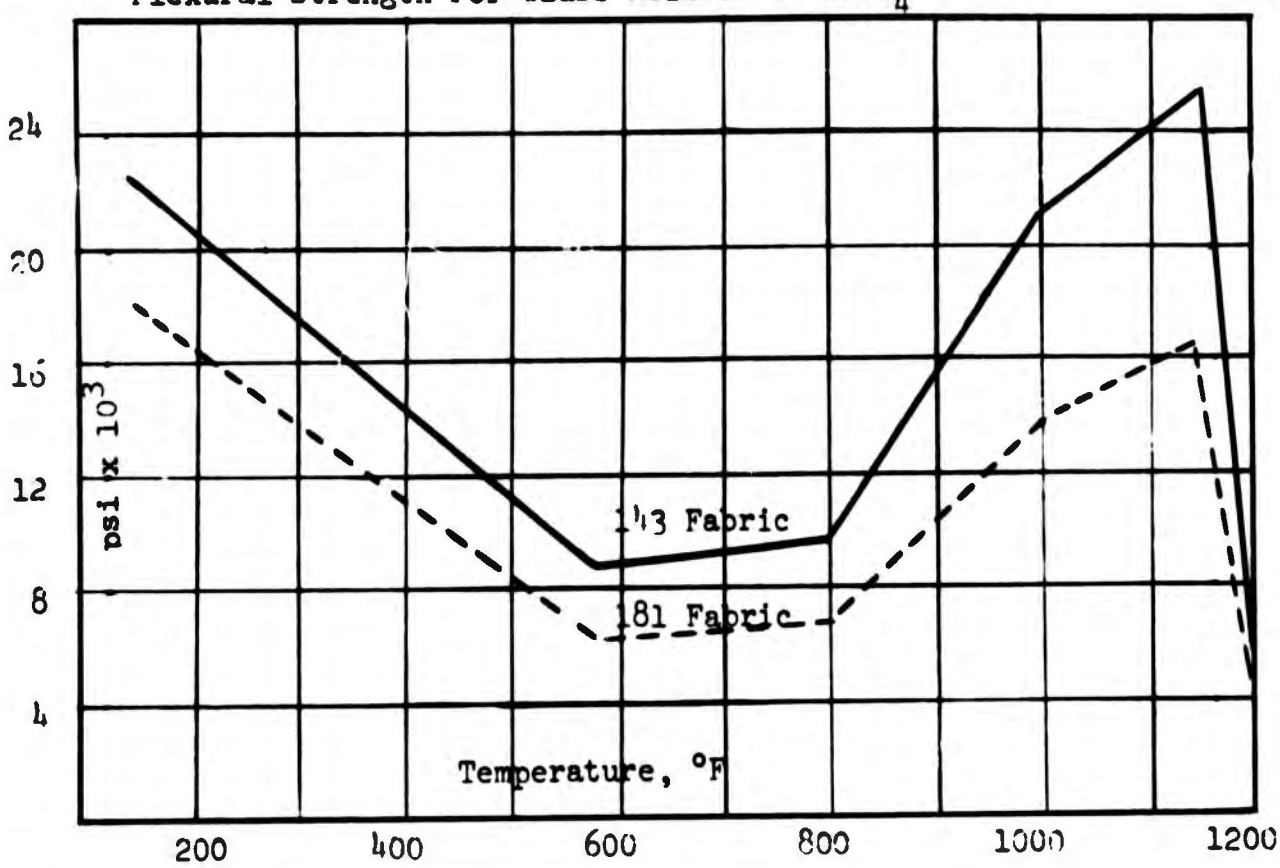

FIGURE 2
Flexural Modulus For Glass Reinforced $AlPO_4$

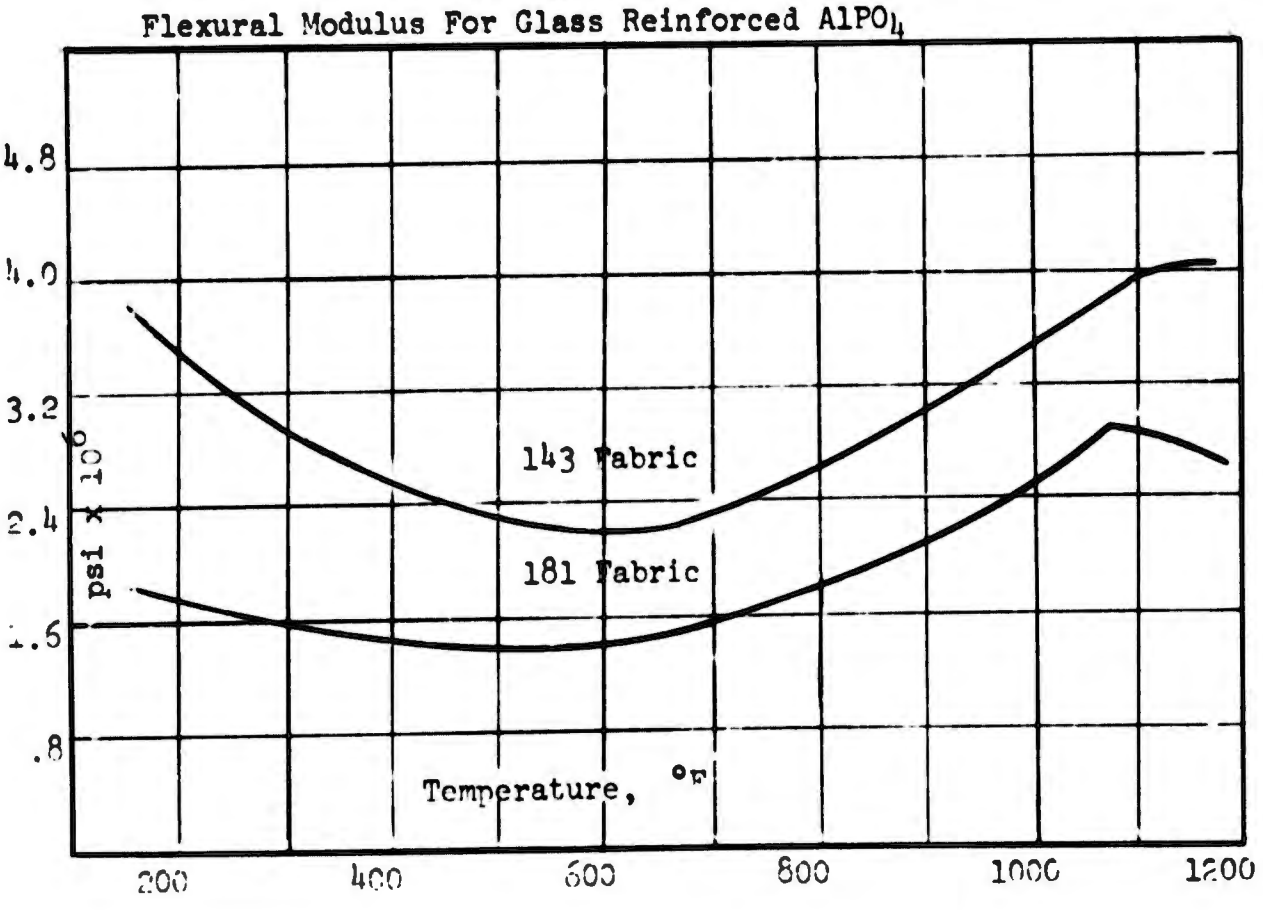

FIGURE 3

Tensile Strength For Glass Reinforced $1PO_4$

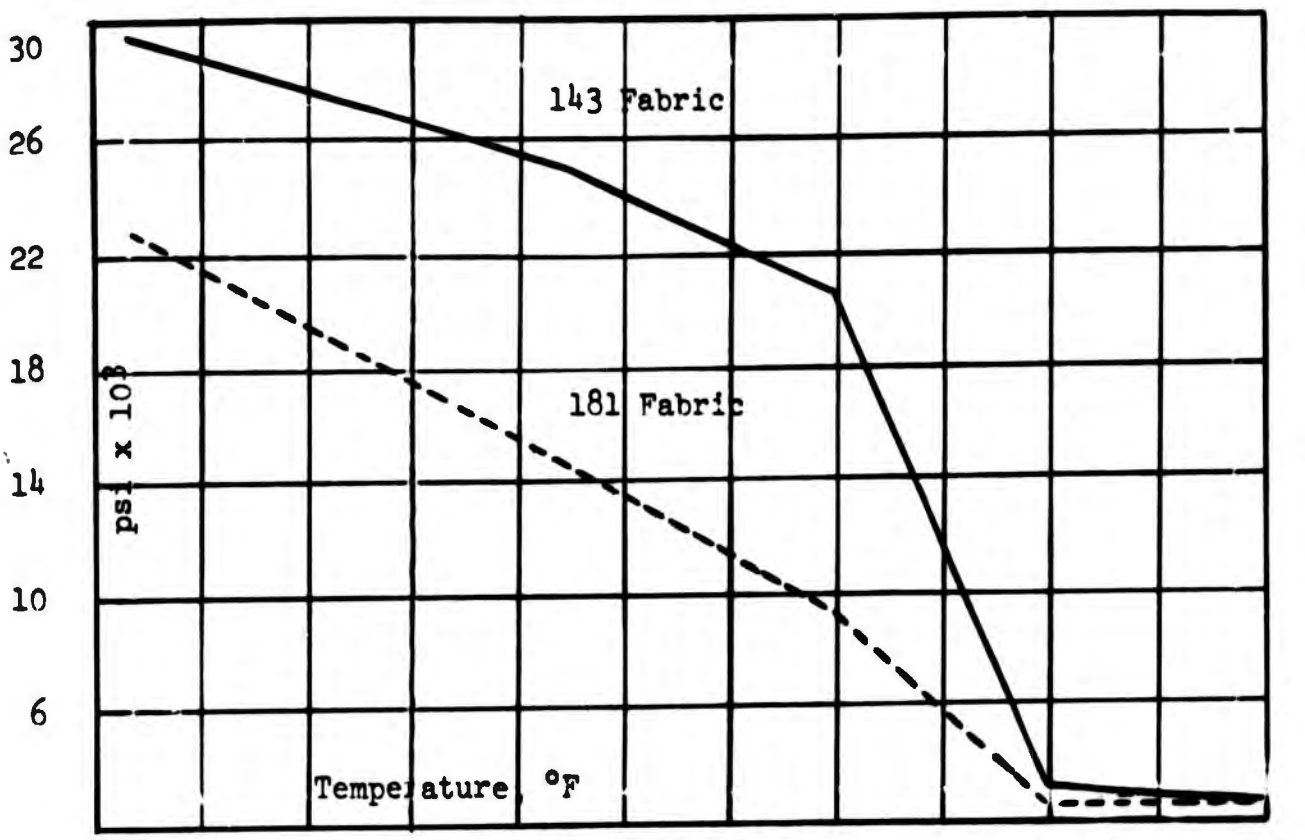

FIGURE 4

Compression Strength For Glass Reinforced $AlPO_4$

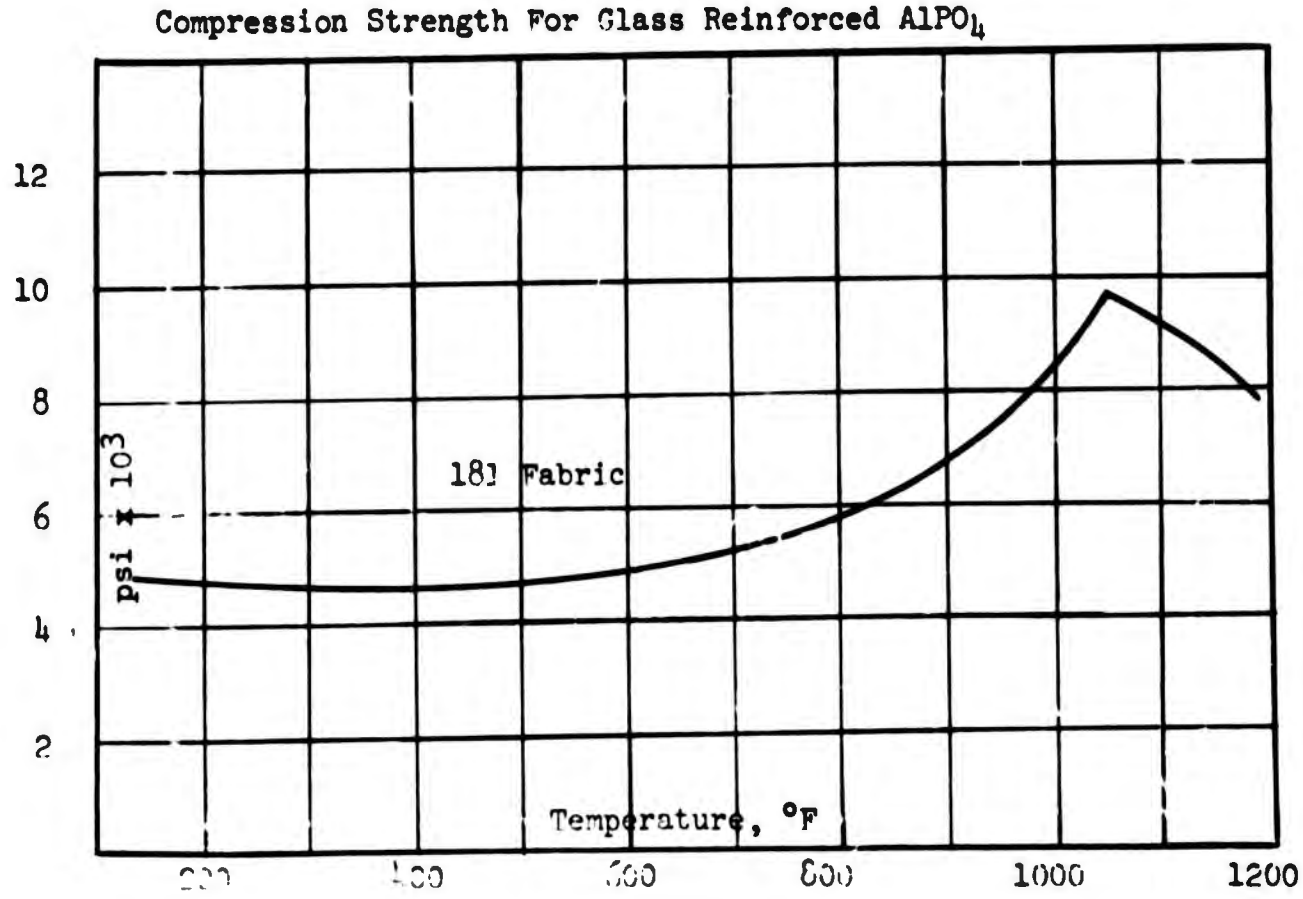

FIGURE 5

DIELECTRIC CONSTANT AND LOSS TANGENT
VERSUS
TEMPERATURE FOR ALUMINUM PHOSPHATE RATIO 1A WITH
S-994 REINFORCEMENT AT 10.0 KMC

Temperature °F.	Dielectric Constant	Loss Tangent
Ambient	3.45	0.0082
200	3.47	0.0089
400	3.54	0.0097
600	3.57	0.0103
800	3.58	0.0113
1000	3.60	0.0150
1200	3.56	0.0191
1100	3.54	0.0154
900	3.48	0.0110
700	3.45	0.0086
500	3.42	0.0075
300	3.38	0.0088
Ambient	3.35	0.0064

FIGURE 6
PERCENT POWER REFLECTION COEFFICIENTS

Angle of Incidence	PERPENDICULAR POLARIZATION Normal (%)	PERPENDICULAR POLARIZATION λ/4 (%)	PARALLEL POLARIZATION Normal (%)	PARALLEL POLARIZATION λ/4 (%)
60°	.038	.022	.022	.022
55°	.038	.022	.022	.022
50°	.060	.022	.038	.022
45°	.038	.038	.060	.022
40°	.022	.022	.038	.022
35°	.038	.022	.038	.022
30°	.038	.022	.038	.022
25°	.038	.038	.038	.038
20°	.085	.060	.060	.060
15°	.085	.060	.085	.060
10°	.085	.060	.060	.038
5°	.022	.022	.022	.038
0°	.022	.022	.022	.022
-5°	.114	.114	.038	.038
-10°	.038	.038	.114	.114
-15°	.114	.114	.060	.060
-20°	.114	.038	.022	.022
-25°	.038	.038	.038	.022
-30°	.038	.022	.038	.038
-35°	.060	.022	.022	.038
-40°	.038	.022	.022	.038
-45°	.038	.038	.038	.038
-50°	.038	.038	.022	.022
-55°	.038	.022	.022	.022
-60°	.038	.022	.022	.010

FIGURE 7

COEFFICIENT OF THERMAL EXPANSION FOR $AlPO_4$ MATRIX

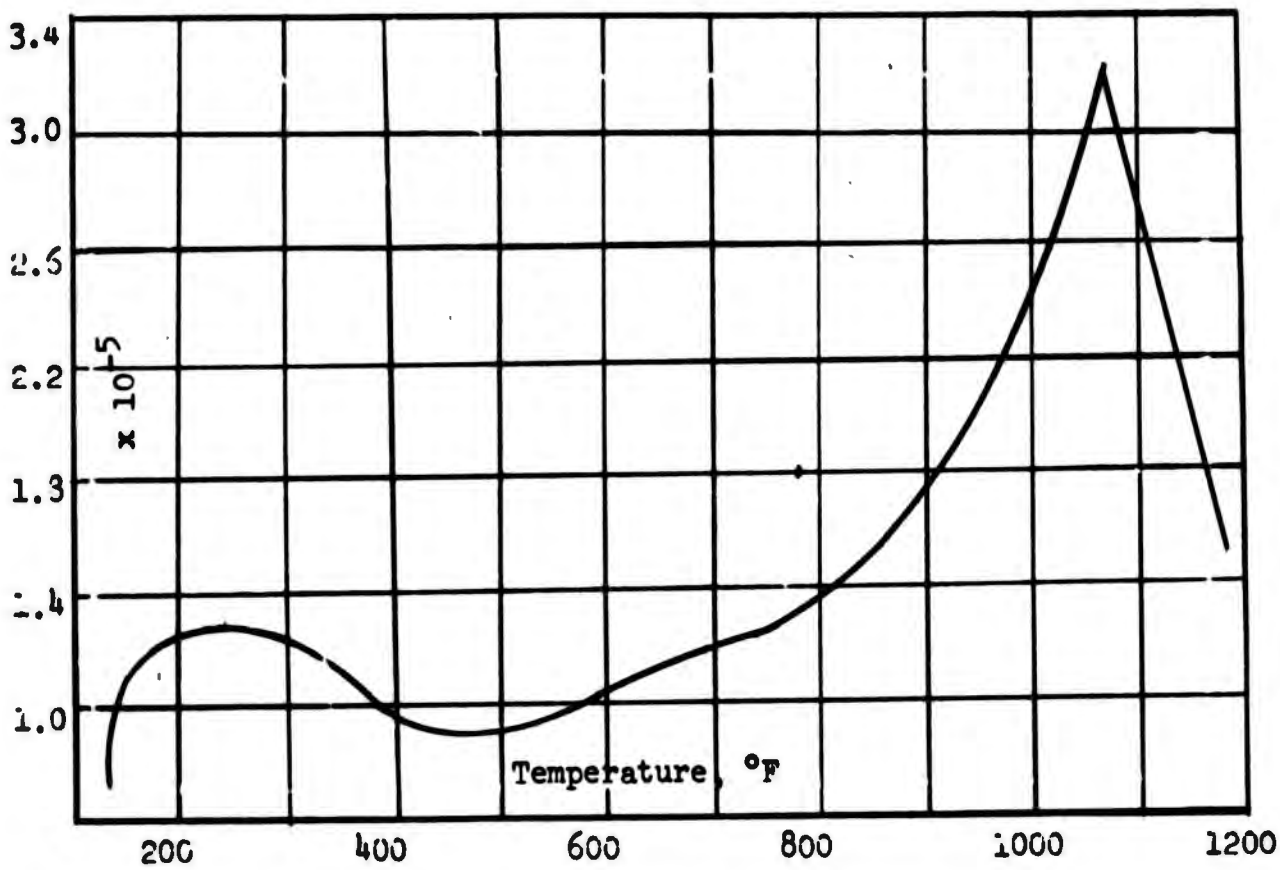

FIGURE 8

PERCENT THERMAL EXPANSION (10% SILICA MODIFIED MATRIX)

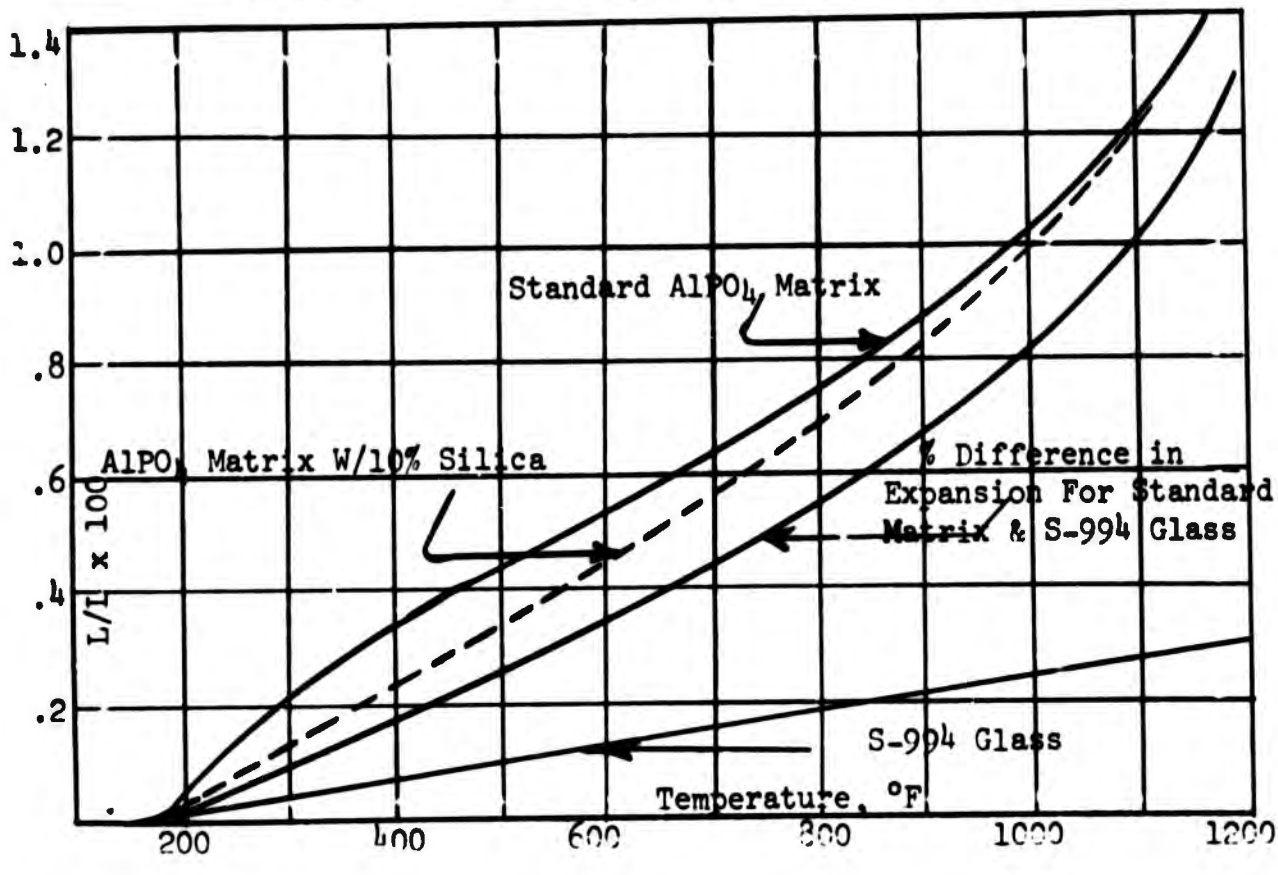

FIGURE 9
SUMMARY OF TARGET GOALS AND ACHIEVEMENTS

ELECTRICAL PROPERTIES Property	Target Goal	Achievements
Dielectric Constant at R.T. & 10.0 KMC	Max. of 5.5	3.44
Dielectric Constant at 1200°F & 10.0 KMC	Max. of 5.5	3.56
Loss Tangent at R.T. & 10.0 KMC	Max. of 0.005	0.0064
Loss Tangent at 1200°F & 10.0 KMC	Max. of 0.02	0.0191
Test Panel Transmission (10.0 KMC ± 60°)	Min. of 85%	85%
Test Phase Reflection (10.0 KMC ± 60°)	Max. of 2.0%	0.2%
Temperature Coefficient of Dielectric Constant	Max. of 5.0×10^{-4}	0.27×10^{-4}
Insertion Phase Delay (10.0 KMC)		Dielectric constant (calculated) varies 0.05 over a 0° to 61.5° incidence angle range

PHYSICAL AND THERMAL PROPERTIES Property	Target Goal	Achievements
Average Thermal Expansion to 1200°F (parallel to ply direction)	----------	$2.2 \times 10^{-}$ °F
Average Thermal Expansion to 1200°F (perpendicular to ply direction)	----------	6.0×10^{-6}/°F
Thermal Conductivity (1200°F)	---------	$4.3 \frac{\text{btu - in}}{\text{hr-ft}^2\text{-°F}}$
Thermal Shock Merit Index	----------	$14.1 \times 10^{3} \frac{\text{btu-in}}{\text{hr-ft}^2}$
Specific Heat (500°F)	----------	Approx. .2 btu/lb/°F
Specific Gravity	----------	1.8
Moisture Absorption (24 hrs) (Laminate aged 200 hours at 1000°F prior to test)	Max. of 1.0%	.63%

FIGURE 9 (Continued)

MECHANICAL PROPERTIES

Property	Target Goal	Achievement
Flexural Strength at R. T.	Min. of 25,000 psi	20,800 psi 32,300 *
Flexural Strength at 1200°F	Min. of 10,000 psi	9,522 psi 25,100 psi at 1100°F
Tensile Strength at R. T.	Min. of 15,000 psi	30,175 psi
Tensile Strength at 1200°F	Min. of 10,000 psi	3,290 psi at 1000°F 6,100 at 1000°F *
Compression Strength at R. T.	----------	5,200 psi
Compression Strength at 1200°F	----------	7,500 psi
Flexural Modulus at R. T.	----------	3.8×10^6 psi
Flexural Modulus at 1200°F	----------	4.2×10^6 psi

* Recent development resulting from modification of matrix.

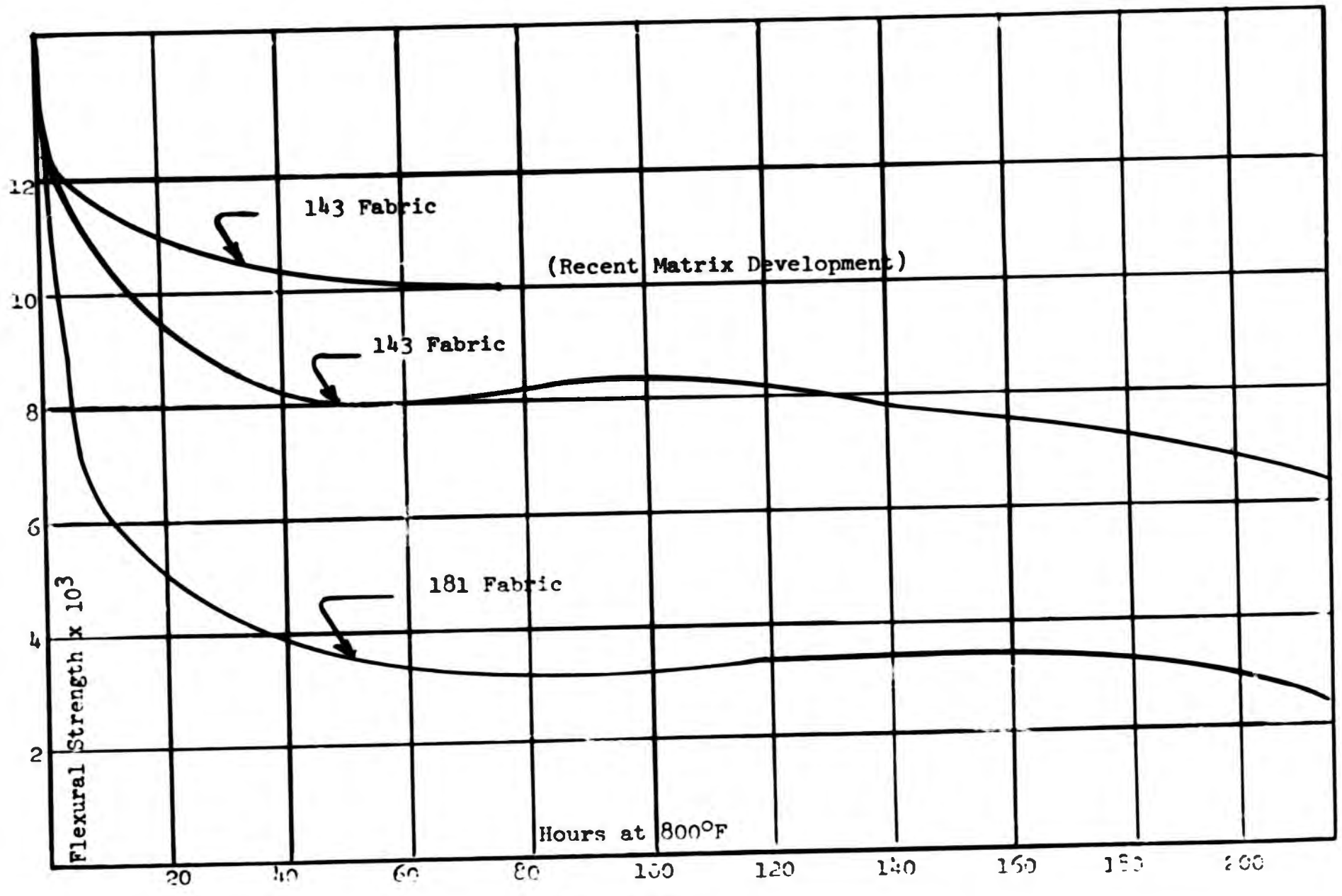

FIGURE 10
Flexural Strength Vs Aging For $AlPO_4$ Laminates

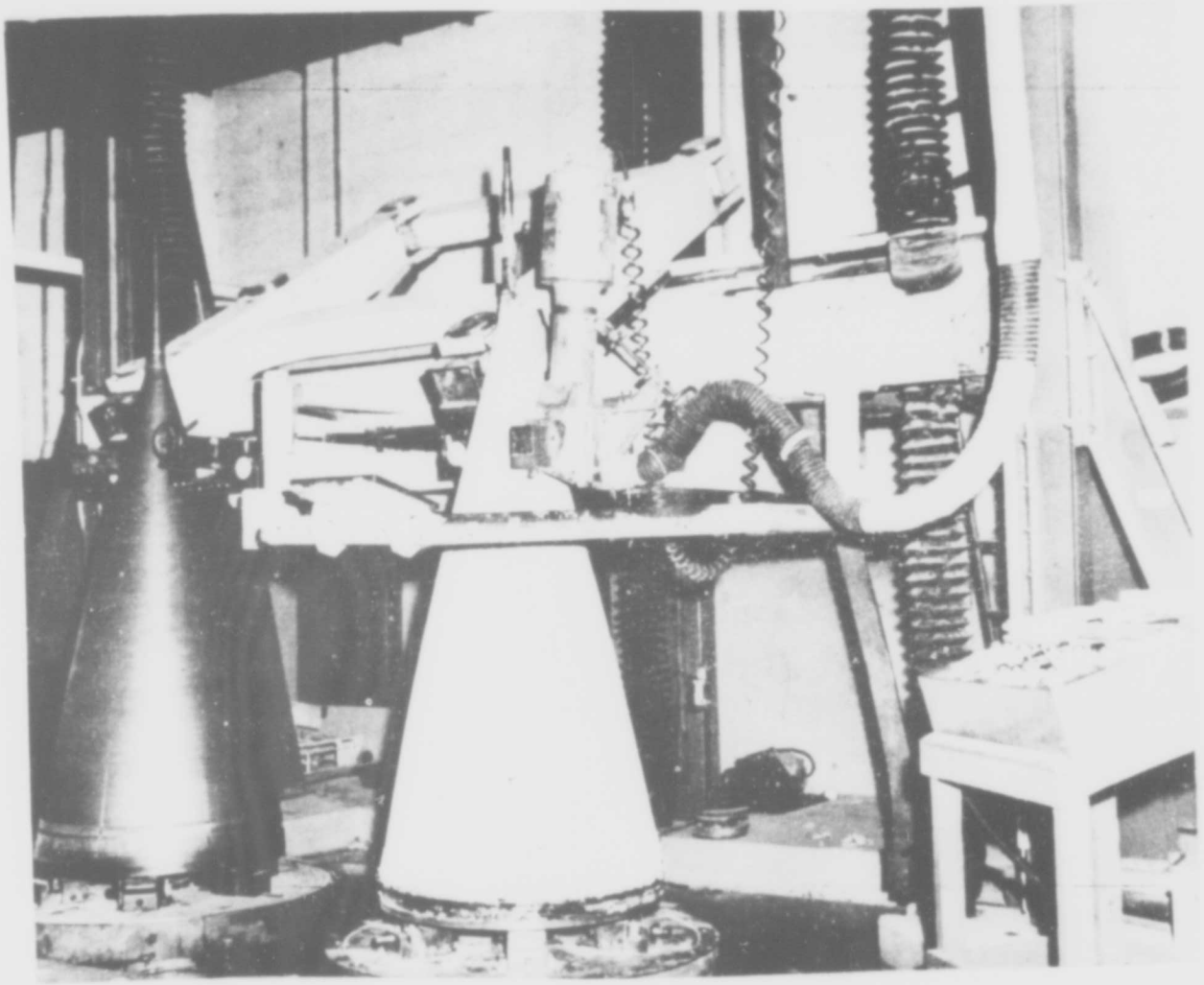

FIGURE 11. GRINDING RADOME TO THICKNESS

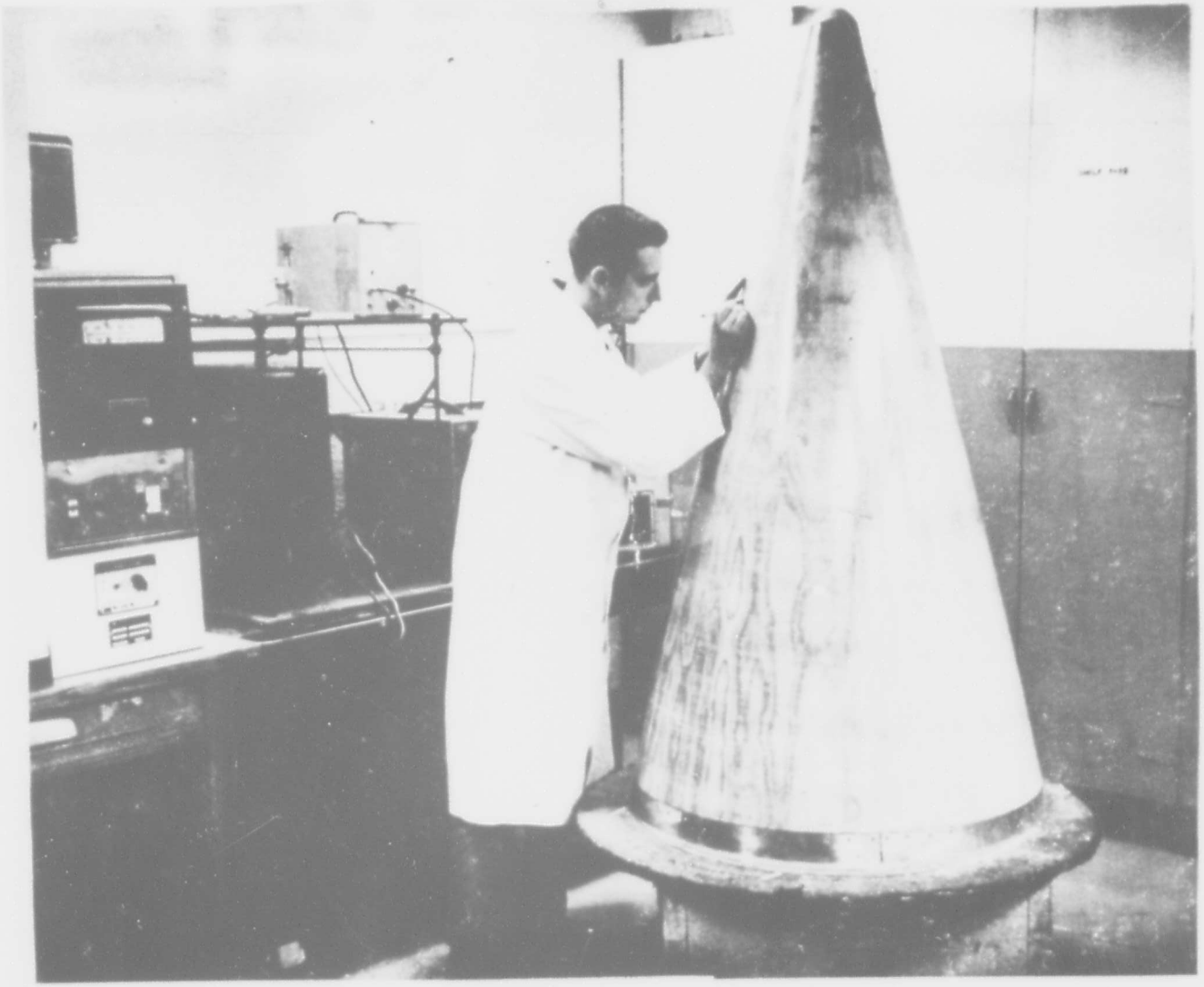

FIGURE 12. FINISHED RADOME

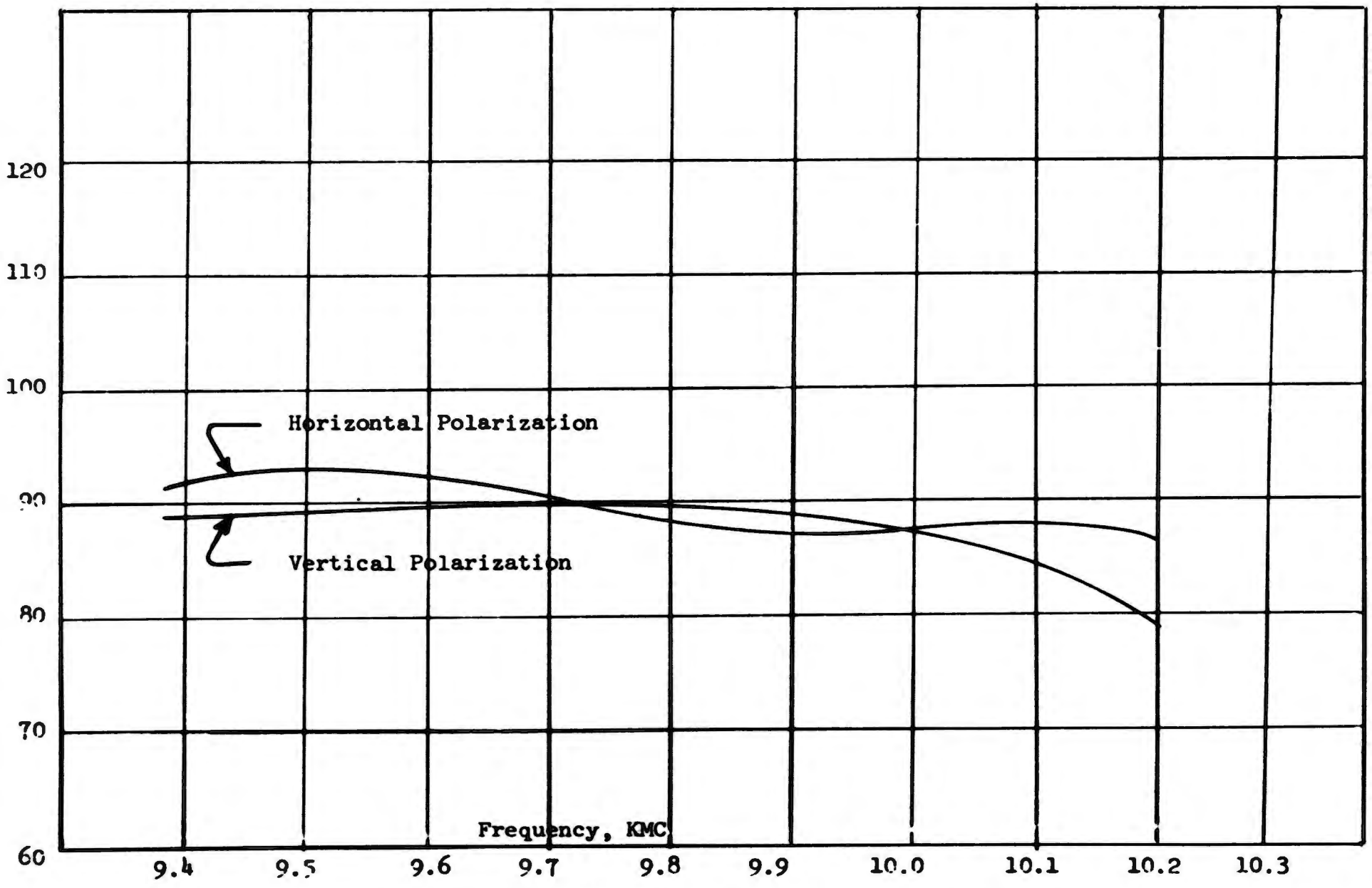

FIGURE 13
RADOME TRANSMISSION AVERAGED OVER ± 40° AZIMUTH SCAN
(ANTENNA LOOK ANGLE - 0° EL. 0° ROLL)

APPENDIX
Item 1

DESIGN ANALYSIS FOR HIGH TEMPERATURE RADOME

Design configuration to be analyzed:

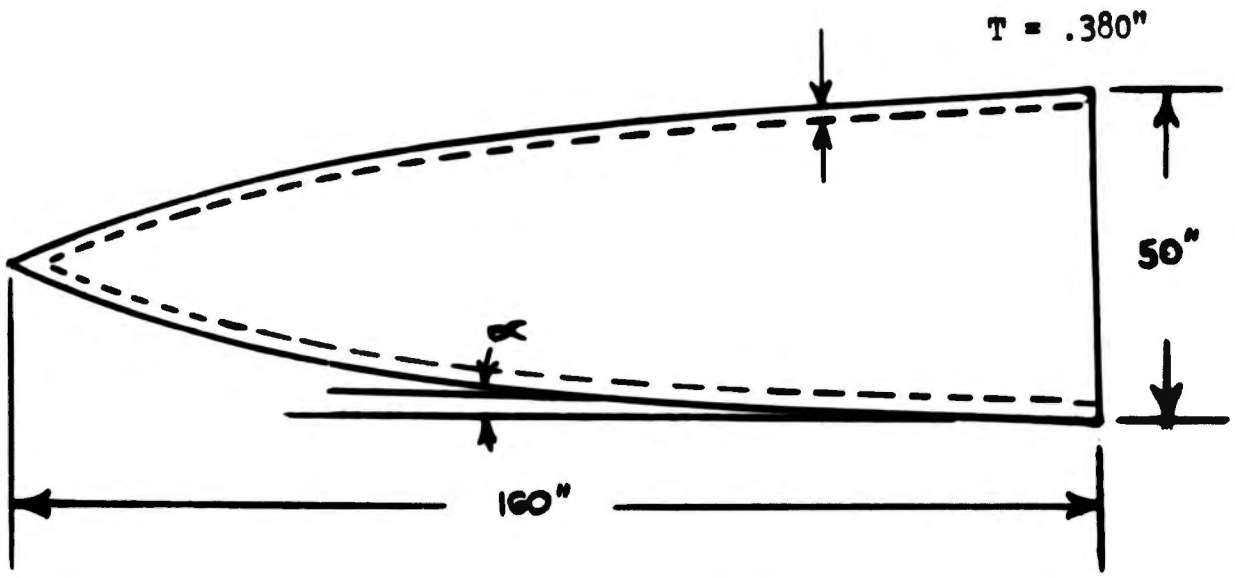

1. Material - S-994 Fabric (181) reinforced phosphate binder.
2. External design limit loads are shown in Figure 1.
3. The wall temperature profile is shown in Figure 2. Nose temperature is 1200°F; temperature at attach area is 900°F.
4. The attachment of the radome to the mating structure is assumed to be continuous, with no high stiffness load paths to cause load concentrations.
5. An ultimate factor of safety of 2.0 shall be used.
6. Allowable material strengths are shown in attached figures.
7. The stresses are determined following:

Due to Bending:

For continuous attachment at the base, the maximum stress due to bending is given by,

$$F_B = \frac{MC}{I \cos\alpha} = \frac{M}{\pi R^2 T \cos\alpha}$$

Where: M = Ultimate Bending Moment

R = Radius at point where stress is desired

T = Wall Thickness

α = Angle between a horizontal line and a tangent to the radome shell at the point where stress is desired

From Figure 3, the limit moment at the base of the radome is, $M_{LIM} = .51 \times 10^6$ pounds. The ultimate moment, then, is, $M_{ULT} = 2.0\ (.51 \times 10^6) = 1.02 \times 10^6$ in pounds.

For the following values, R = 25, T = .380, $\alpha = 5^\circ$, and $M_{ULT} = 1.02 \times 10^6$ the maximum bending stress is, $F_B = \dfrac{1.02 \times 10^6}{(25)^2\ (0.380)(.995)} = 1{,}380$ psi

This stress occurs in tension on the upper surface of the shell and compression on the lower surface.

From Figure 4, the tensile strength of this material at 900°F is, $S_T = 5600$ psi.
From Figure 4, the compressive strength of this material at 900°F is, $S_C = 6200$ psi.
The margin of safety for tensile stress is, M.S. $= \dfrac{5600}{1380} - 1 = 3.06$

The margin of safety for compressive stress is, M.S. $= \dfrac{6200}{1380} - 1 = 3.49$

Stability Check

In order to evaluate the structural stability of the radome, the radome geometry is replaced by a cylinder that has equivalent buckling resistance. An analysis is then performed on the cylinder. The equivalent cylinder is determined on the following page. The shell is first approximated by a frustum of a cone. The frustum is then converted into a cylinder of radius R_{EQ} and length L_{EQ} equal to,

$$L_{EQ} = \left[\frac{R_1 - 1.2\ R_2}{2.2\ R_2} \right] L \qquad R_{EQ} = \frac{R_2}{\cos \alpha}$$

For the values shown in the following sketch, $L_{EQ} = 115$ and $R_{EQ} = 25.1$

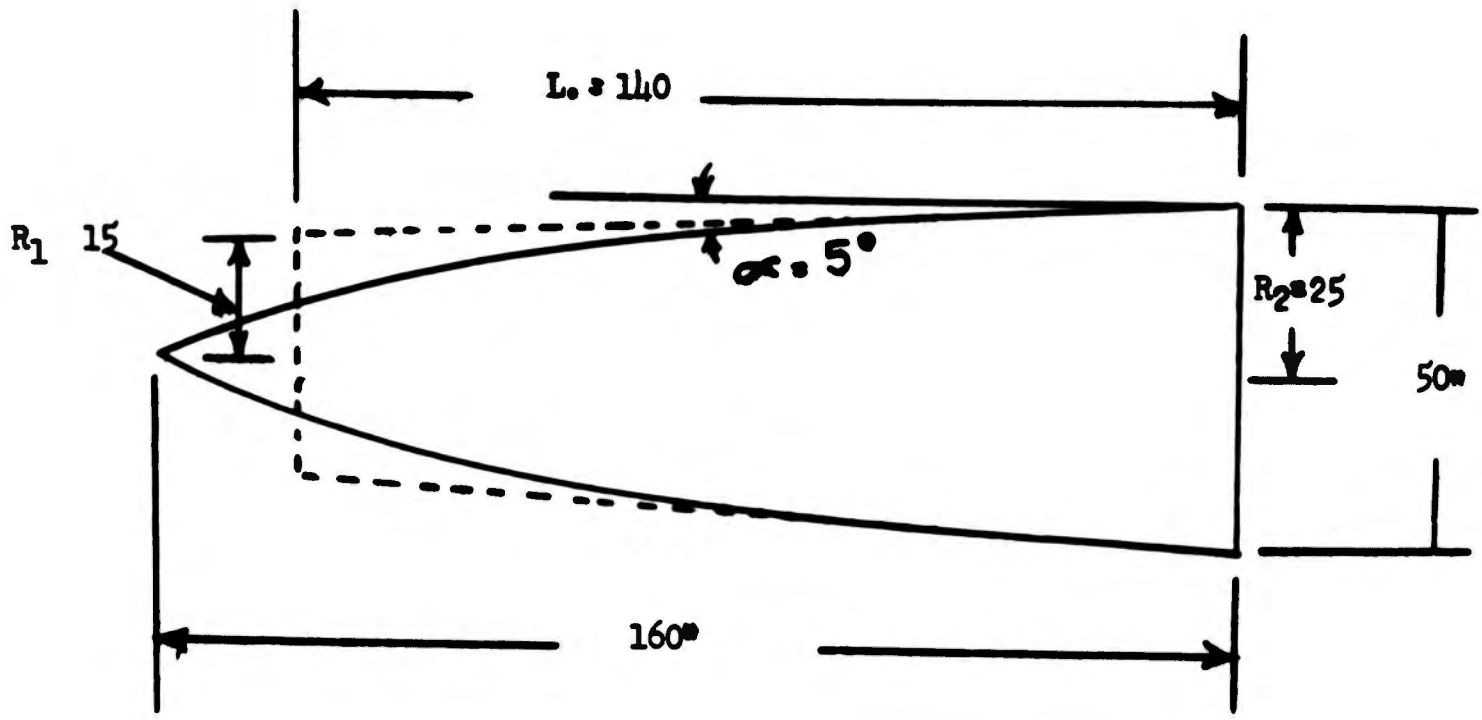

For this particular radome the compressive loading on the bottom surface of the shell (resulting from bending and drag) represents the more severe buckling load. The maximum value of this compressive load at the aft end of the shell is given by,

$$N\phi = \frac{M}{\pi R^2 \cos \alpha} + \frac{D}{2 \pi R \cos \alpha}$$

Where "D" represents the ultimate drag and "M", "R", and α are as previously defined.

For the following values, $M = 1.02 \times 10^6$, $R = 25$, $\alpha = 5^\circ$, and $D = 3400$

$$N\phi = \frac{1.06 \times 10^6}{\pi (25)^2 (.995)} + \frac{3400}{2 \pi (25)(.995)} \approx 556 \text{ \#/In.}$$

Timoshenko and Gere[1] give the following expression for the critical buckling load of a cylindrical shell,

$$N\phi_{CR} = \frac{0.30\ ET^2}{R} \quad \text{if } L > = 2(1.72\ \sqrt{RT})$$

Since $R_{EQ} = 2.51$, $T = .380$ and $L_{EQ} = 115$

$2(1.72)\sqrt{R_{EQ}T}) = 2(1.72\sqrt{25.1(.380)} = 10.6$ ∴ the equation applies. From Figure 2 the flexural modulus for this material at 900°F is, $E = 2.3 \times 10^6$ psi.

The critical buckling load then is:

$$N\phi_{CR} = \frac{0.30\ (2.3 \times 10^6)(.380)^2}{25.1} = 3970 \text{ lbs/in}$$

Thus the margin of safety for stability is:

$$M.S. = \frac{3970}{566} - 1 = 6.02$$

The preceeding analysis verifies the structural feasibility of a high temperature radome.

1 Timoshenko and Gere, Theory of Plastic Stability, McGraw Hill Book Company; New York, New York 1961.

NOTES:

1. Loads shown are limit
2. These loads are applicable at maximum temperature.
3. Higher surface pressures are possbile, but with lower shears and moments.
4. Use straight line pressure variation from one side to other around the periphery.
5. Shear and bending moment are applicable in all cross directions.
6. Drag is in the longitudinal direction.
7. Pressures shown give maximum cross-wise differential and are applicable at at any point around the periphery.

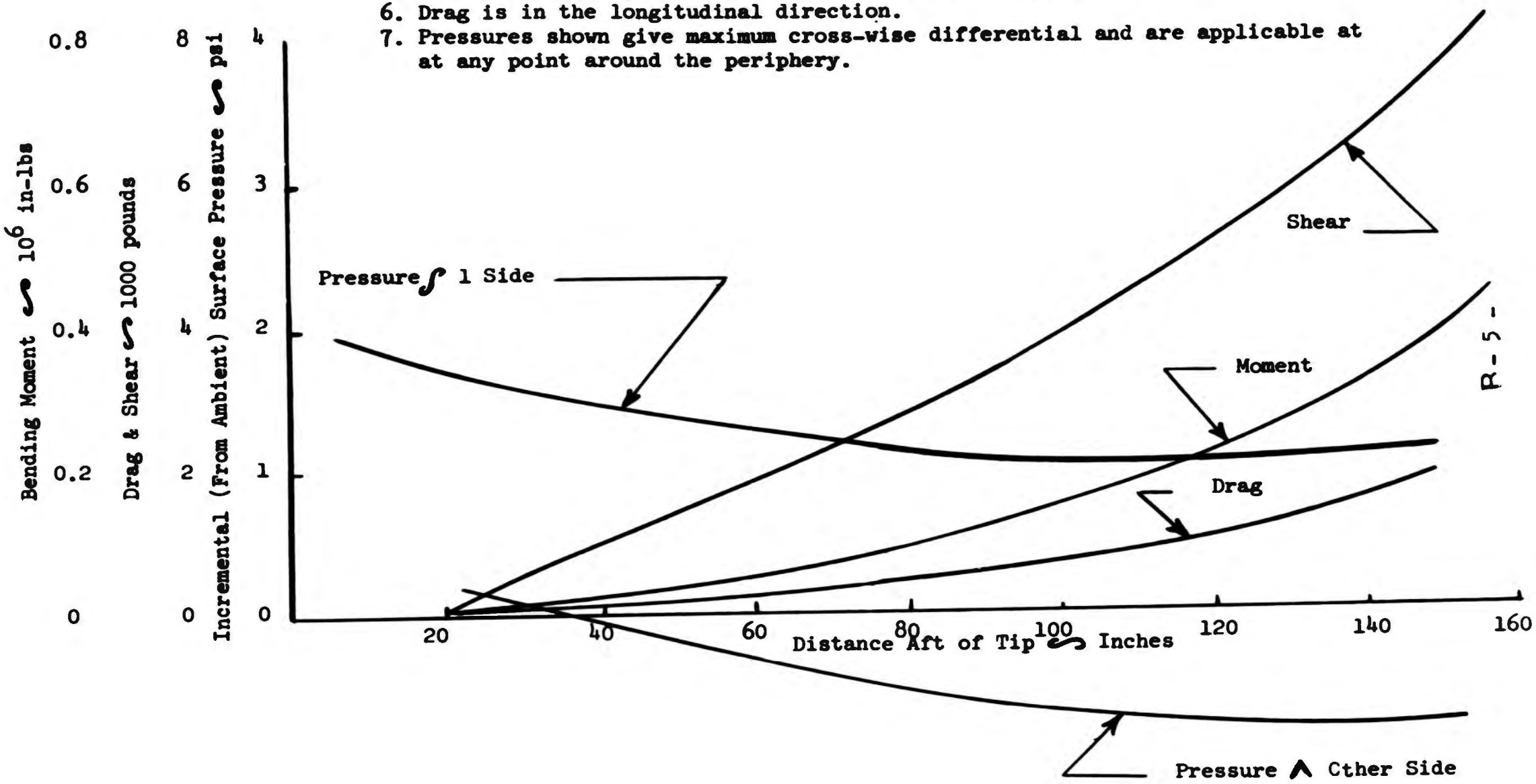

Figure 1
Radome External Loads

Figure 2

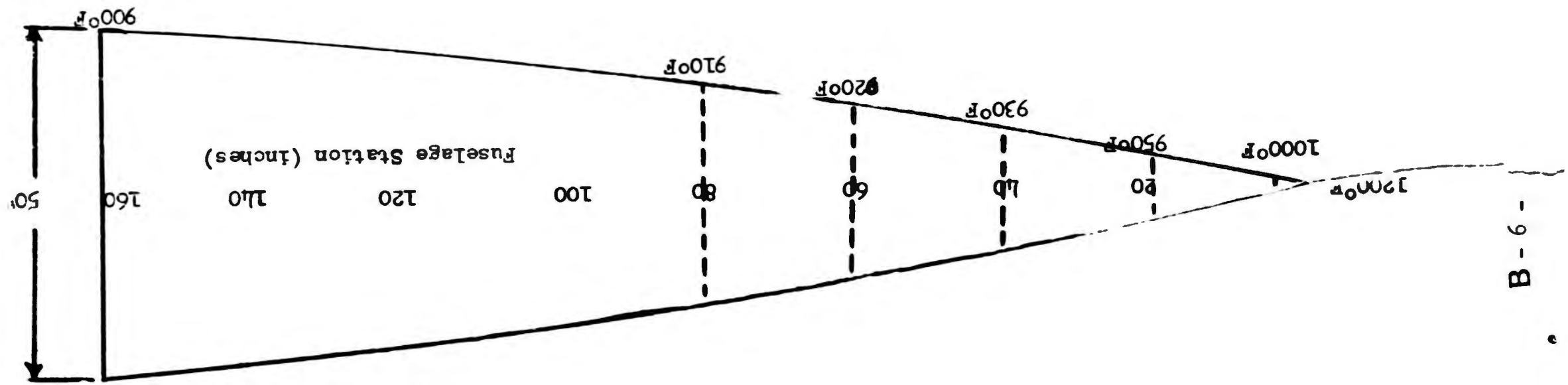
900°F
910°F
920°F
930°F
950°F
1000°F
1200°F
Fuselage Station (inches)
50
160
140
120
100
80
60
40
20

UCRL-7795

UNIVERSITY OF CALIFORNIA
Lawrence Radiation Laboratory
Livermore, California

Contract No. W-7405-eng-48

SILICON NITRIDE AS A HIGH-TEMPERATURE RADOME MATERIAL

William M. Wells

May 19, 1964

C

SILICON NITRIDE AS A HIGH-TEMPERATURE RADOME MATERIAL

William M. Wells

Lawrence Radiation Laboratory, University of California
Livermore, California

ACKNOWLEDGMENTS

This work was done under the auspices of the U. S. Atomic Energy Commission. Douglas W. Hanner and Peter B. Mohr maintained liaison with suppliers doing work sponsored by Lawrence Radiation Laboratory (LRL) elsewhere, and together with Roy S. Cornwell were responsible for generating the bulk of the data produced at LRL. Klaus Ernst was responsible for the electrical measurements.

ABSTRACT

LRL has investigated silicon nitride fairly thoroughly for application as structural elements in high-temperature, air-cooled reactors. Measurements show that it can easily have values for the two common thermal stress parameters which are substantially higher than those for either alumina or beryllia. In addition, its long-time high-temperature strength (to at least 2700°F) is substantially better than either of these two oxides. Its oxidation resistance is very good. Most of its exceptional thermal stress resistance can be attributed to its low modulus of elasticity and low coefficient of thermal expansion. Actual experience with purchase of the same shape made from both alumina and silicon nitride show that the nitride is the cheaper. Of the properties of silicon nitride which are significant in radome applications, the electrical properties are least known. However, the one available published value of dielectric constant (9.4) seems reasonable.

INTRODUCTION

LRL has the responsibility of demonstrating the feasibility of a reactor for use as a power plant for a low-altitude, high-Mach-number missile. This reactor is literally a very high power air heater which must work at temperatures in excess of 2000°F. The reactor is exposed to high loads so one of the primary problems is providing high temperature structure. Considerable effort has been devoted to developing ceramic structural elements. One of the materials considered for this purpose is silicon nitride. In ceramic structural elements operating over large temperature ranges, a major problem is coping with thermal stress. In this respect there is a similarity with the radome problem. The work on silicon nitride at LRL consisted of limited fabrication studies (principally for familiarization), measurement of properties of interest to the application, and funding of fabrication scale-up efforts.

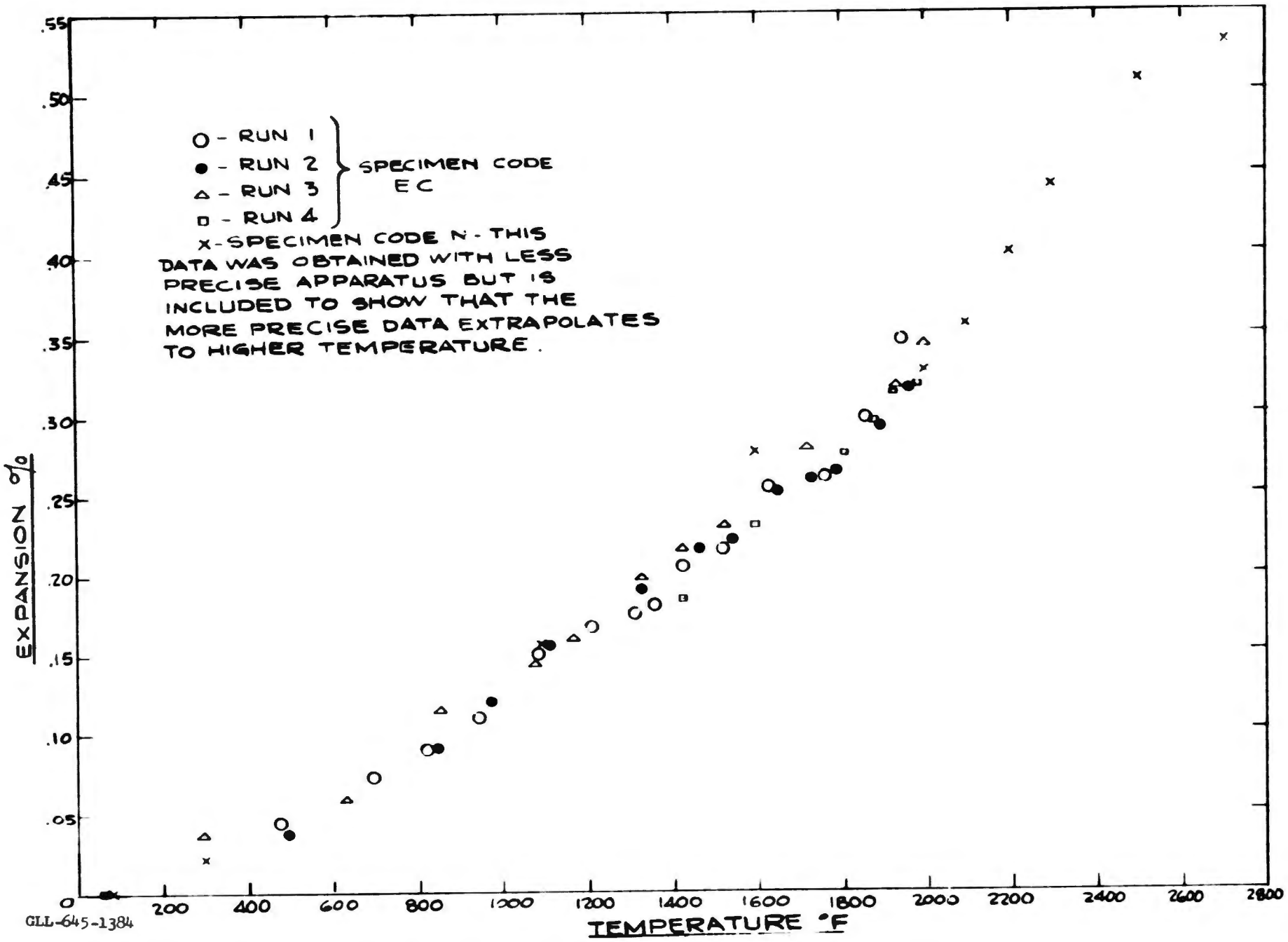

Fig. 1. Thermal expansion of silicon nitride.

PROPERTIES AND DATA

Silicon nitride occurs in two crystalline forms having nearly the same density and similar crystallographic structure. The density of the two forms is as follows: α phase, 3.16 g/cc; β phase, 3.15 g/cc. These densities were determined from lattice constants taken from ref. 1. Apparently the temperature at which the nitride forms is the most important factor in determining which phase forms.[2] Insofar as we were able to determine, no reason has been found for preferring one phase over the other.

Bulk densities of the reaction-sintered material cover the range of about 2.0-2.6 g/cc, implying a porosity of 17.6 to 36.6%. While we are not aware of permeability measurements, it is clear that some permeability is required for nitridation to occur. If impermeability is required in the application, resort to some sealing technique would be required. Observation of oxidation specimens and bend strength specimens which were held at high temperatures for substantial times shows that a glassy layer forms which may be useful in this connection.

Figure 1 shows an expansion curve produced at LRL. The room temperature coefficient of expansion from this data is $1.1 \times 10^{-6}/°F$ and the average coefficient of expansion between room temperature and 2800°F is $2.0 \times 10^{-6}/°F$. The specimen was $4 \times \frac{1}{2} \times \frac{1}{2}$ in. and its bulk density was approximately 2.3 g/cc (for runs 1-4).

Table 1 gives modulus-of-rupture data for silicon nitride specimens at various temperatures for samples purchased by LRL from several sources. The samples were all $\frac{1}{2} \times \frac{1}{2} \times 5$ in. and were loaded in three-point bending on a span of 4 in.

Two values of modulus of elasticity were obtained at LRL. These were obtained by driving a $\frac{1}{2} \times \frac{1}{2} \times 5$ in. bar at its fundamental vibrational mode, measuring the frequency, and calculating the modulus. The data is in Table 2.

Thermal conductivity was measured in an apparatus developed principally for thermal stress measurements in ceramics.[3] Because it produces a radially outward heat flow which is easily measured electrically, it is readily adaptable to thermal conductivity measurement. Holes are drilled in the specimen as shown in Fig. 2. Since our primary interest was in high temperatures, the temperature measurement was made with an optical pyrometer thus setting a low temperature limit at which the measurement could be made. Having the power flow, the geometry, and the temperatures at two points, the thermal conductivity can be readily obtained. This has proven to be an easy and repeatable technique, though not highly precise. The specimens are approximately $1\frac{1}{4}$ in. o.d. $\times \frac{1}{4}$ in. i.d. $\times 1\frac{1}{4}$ in. long. The data is given in Figs. 3-7.

Approximate values of two thermal stress parameters, $\sigma K/E\alpha$ and $\sigma/E\alpha$, were obtained in the course of the tests which yielded the thermal conductivity values. The technique used is described in ref. 3. In the course of raising the radially outward power flow to measure thermal conductivity the thermal stress can be expressed in terms of this power

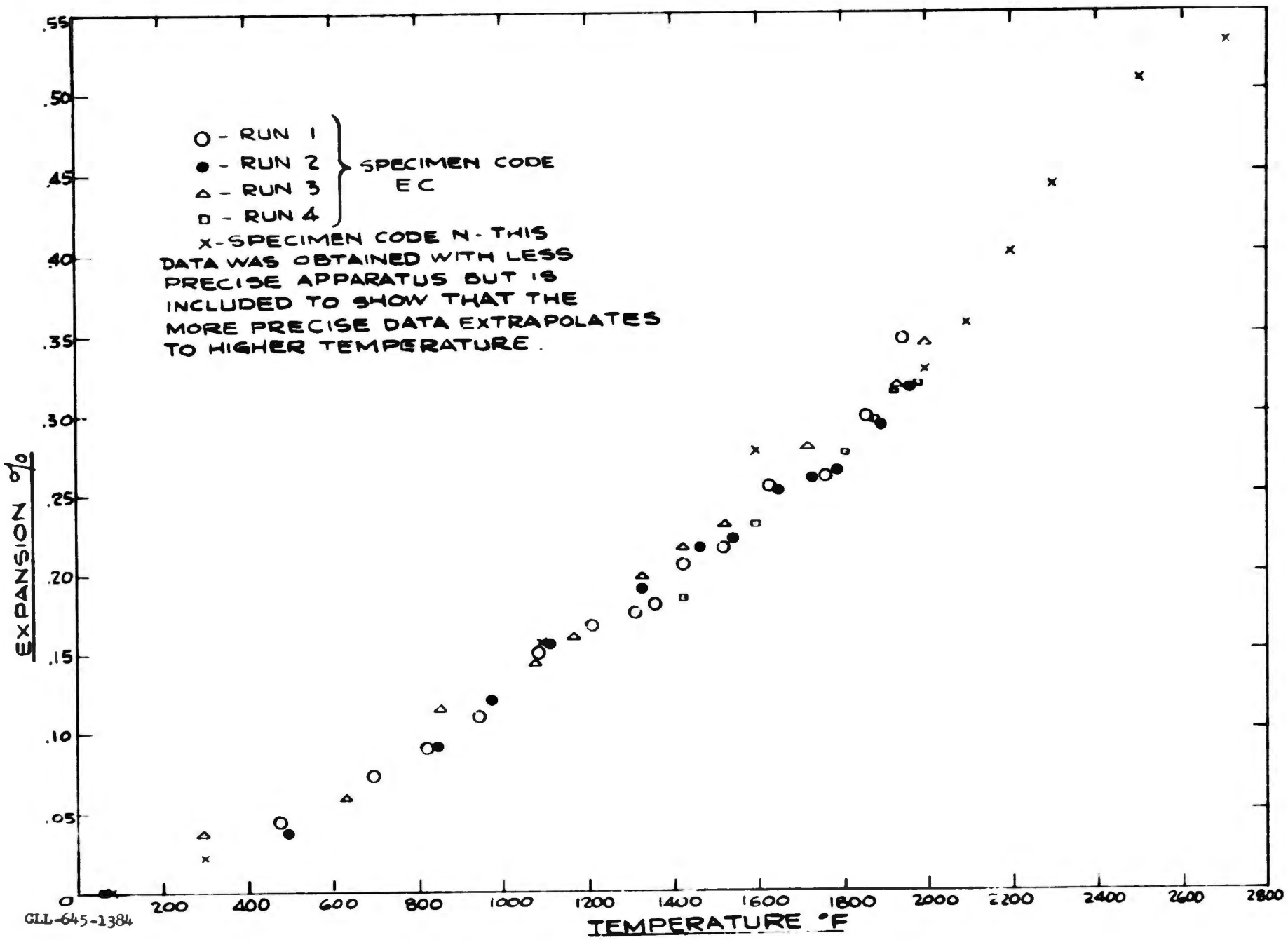

Fig. 1. Thermal expansion of silicon nitride.

Table 1. Modulus-of-rupture results for silicon nitride.

Specimen No.	Bulk density (g/cc)	Fracture temp (°F)	Modulus of rupture (psi)	Remarks
Group A				
H-1-FB	2.40	2700	15,000	Stress constant for 60 sec before fracture
H-3-FB	2.30	"	16,200	
H-4-FB	2.37	"	17,000	
H-5-FB	2.35	"	20,000	Specimen did not fracture
H-6-FB	2.40	"	19,400	
H-7-FB	2.40	2500	20,400	
H-8-FB	2.34	2700	8,500	
H-9-FB	2.40	"	11,300	Stress constant for 21 min before fracture
Group B				
EC-1-FB	2.25	2700	10,400	
EC-2-FB	2.27	"	14,600	At 2700°F for 19 hours before fracture (unstressed)
EC-9-FB	2.27	"	9,400	
EC-10-FB	2.27	"	10,700	
EC-16-FB	2.27	"	9,900	
EC-18-FB	2.27	"	12,700	
EC-19-FB	2.27	"	12,800	
EC-20-FB	2.26	"	14,100	One full cycle to 2700°F before fracture (unstressed)
EC-12-FB	2.29	72	8,800	
EC-13-FB	2.21	"	8,400	
EC-11-FB	2.25	"	8,400	
EC-14-FB	2.30	"	10,400	
EC-15-FB	2.22	"	8,500	
EC-6-FB	2.20	2850	7,500	
EC-8-FB	2.27	"	8,100	
EC-3-FB	2.30	72	8,900	One full cycle to 2700°F before fracture (unstressed)
EC-4-FB	2.26	"	9,700	
Group C				
N-7-FB	2.26	2700	11,500	One full cycle to 2700°F before fracture (unstressed)
N-2-FB	2.32	"	19,500	
N-16-FB	2.29	"	13,400	
N-18-FB	2.42	"	22,800	
N-4-FB	2.24	"	9,900	
N-17-FB	2.32	"	27,000	
N-13-FB	2.43	"	14,000	
N-8-FB	2.44	"	14,900	
N-14-FB	2.30	"	13,400	
N-11-FB	2.32	"	18,100	
N-6-FB	2.44	"	20,400	At 2700°F for 19 hours before fracture (unstressed)
N-1-FB	2.31	72	11,400	

Table 1. (Continued)

Specimen No.	Bulk density (g/cc)	Fracture temp (°F)	Modulus of rupture (psi)	Remarks
Group C (Continued)				
N-3-FB	2.20	72	12,400	
N-5-FB	2.43	"	5,200	
N-19-FB	2.29	"	1,300	One cycle to 2700°F before fracture (unstressed)
N-20-FB	2.30	"	1,340	
N-12-FB	2.23	2850	11,600	
N-10-FB	2.21	"	2,270	One full cycle to 2700°F before fracture (unstressed)
N-9-FB	2.31	72	1,220	
Group D				
CS-5-FB	2.06	2700	7,300	One full cycle to 2700°F before fracture (unstressed)
CS-8-FB	2.16	"	7,000	
CS-2-FB	2.12	"	7,400	
CS-10-FB	2.10	"	5,100	
CS-4-FB	2.11	72	4,200	
CS-6-FB	2.08	"	3,900	
CS-7-FB	2.10	"	3,200	
CS-3-FB	2.09	2700	7,800	
CS-1-FB	2.08	2850	6,000	
Group E				
Y-4-FB	2.17	2700	7,500	One cycle to 2700°F before fracture
Y-5-FB	2.38	"	9,700	
Y-2-FB	2.31	"	11,200	
Y-3-FB	2.26	"	8,900	
Y-8-FB	2.30	"	10,000	
Y-9-FB	2.30	"	9,500	At 2700°F 19 hours before fracture (unstressed)
Y-7-FB	2.11	72	3,500	
Y-10-FB	2.22	"	5,800	
Y-6-FB	2.36	"	6,000	
Group F				
Y-20-FB	2.50	2700	20,800	At 2700°F 19 hours before fracture (unstressed)
Y-11-FB	2.49	"	13,800	
Y-12-FB	2.45	"	12,000	
Y-13-FB	2.48	"	20,600	
Y-14-FB	2.49	"	17,000	
Y-15-FB	2.47	"	16,000	
Y-18-FB	2.49	2850	15,500	
Y-17-FB	2.42	72	8,200	
Y-19-FB	2.41	"	8,500	

Table 2. Modulus of elasticity for two silicon nitride specimens.

Specimen code	Density (g/cc)	Modulus of elasticity (10^6 psi)
H	2.35	15.1
EC	2.25	9.6

flow[4] and it can be expressed as follows for the plane stress case (that for a thin washer specimen):

$$\frac{\sigma K}{E\alpha} = \frac{q}{4\pi}\left[1 - \frac{2}{(b/a)^2 - 1}\ln\frac{b}{a}\right] \qquad (1)$$

where

σ = stress,
K = thermal conductivity,
E = modulus of elasticity,
α = expansion coefficient,
q = power flow per unit of axial length,
b = outer radius,
a = inner radius.

For the case of plane strain (very long cylinder) the relationship is altered by the multiplier $(1 - \nu)$ on the right-hand side, where ν is Poisson's ratio. The quantity on the left-hand side of the equation has generally been called a thermal stress parameter. In general the temperatures are in a range where some deviation from elastic action occurs, thus equation (1) has some invalidity. For this reason we have chosen to call the data obtained from such tests with equation (1) an "apparent" thermal stress parameter.

During the course of the thermal conductivity test, as the power and temperature were raised the specimen cracked, allowing light to be seen along the cracks. Power and specimen temperature were recorded at that point. Equation (1) allows computation of the apparent thermal stress parameter from power and geometry. Table 3 gives data obtained in this fashion. Because of the relatively small number of data points and other uncertainties, this data must be regarded as approximate.

Table 3. Thermal stress parameters.

Specimen code	Density (g/cc)	Apparent $\frac{\sigma K}{E\alpha}$ (watts/in.)	Inner radius temp at fracture (°F)	K (from Figs. 3-7) $\left(\frac{\text{Btu-in.}}{\text{ft}^2\text{-°F-hour}}\right)$	Apparent $\frac{\sigma}{E\alpha}$ (°F)
H	2.3(approx)	27	2100	40	330
EC	2.1	31	Not recorded	60(approx)	250
LRL	2.5	30	2370	100	150

The last specimen was treated as a case of plane strain, since its L/D was about 2. The others were treated as cases of plane stress, since their L/D was about 1. Experience justified this to some degree.[3] An experimental

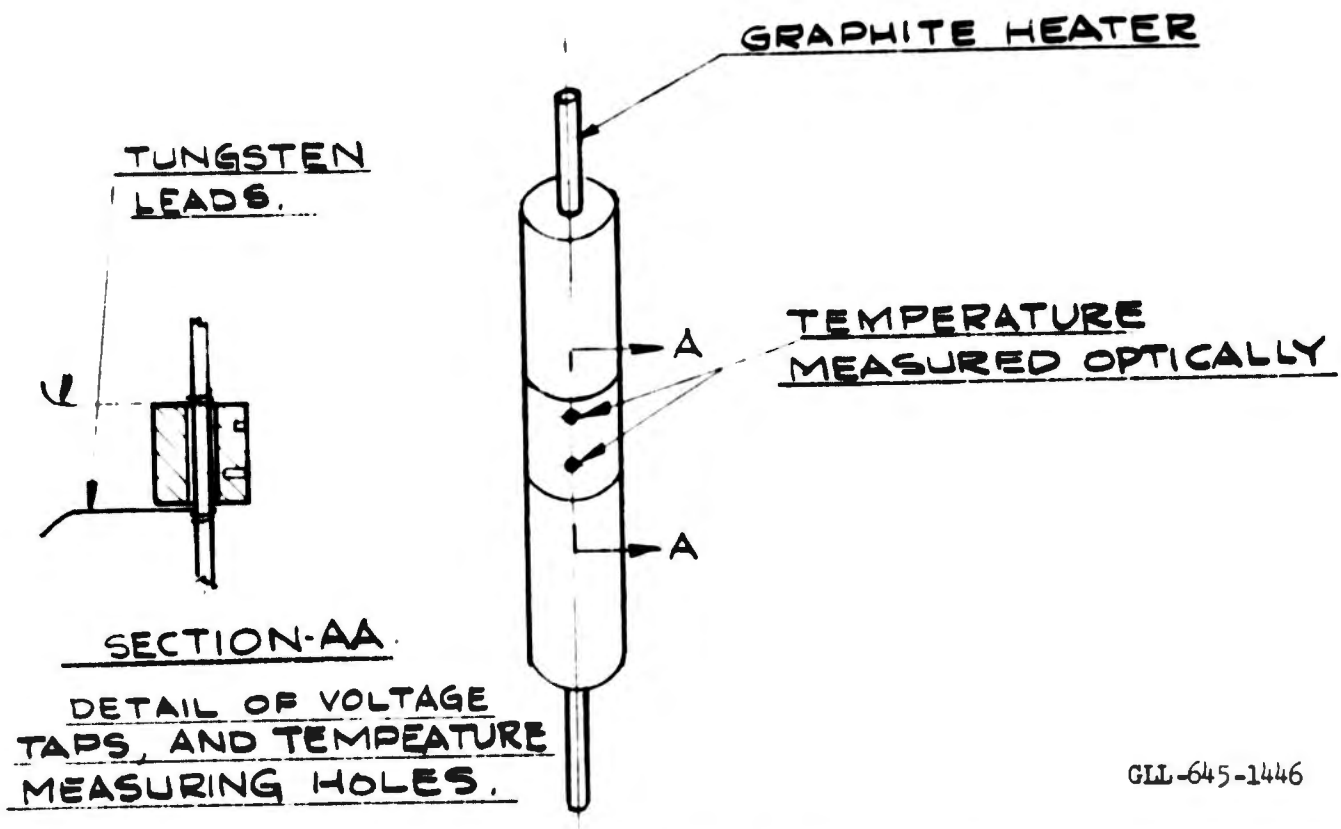

Fig. 2. Specimen configuration and test setup for measuring thermal conductivity. The measurement is made under thermal stress in an argon atmosphere.

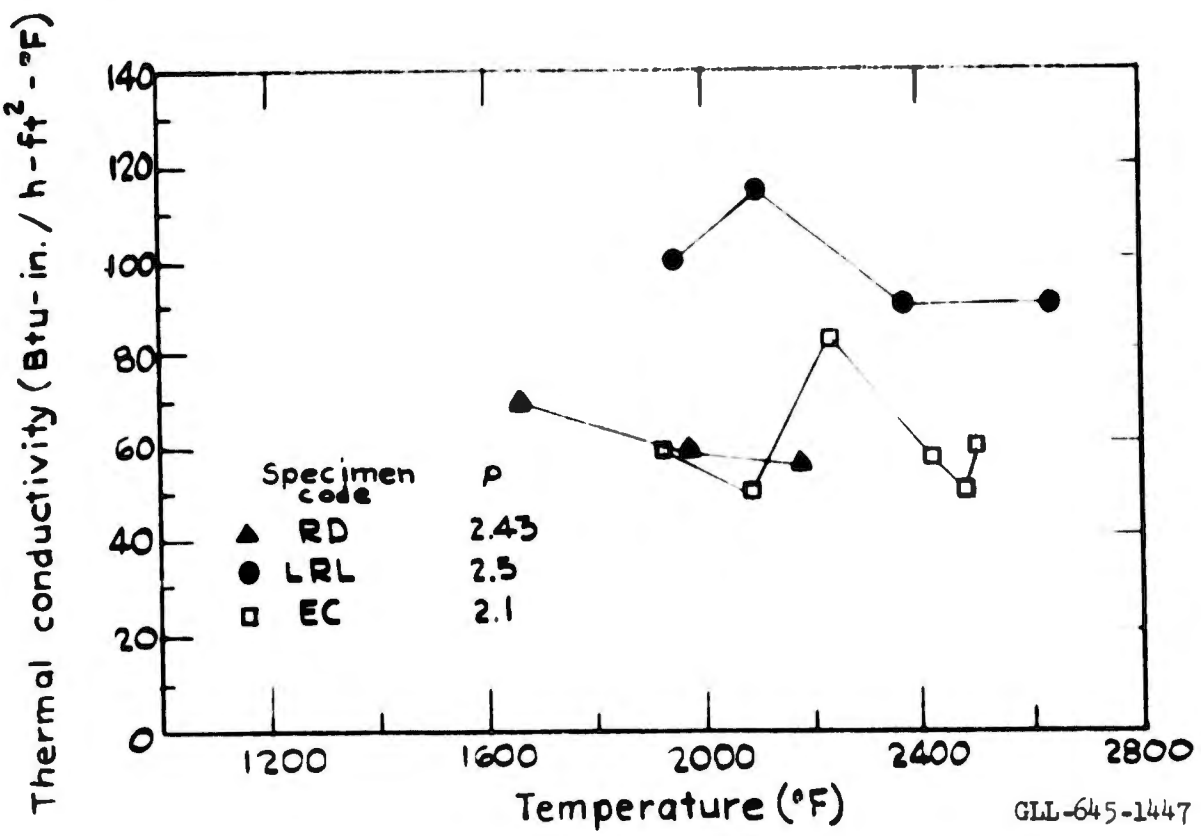

Fig. 3. Thermal conductivity of silicor nitride of various densities.

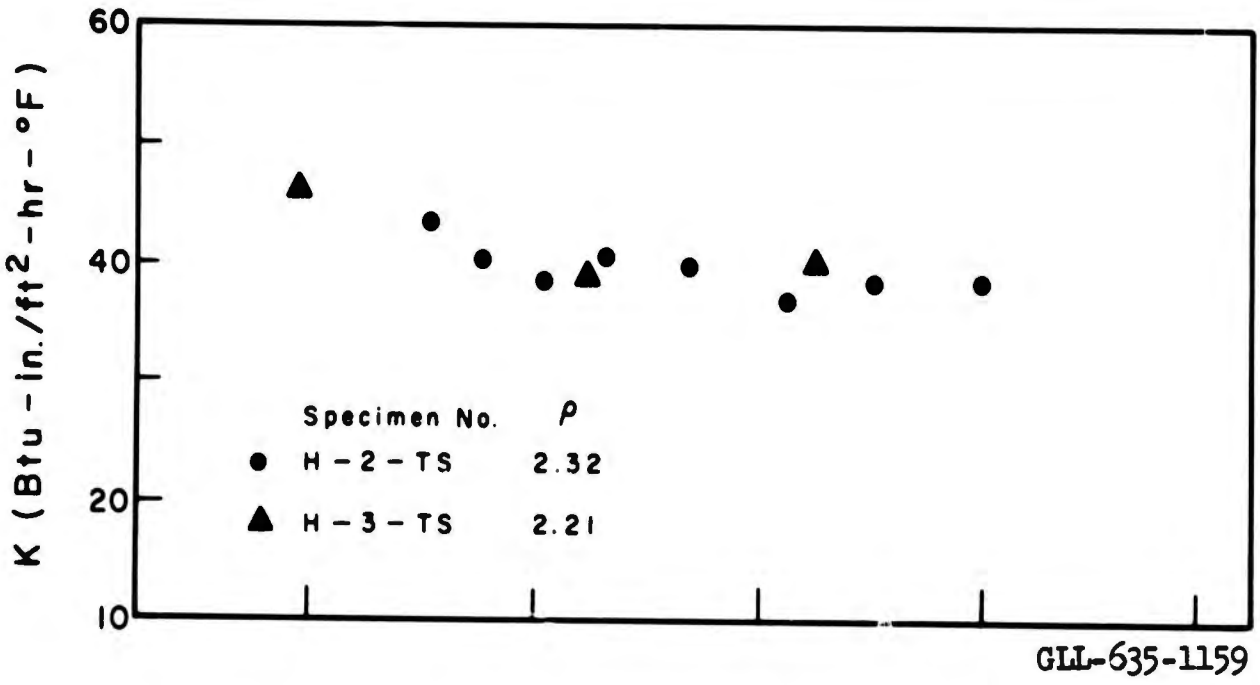

Fig. 4. Thermal conductivity of silicon nitride (group A).

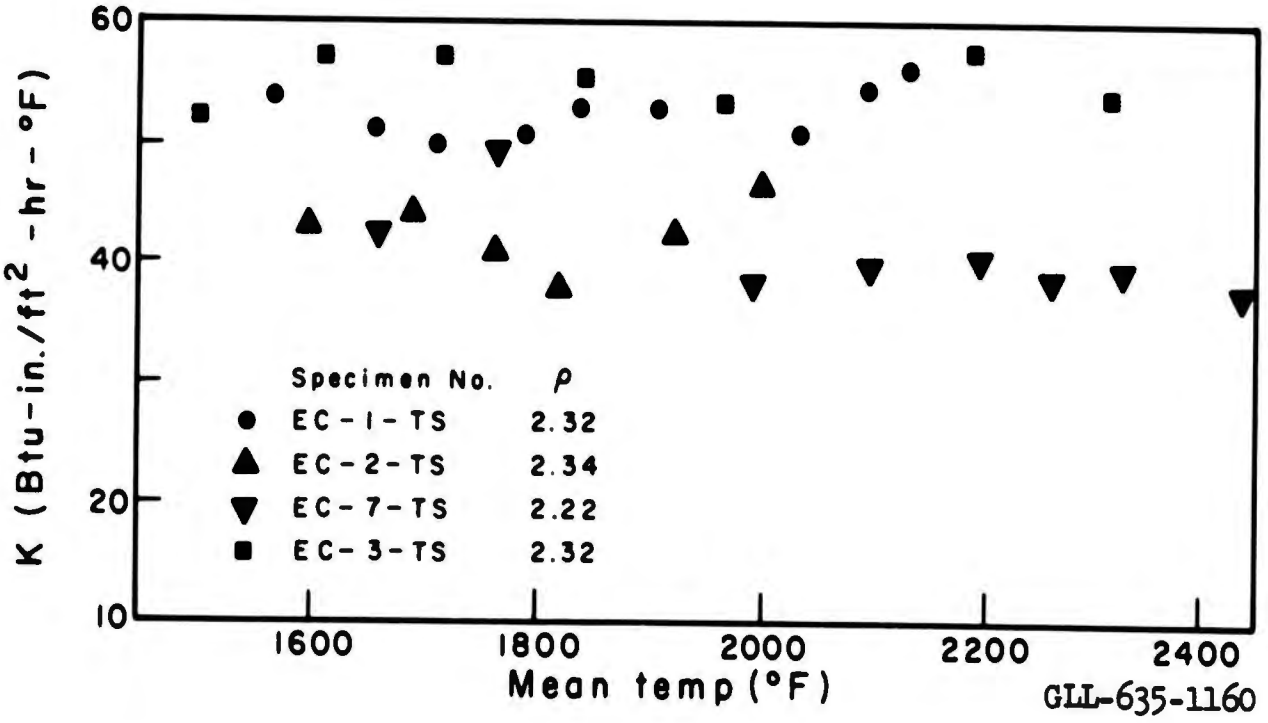

Fig. 5. Thermal conductivity of silicon nitride (group B).

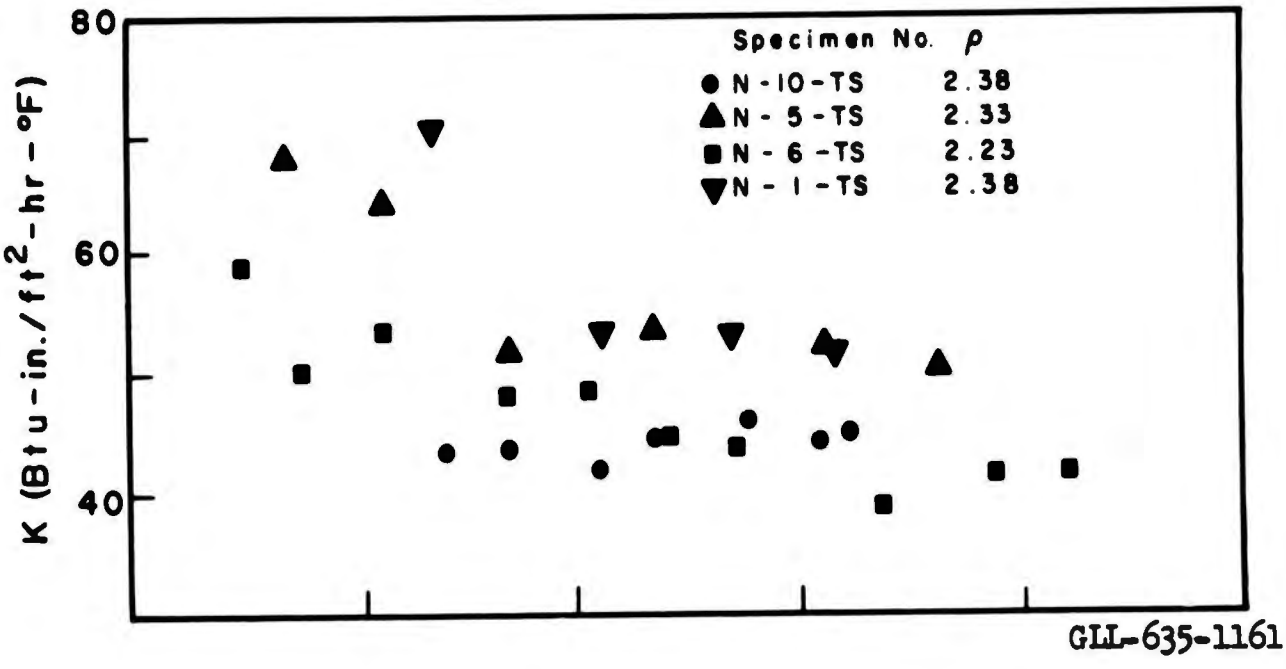

Fig. 6. Thermal conductivity of silicon nitride (group C).

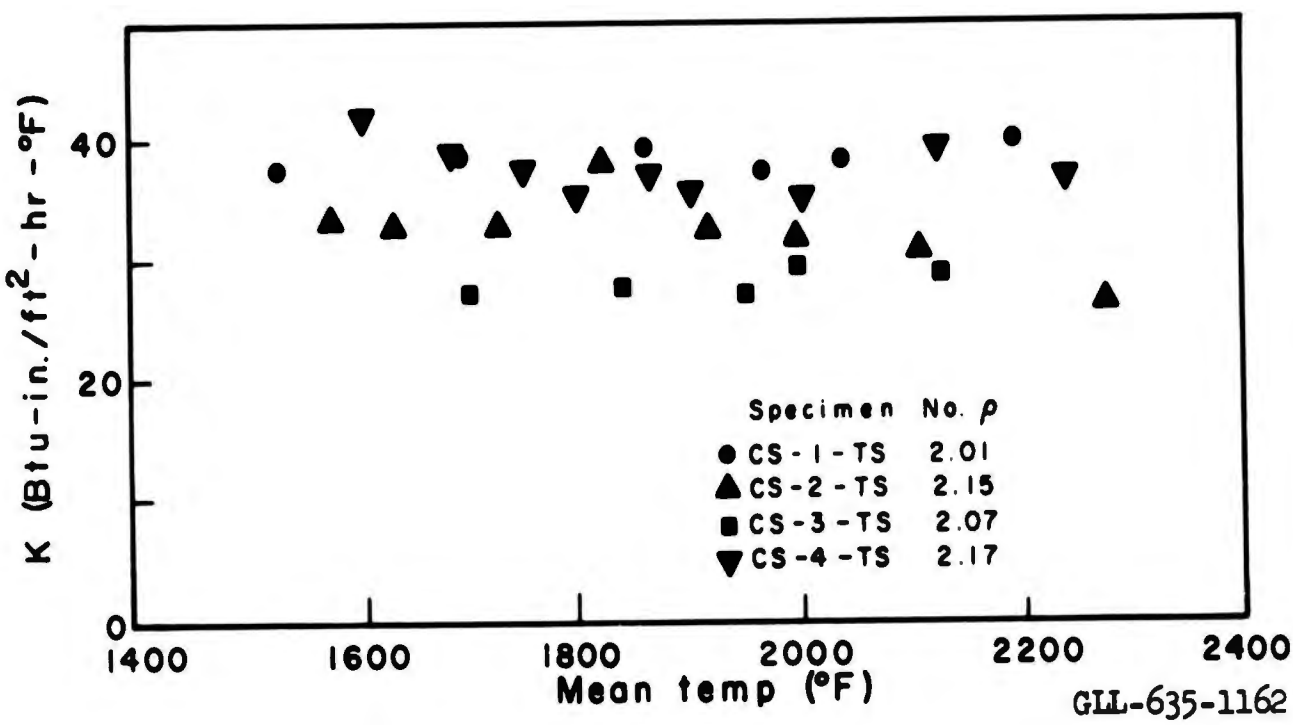

Fig. 7. Thermal conductivity of silicon nitride (group D).

study with Al_2O_3 specimens,[5] dealing specifically with the effect of L/D on cracking, provides further justification.

The value of $\sigma/E\alpha$ was obtained by dividing $\sigma K/E\alpha$ by the value of thermal conductivity K. The significance of this second thermal stress parameter becomes apparent when it is realized that expressions for thermal stress in common situations where there are no severe stress concentrations can be put in the form

$$\sigma = CE\alpha\Delta T$$

where C has a value generally like $\frac{1}{2}$. This makes it apparent that the temperature difference in the piece necessary to cause cracking is about twice the value of $\sigma/E\alpha$. It is apparent that it is necessary to develop ΔT's in silicon nitride of 300 to 700°F in order to cause fracture.

Reference 3 shows typical values of $\sigma K/E\alpha$ in BeO of less than 20 watts per inch. The corresponding value of $\sigma/E\alpha$ is about 85°F. Reference 3 shows a few data points for BeO where the apparent $\sigma K/E\alpha$ approaches those of Si_3N_4, but this is primarily because the BeO is very fine grained and exhibits large creep strains. Because of this it is probably inappropriate to compare Si_3N_4 with these few BeO data points. BeO is generally regarded as comparable to or superior to Al_2O_3 in the two thermal stress parameters, depending principally on the temperature range.

Figure 8 gives compressive creep data obtained on two specimens. The data was obtained in an apparatus which was developed principally for taking data in BeO.[6] The specimens were 3/4 in. in diameter by 2 in. long. Sapphire extensometer rods rested in small gauge holes 1 in. apart on the side of the specimen for strain measurement.

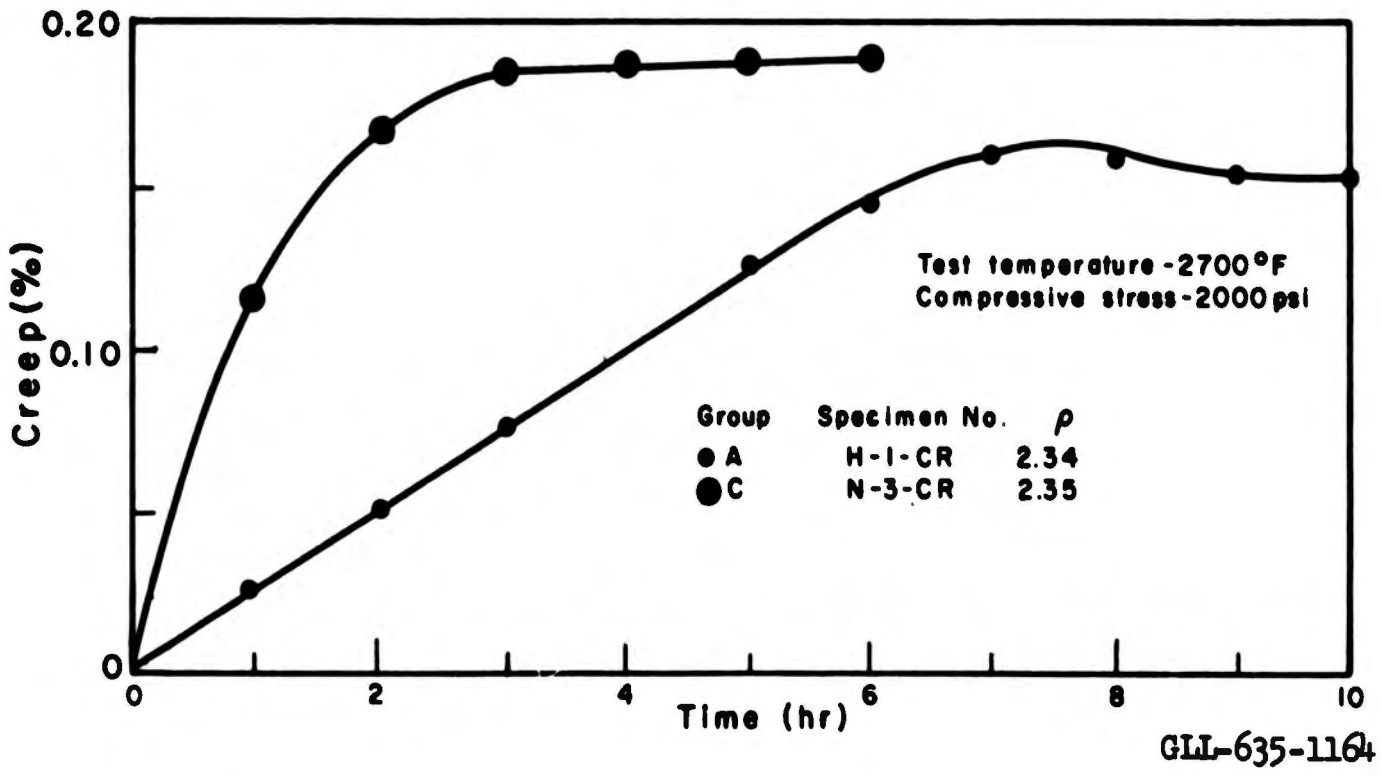

Fig. 8. Compressive creep data for silicon nitride.

Several specimens with densities between 2.1 and 2.5 g/cc were exposed to 2700°F in static air at 1 atmosphere for times up to 60 hours. The weight changes were all increases and were mostly less than ½%. This would seem to indicate satisfactory oxidation behavior for radome application at temperatures where the properties are otherwise satisfactory. This data is supported to some degree by some of the long exposures described in Table 1. Exposure at high air pressures and flow rates also indicate satisfactory performance. This data is somewhat at variance with that reported on p. 205 of ref. 7 and on p. 3 of ref. 8. Both of these indicate relatively poor oxidation behavior above 2550°F.

Exposures under vacuum conditions, however, produce less satisfying data. A specimen fabricated at LRL having a density of 2.33 g/cc and an initial weight of 3.15 g was exposed in vacuo at 2500°F. At 17 hours it had lost 7.1% of its weight, and at 57 hours it had lost 20.7% of its weight. This may also occur at reduced pressures of air.

Only one value of dielectric constant and one value of loss tangent were found. Reference 9 gives a dielectric constant of 9.4 and a loss tangent of 0.001-0.01 at 1 Mc. Because of the paucity of data on electrical properties of interest, room temperature measurements were made of the dielectric constant. These measurements were made using a transmission line method.[10] They were made over a frequency range of 8.2-12.4 kMc and are given in Table 4.

Table 4. Dielectric constant measured at 8.2-12.4 kMc.

Specimen code	Density (g/cc)	Dielectric constant ϵ'
H	2.37	5.5 ± 0.9
EC	2.30	6.3 ± 0.5

Experience with similar material from the same suppliers indicates that the H specimen contains substantially less free silicon than the other. The two samples are from different suppliers, and the processes differ significantly. The H specimen had been heated to 2700°F in air. The EC specimen had never been heated in air. In both cases specimens were cut from broken modulus-of-rupture specimens in Table 1.

FABRICATION PROCESSES AND COST CONSIDERATION

The most common fabrication process is that of forming a powder compact from silicon powder by conventional ceramic and powder metallurgy techniques, then heating this compact in a nitrogen (or ammonia) atmosphere to produce Si_3N_4. Some work has been done where the process is the same except that some Si_3N_4 powder is added to the starting silicon powder. Also some hot pressing has been done.[11] Relatively pure Si_3N_4 is reported as unsinterable; to overcome this, these hot pressing studies used a few weight percent of various additives.

Because the bulk of experience, both ours and others', deals with the process using only silicon powder as the starting material, the following discussion of fabrication factors will deal only with that process.

Silicon Powder Requirements and Forming of Powder Compacts

Our experience, verifying that of many others, is that relatively impure silicon powder is probably superior for the intended purpose. Most of our trial fabrication was done with 98% pure, minus 200 mesh powder (all passing a 200 mesh screen). This is currently available at 35¢ per pound in 500-pound lots. Powder having a purity of 99.6%, also minus 200 mesh, is available at $12.00 per pound, and 99 99% at $25.00 per pound, in the same lot size. The consequence is that starting material cost is practically a negligible factor in final cost of critical components of reasonably complex shape.

The problem of forming the powder compact has of course been highly developed with other materials. Silicon powder compacts have been formed by slip casting, vibratory compaction, tamping, and isostatic pressing both dry and with lubricants and plastic binders.

Two factors which may affect the choice of powder compaction method are:

1. The fact that the material may be partially fired, then removed and machined as described under "Machining."

2. The dimensional change from the powder body to the hard fired state is an expansion of less than 1%.[12] This suggests the possibility that a fragile powder compact formed to a radome shape can be supported on a mandrel during the firing process.

The bodies of interest to us were massive perforated shapes. The methods used in our few limited trials at LRL, and those of the three suppliers, all differed substantially, yet they all seemed to have the potential of success. That at LRL involved isostatic pressing. We are not free to reveal the other processes because of proprietary considerations. Figure 9 shows some of the trial procurements. C2820 and C3330 are not silicon nitride, but the rest are. None of these are crack-free, but eliminating the cracks seemed straightforward.

Firing Cycle Considerations

Most firing cycles involve a two-stage process. The first portion involves nitriding at a temperature less than the melting point of silicon. The melting point of silicon is about 2580°F and a typical first-stage firing temperature would be 2200°F. This causes nitridation of the surface of the silicon grains and the reaction rate slows down and approaches saturation. It is then possible to raise the temperature above the melting point of silicon and complete the reaction of the remainder of the silicon in short time. Care must be exercised in programming the temperature such that the molten silicon does not transfer to another location (e.g., outside the body). In general the firing process takes less than 100 hours.

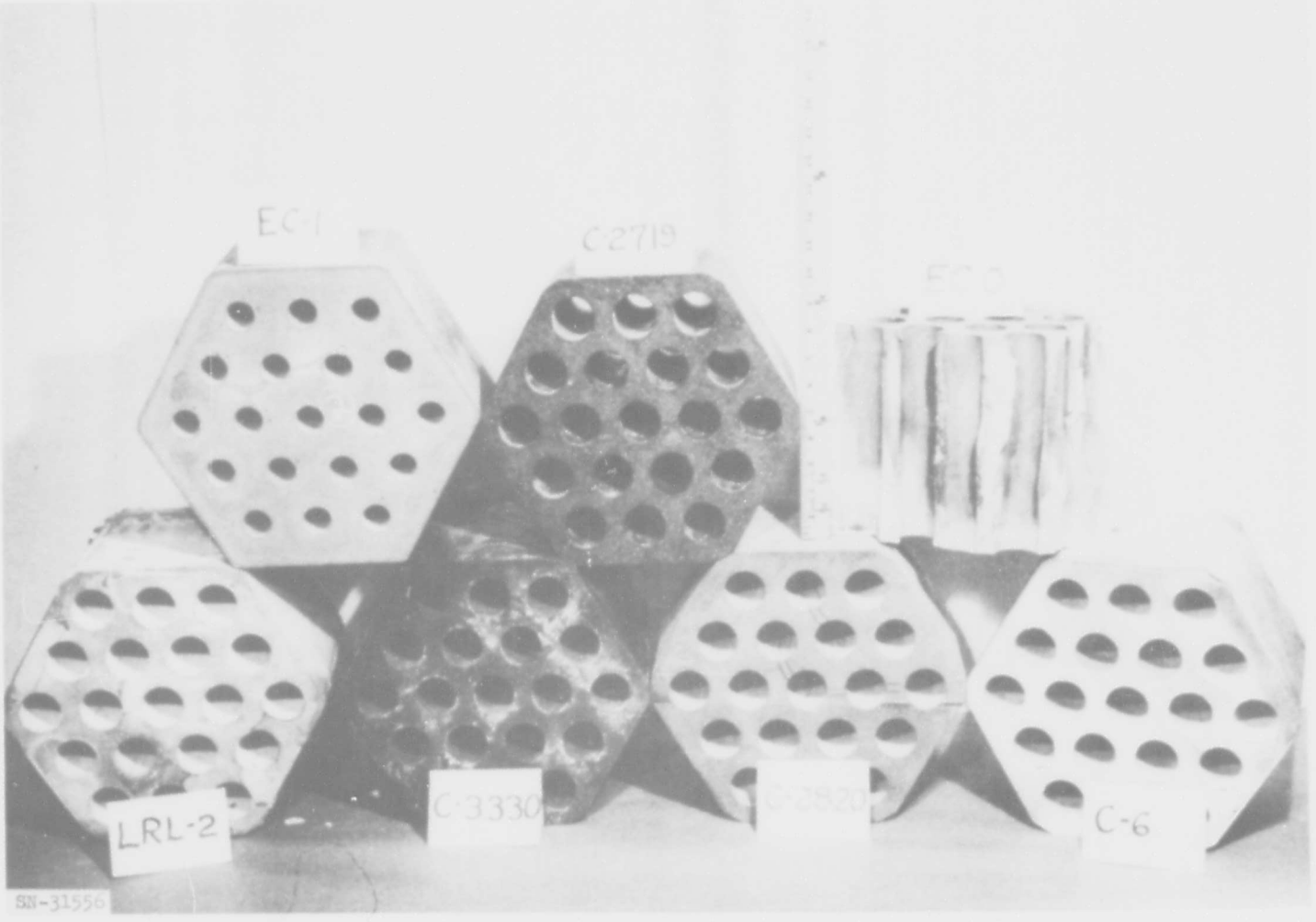

Fig. 9. Ceramic specimens produced by various commercial sources in developing fabrication techniques.

Following are the three most common difficulties which we have observed in this type of firing sequence:

1. Flow of molten silicon (e. g., oozing from the surface).

2. Incomplete reaction. As one would expect, penetration limitations occur with thicker sections. In our experience such difficulties have occurred at distances from the surface of about 1/4 to 1/2 in. This would suggest that a radome 1/2 to 1 in. thick could be fired without difficulty. Of course this is very much dependent on the initial compact density and particle size. Also it is subject to improvement by using longer furnace times and tricks such as alternating furnace pressure ("pumping" the nitrogen).

3. For thick sections (several inches), the combined effect of the exothermic nitridation and temperature sensitivity of the reaction can produce large temperature differences in the piece. This can lead to several difficulties including cracking and premature melting of the silicon.

These difficulties are subject to control and much has been done by commercial fabricators to eliminate them. The point in listing them is to benefit the application-oriented individual rather than to deal with overcoming them.

Machining

As briefly mentioned earlier, the material can be nitrided a relatively small percentage of the total, removed from the furnace, and machined with essentially conventional metal-working techniques. High-speed steel cutting tools can be used, but require frequent sharpening. Carbide and alumina cutting tools are more satisfactory. Dimensional change after machining is less than 0.1%.[12] This suggests the possibility that expensive grinding of hard fired radomes may be eliminated. This type of machining is discussed further in several of the British references.[7,11,13]

The hard fired material can be diamond ground with essentially the same techniques used on other ceramics.

Cost Consideration

The cost of the silicon powder starting material is nearly negligible (35¢ per pound, as indicated above). Relative to alumina, the firing process differs in two essential ways. A nitrogen atmosphere must be provided for Si_3N_4, but the maximum firing temperature is lower, about 2800°F compared to about 3200°F for alumina. Where a substantial number of items are concerned, so that setup costs are minimized, we believe that temperature is apt to affect firing cost more than atmosphere control, resulting in lower firing costs for Si_3N_4. The following limited experience tends to bear this out.

Figure 10 is an assembly of sleeves used as a liner for an air heater. The shapes are roughly similar to shapes that might be used for radomes. Both alumina and silicon nitride were considered for the application. Following are bids obtained for fabricating these shapes from the two materials in

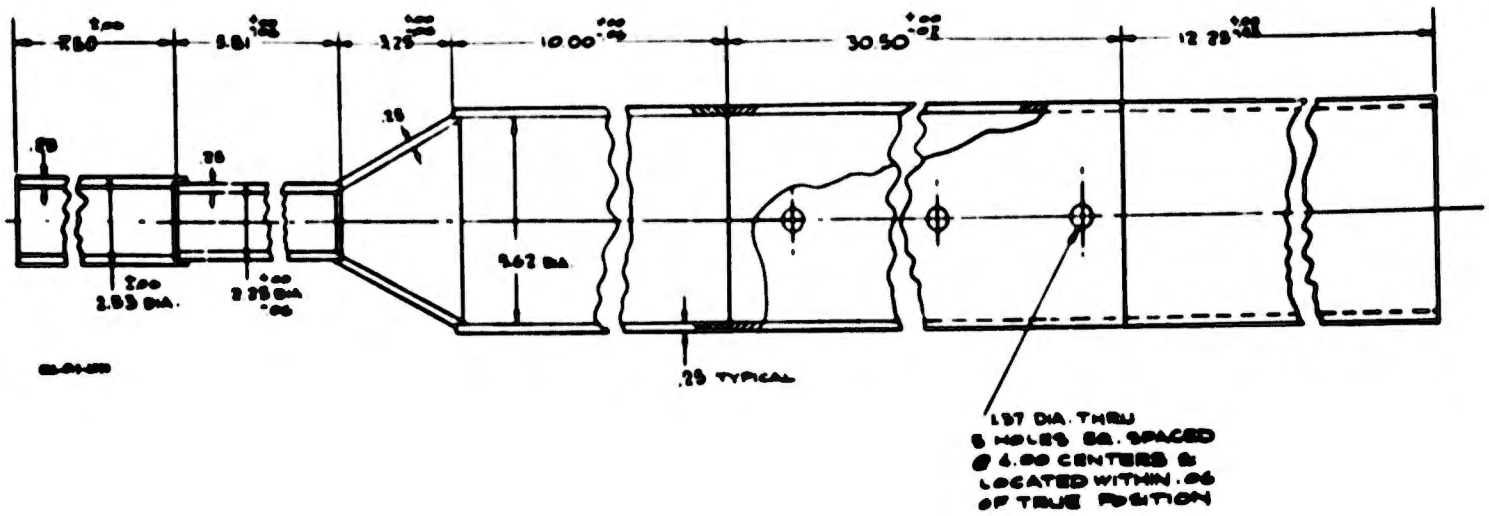

Fig. 10. Assembly for which fabrication costs (bids) were compared: silicon nitride vs alumina.

late 1961

Si_3N_4		$ 812.10
97.5% or purer Al_2O_3	Bid 1	$ 929.38
	Bid 2	$1,897.10
	Bid 3	$2,288.00

These were firm price bids, and the assembly was procured under the first bid.

APPLICATIONS

The British Admiralty Materials Laboratory has placed a contract[14] where the objective is to build and operate a rudimentary ceramic engine. It is believed that it will be made of silicon nitride and that it will take the form of a rotary piston engine. The De Havilland Engine Co., Ltd., was reported[7] to be using silicon nitride as a bushing for holding compressor blades during heating prior to extrusion. The material was apparently considered in England for stator blading in gas turbines, but this interest apparently waned because of lack of impact strength.

A perusal of the list of references makes it apparent that generation of data on this material has received much more attention in England than it has here, although there is no lack of fabrication capability in this country.

A review of all the factors affecting application of ceramics to both defense and commercial purposes suggests that Si_3N_4 might well displace more common ceramics such as Al_2O_3, and that the reason it has not is that its properties are not well publicized. Reference 13 gives additional data which may be of interest to application-oriented individuals.

REFERENCES

1. "X-ray Powder Data File," Published by ASTM, Card Nos. 9-250 and 9-259.

2. Parr, N. L., et al., "Structural Aspects of Silicon Nitride," Powder Metallurgy, 1961, No. 8.

3. Wells, Wm. M., and C. F. Cline, "Thermal Stress Fracture Characteristics of BeO," UCRL-7430. Also available as ASME paper no. 63-WA-297.

4. Timoshenko, S., Theory of Elasticity (McGraw-Hill, New York).

5. Gordon, G. M., and D. A. Brown, "Tungsten and Rocket Motors," Stanford Research Institute, May 31, 1962. Final report under Contract NOrd-18619 (FBM).

6. Vandervoort, R. R., and W. L. Barmore, "Compressive Creep of Ceramics for High Temperature Nuclear Reactors," UCRL-6826.

7. Sage, A. M., and J. H. Histed, "Applications of Silicon Nitride," Powder Metallurgy, 1961, No. 8.

8. Brochure entitled "Haynes Silicon Nitride," March 1962. Published by Haynes Stellite Division of Union Carbide.

9. Data sheet on "Roydazide," June 1962. Published by Doulton Industrial Porcelains, Ltd. The electrical data is attributed to British Ceramic Research Ass'n.

10. "Handbook of Microwave Measurements," Microwave Research Institute, Vol. II, 3rd Ed., 1963.

11. Deeley, G. G., et al., "Dense Silicon Nitride," Powder Metallurgy, 1961, No. 8.

12. Popper, P., et al., "The Preparation, Properties and Structure of Silicon Nitride," Trans. Brit. Ceram. Soc., Sept. 1961.

13. Glenny, E., and T. A. Taylor, "Mechanical Strength and Thermal-Fatigue Characteristics of Silicon Nitride," Powder Metallurgy, 1961, No. 8.

14. Private communication with D. J. Godfrey of British Admiralty Materials Laboratory.